451331

Report Status:
✓ Report Submitted to Sponsor (Award File Copy)
____ Send to Sponsor (Mailing Instructions Attached)
Date: 1/18/06
Administrator: PBonifazi

STRUCTURE AND PETROLOGY OF THE KERN CANYON FAULT, CALIFORNIA: A DEEPLY EXHUMED STRIKE-SLIP FAULT

Final Technical Report
USGS Award No: 00HQGR0056
Earthquake Hazards Program

Judith S. Chester
Texas A & M University
Department of Geology and Geophysics
College Station, TX 77843
Tel: 979-845-1380; Fax: 979-845-6162
e-mail: chesterj@geo.tamu.edu

☐ Reports Monitoring Updated
☑ Pending List Updated
updated 6/4/05
☐ Report not listed on either
HCM 1/18/06

Research supported by the U.S. Geological Survey (USGS), Department of the Interior, under USGS award number (J.S. Chester, 00HQGR0056). The views and conclusions contained in this document are those of the authors and should not be interpreted as necessarily representing the official policies, either expressed or implied, of the U.S. Government.

STRUCTURE AND PETROLOGY OF THE KERN CANYON FAULT, CALIFORNIA: A DEEPLY EXHUMED STRIKE-SLIP FAULT

Final Technical Report
USGS Award No: 00HQGR0056
Earthquake Hazards Program

Judith S. Chester
Texas A & M University
Department of Geology and Geophysics
College Station, TX 77843
Tel: 979-845-1380; Fax: 979-845-6162
e-mail: chesterj@geo.tamu.edu

Research supported by the U.S. Geological Survey (USGS), Department of the Interior, under USGS award number (J.S. Chester, 00HQGR0056). The views and conclusions contained in this document are those of the authors and should not be interpreted as necessarily representing the official policies, either expressed or implied, of the U.S. Government.

USGS Award No: 00HQGR0056

STRUCTURE AND PETROLOGY OF THE KERN CANYON FAULT, CALIFORNIA: A DEEPLY EXHUMED STRIKE-SLIP FAULT

Judith S. Chester
Texas A & M University
Department of Geology and Geophysics
College Station, TX 77843
Tel: 979-845-1380; Fax: 979-845-6162
e-mail: chesterj@geo.tamu.edu

TECHNICAL ABSTRACT

The mesoscopic structure and petrology of the Kern Canyon fault at Engineer Point, Isabella Lake, is characterized to better understand the physical and chemical processes that control earthquake nucleation and rupture propagation along mature faults in the middle to lower seismogenic zone of the continental crust. The 140 km long Kern Canyon fault is an exhumed, large displacement fault that cuts batholithic and metamorphic rocks in the southern Sierra Nevada Mountains, California. At Engineer Point, the Kern Canyon fault displays approximately 15 km of right lateral separation, and consists of a fractured, sheared and mineralogically altered zone several hundred meters thick. At least three distinct phases of deformation are recorded in the zone: an early phase of ductile shear within an S-C phyllonite, a subsequent, dominant phase of brittle faulting characterized by a throughgoing zone of cataclastic rocks, and a late stage of minor faulting along thin, hematitic gouge zones. The phyllonite zone trends N20-40E and displays extensive retrograde alteration primarily involving transformation of feldspar to mica, calcite and quartz. The cataclastic zone cuts the phyllonite, trends N20E, and consists of a relatively narrow core of foliated cataclasites cut by mesoscopic slip surfaces. Mesoscale fracture intensity decreases linearly with log distance from the cataclastic core and approaches background levels at approximately 50 m. S-C fabrics and subsidiary fault slip data indicate that both the phyllonitic and cataclastic shear zones were dominantly strike-slip. Slip lineations on the hematitic gouge zones suggest normal oblique-slip. The damage zone of the fault contains many quartz- and calcite-filled veins and the cataclastic rocks often are calcite-cemented. Some quartz veins are greater than 1 m thick. Fault-parallel and pinnate veins exist along the foliated cataclasites and localized slip surfaces. Cross cutting relations indicate quart-filled veins began forming during the phyllonite phase, and calcite-filled veins formed largely during the cataclastic-faulting phase. The structures and synfaulting mineral reactions record faulting under evolving fluid chemistry and metamorphic conditions possibly associated with progressive unroofing during faulting.

INTRODUCTION

A long-standing problem in earthquake mechanics is our incomplete understanding of the physical and chemical processes that control earthquake nucleation and rupture propagation along mature faults, such as faults of the San Andreas system, California. To date, numerous hypotheses have been put forward to explain the apparent weakness of the San Andreas fault (e.g., Scholz, 2000; Hickman et al., 1994; Zoback et al., 1987). Similarly, a number of hypotheses have been proposed to explain observations of seismicity on faults, including the depth extent of seismogenesis, occurrence of aseismic creep, and complexity of earthquake rupture, such as heterogeneous moment release, and triggered slip. Critical to many of these hypotheses are specific assumptions about the structure,

petrology, and fluid environment of fault zones. Although we have increased our understanding of these parameters significantly through detailed field studies of exhumed faults, there is a general lack of observations of large-displacement, strike-slip faults at depths greater than about 5 km, i.e., from the middle of the seismogenic zone in the continental crust. As such, too few data are available to constrain or test many of the existing hypotheses for fault weakening and earthquake mechanics. This study is the first part of a detailed structural and petrological investigation of the mechanics and mechanisms of seismic faulting in the mid- to lower-portion of the seismogenic regime. The goal is to provide critical information on the physical and chemical processes that operate within this zone over the earthquake cycle through field study of the Kern Canyon fault, CA (Figure 1).

GEOLOGY OF THE KERN CANYON FAULT ZONE

The Kern Canyon fault zone is part of a deeply exhumed, large displacement, strike-slip fault system in batholithic, metasedimentary and metavolcanic rocks of the southern Sierra Nevada (Figure 1; e.g., Moore and du Bray, 1978). The system is approximately 140 km in length and parallels the marginal faults of the Sierra Nevada (Moore, 1981; Moore and Sisson, 1984; Ross, 1986), extending from south of Isabella Lake northward towards Mt. Whitney. The Kern Canyon fault zone generally is regarded as a narrow, brittle fault zone of Cenozoic age (Moore & du Bray, 1978; Ross, 1986). Along the central and northern portions of the Kern Canyon fault zone there is evidence of an earlier, wider zone of ductile shearing referred to as the proto-Kern Canyon fault zone (e.g., Busby-Spera & Saleeby, 1990). The proto-Kern Canyon fault zone is a regionally extensive, synplutonic dextral shear zone that may be the southern continuation of the axial intrabatholithic break of the Sierra Nevada (Saleeby and Busby, 1993; Kistler, 1993).

The proto-Kern Canyon and Kern Canyon fault zones diverge at about Kernville. The Kern Canyon fault continues to the southwest through Engineer Point and the dam at Isabella Lake (Ross, 1986), and the proto-Kern Canyon fault continues southeast to the eastern end of the Tehachapi Mountains (e.g., Busby-Spera & Saleeby, 1990; Saleeby & Busby-Spera, 1993).

The proto-Kern Canyon fault zone is interpreted to represent a major, ancient intra-arc strike-slip fault associated with right-oblique convergence during subduction of the Farallon plate or possibly the northward component of convergence of the Kula plate from mid(?)- to Late Cretaceous time (Busby-Spera and Saleeby, 1990). Deformation associated with this phase of movement is characterized by a 0.5-3 km wide mylonite-phyllonite shear zone. S-C fabrics in the mylonitic rocks are consistent with right-lateral shear with a minor component of uplift of the east side relative to the west. Metamorphism and deformation are assumed to have occurred during emplacement of the mid-Cretaceous plutons, at a pressure of 3+ 0.5 kbar. About 8-10 km of structural relief across the fault zone is indicated by geobarometric data. The magnitude of lateral displacement is poorly constrained, however, field evidence for dominantly strike-slip separation and approximately 10 km of vertical separation at some localities suggests that at least 40 km of strike-slip separation may have occurred.

Along the central portion of the Kern Canyon fault, the intensity of mylonitization increases towards the fault suggesting that the Cenozoic fault trace coincides with the locus of maximum slip on the proto-Kern Canyon fault in this region. Most previous workers are in agreement regarding the existence and location of the Kern Canyon fault north of Kernville. However, the movement history and relation of the southern portion of the fault to the Breckenridge and the White Wolf faults are not entirely clear (Figure 1; e.g., Ross, 1986; Saleeby, 1992). Geologic mapping shows that the Kern Canyon fault cuts granites as young as 80 Ma, but does not cut a 3.5 Ma overlying basalt flow. Thus, the fault may be associated with Cenozoic basin-and-range extension (Dellinger and Zilka, 1984). Although the fault trace often is mapped as continuous and relatively straight or smoothly curving, the limited number of exposures do not preclude a segmented character. Moore and du Bray (1978)

demonstrated right-lateral, strike-slip separation of igneous and metamorphic rock units along the northern section of the fault, and Ross (1986) showed compatible offset of units further south. The mapped separation increases from several km at the northern end to about 13 km along the southernmost portions of the fault. Moore and du Bray note that the contacts of the offset units are variably and steeply dipping, and thus the offset patterns imply that the fault is dominantly strike-slip.

The Kern Canyon fault zone generally consists of a zone of brittle shear 100 m wide or less within a broader zone up to 1 km wide containing subparallel and secondary faults (Moore & du Bray, 1978; Ross, 1986). The smaller faults have sympathetic shear to the Kern Canyon fault zone. At the northern portion of the Kern Canyon fault zone, displacements may be partly accommodated on a network of north-trending joints and sheared joints that occur over a broad region of the Sierra Nevada (Lockwood and Moore, 1979; Segall and Pollard, 1983). Several studies have noted the presence of cataclastically deformed, highly sheared and altered rocks within the fault. Probably the most complete study of the fault structure was that done by Treasher (1948) as part of the siting of the Isabella auxiliary dam. Surface study, trenching and drilling in the vicinity of the dam abutment at Engineer Point showed that the zone of faulting and hydrothermal alteration there is about 250 m wide, and that the fault contains a narrower zone of intense shear on the order of 90 m wide. As reported by Treasher (1948) and Ross (1986), fault rocks range from fault gouge and fault breccia to microbreccia and protomylonite. Optical microscopy reveals that significant alteration to white mica, chlorite and calcite (Ross, 1986).

KERN CANYON FAULT ZONE AT ENGINEER POINT

Excellent exposures of the Kern Canyon fault exist along Engineer Point at the south end of Isabella Lake (Figure 2). Engineer Point is a prominent peninsula extending northward into the lake between the main dam on the west and auxiliary dam on the east. The fault is located along and strikes approximately parallel to the eastern side of the peninsula. Correlation of offset plutonic and metamorphic rocks across the Kern Canyon fault in the vicinity of this peninsula suggests dextral separation of approximately 15 km (Ross, 1986; Moore & du Bray, 1978). Previous reports also suggest that there may have been a significant component of dip-slip in this region (Treasher, 1948; Engel, 1963; Saleeby, 1992). Rock exposures are present over the peninsula and along the wave cut beaches. We visited the fault during mid-summer months when water levels in the reservoir are moderate to high (~780-790m), and at relatively low-water levels (~775m) when a greater portion of the fault zone is exposed and most of the peninsula is dry and accessible.

Work to date has focused on documenting the overall petrology and structure of the fault zone at Engineer Point. Fault rock structures, relative intensity of hydrothermal alteration, and protolith rock type were mapped at a scale of 1:6000. Mesoscopic scale fracture density traverses and fault and fracture orientations have been measured at the regional and fault zone scales. Approximately 30 oriented samples representative of the various protoliths and fault rocks were collected for preliminary optical microscopy and quantitative microprobe analyses.

Through field mapping we have documented that the Kern Canyon fault zone at Engineer Point consists of two distinct shear zones, a phyllonite and a cataclastic zone. Within the cataclastic zone two distinct types of cataclastic fault rocks exist recording two brittle phases of faulting. The dominant cataclastic zone trends N20°E and contains breccias, cataclasites, and foliated cataclasites, and displays mesoscopic, localized slip surfaces. This zone displays mineralogies that are similar to the phyllonite, except that it contains greater volumes of calcite. The internal structure of the cataclastic zone is similar to that of other large displacement faults in that it consists of a broad zone of fractured and altered rock bounding a relatively narrow core of highly sheared fault rocks (Figures 3 and 4; Chester et al., 1993).

The dominant cataclastic zone is cut by faults formed during the second phase of brittle deformation. Distinctly younger shears occur within and are roughly parallel to the cataclastic zone, and are lined with thin layers of hematite-cemented gouge. The hematite-cemented gouge consists of an extremely fine grained matrix containing porphyroclasts of older cataclasites. Clast compositions vary, and most show evidence for alteration and replacement reactions. Slip lineations in the gouge suggest a large component of dip-slip. On the basis of cross-cutting relations and relative development of the different brittle fault rocks, it appears that the gouge represents the latest stage movements and that the magnitude of dip-slip motion is small relative to that accommodated by the prominent right-lateral cataclastic zone. Although locally variable in thickness and deformation intensity, the overall damage zone generally displays an ordered progression of mesoscopic scale structures recording increased deformation towards the fault core (Figure 5).

The phyllonite zone trends N40°E, and is located west of the cataclastic zone (Figure 4). At the southern end of Engineer Point, the phyllonite is spatially separate from the cataclastic fault and is relatively unaffected by brittle deformation. The phyllonite is cut by the cataclastic fault in the central portion of the peninsula and segments of the phyllonite zone are present within the cataclastic zone further north. The phyllonite zone is on the order of 10 m wide and consists of a narrow layer of phyllonitic material bounded by protophyllonite that grades into altered host-rock. Fault-related mineral alteration reflects the transformation of feldspars to white mica, quartz, calcite, and albite (Figure 6, Table 1). Quartz fabric and synshearing mineral reactions imply phyllonite formation at brittle-plastic transitional conditions.

Timing Relations

Offset of igneous contacts and acidic dikes across the phyllonite suggest approximately 300 m of right-lateral separation (Figure 6). The phyllonite is cut and dissected by the westernmost observed trace of the cataclastic fault. Fault-bounded slices of exotic rocks, such as tuff and limestone, within the cataclastic fault zone imply kilometers of slip on the slip surfaces.

Quartz and calcite fracture-fill is common in the damaged zone of the cataclastic fault and veins up to several decimeters thick are present near the fault core. In general, the thickness of veins decreases with distance from the fault core. Individual veins show evidence of more than two fracture and cementation events, and the veins and cataclastic shears are mutually cross-cutting indicating that fracture and cementation occurred during faulting.

Synfaulting Alteration

Map-scale zones of mineral alteration roughly correlate with the damaged zone of both the phyllonite and cataclasite zones. Rocks with greatest degree of alteration occur closest to the fault cores and larger subsidiary faults in the surrounding host rock (Figure 4 and 7). Smaller alteration halos about brittle fractures and small brittle shears also are displayed in outcrop. Fault-related mineral alteration reflects the transformation of feldspars to albite, white mica, quartz, and calcite to produce an overall decrease in feldspar and biotite, and increase in white mica and quartz (Figures 4 and 7; Table 1). The detailed spatial distribution of mineral alteration suggests the alteration primarily was associated with the formation of the phyllonite shear zone. Quartz fabric and synshearing mineral reactions imply phyllonite formation at brittle-plastic transitional conditions.

A traverse across the phyllonite zone (at K16 in Figure 4) from the undeformed protolith (Wagy Flat granodiorite) on the east to the Alta Sierra granodiorite on the west was used to characterize the syndeformation-alteration reactions important during the ductile phase of faulting. The protolith (Wagy Flat granodiorite) is a coarse-grained granoblasitc rock composed of zoned plagioclase (An40-

45 cores to An25 rims), potassium feldspar, biotite, quartz, sphene and minor amounts of hornblend. At the microscopic scale the quartz grains display a relatively low density of intragranular microfractures, and biotite crystals are slightly undulose. Four domains may be distinguished within the damage zone of the phyllonite on the basis of a progressive increase in deformation and different chemical reaction products. Preliminary quantitative microprobe analyses show that the outermost domain of the damage zone is characterized, in part, by the pseudomorphic replacement reactions of anorthite to albite (An02-00)+muscovite+calcite; biotite to vermiculite, and sphene to rutile+quartz. In higher strained, domains vermiculite has altered to chlorite, and albite has altered to mica+quartz. Microscopic phyllonite zones appear along albite-albite grain boundaries and along boundaries between different phases. These zones are composed phengitic mica and display strong lattice preferred orientation and well-developed mica contiguity. The two additional domains display increasing degree of phyllonite development and increasing deformation, healing, sealing and recrystallization of quartz, and consumption of feldspars. In support of previous studies (e.g., Wintsch et al., 1995; Shea and Kronenberg, 1993) we have found that the alteration of anorthite and albite to muscovite alone clearly were not sufficient to localize strain, as there is no evidence that early formed micas from these reactions were reoriented and concentrated by shear to form phyllonite zones. It appears that calcite produced by alteration of primary plagioclase (An40) either left the system, or may have concentrated in veins at shallower depths.

The only deformation associated with the first stage of reactions is fracturing, and most fractures were sealed and healed. Thus, these initial reactions were chemically driven in an open system, probably from the influx of acidic meteoric waters along fracture permeability, provided a source for Ca++, and were independent of phyllonite formation and apparently independent of significant strain. With further strain, it appears that the quartz and mica reaction products are spatially differentiated through diffusive mass transfer to produce the concentrated mica seams and zones of finely recrystallized quartz. The distribution of phases suggests that some reactions require deformation or at least a directed stress. Overall, the field relations suggest that the faults were fluid-saturated, the faulting environment was hydrothermal, and that fluid flow and mineralization was episodic and coupled with fault-slip.

Fault and Fracture Fabric

The regional fracture fabric is characterized by two steeply dipping fractures sets striking approximately N05E and N60W (Figure 8a). In contrast, the fractures at Engineer Point display a strong preferred orientation characterized by steeply dipping fractures striking N60E, and a weaker set that reflects the regional fracture fabric (Figure 8b). Fractures filled with quartz and calcite, clearly associated with synfaulting alteration and deformation, display two broad sets, a fault-parallel set, and a set that is oriented at approximately 45° to the Kern Canyon fault and consistent with right-lateral strike-slip (Figure 8c). Subsidiary faults are common in the intensely fractured rock of the damage zone near the foliated cataclastite fault core. The subsidiary faults constitute a quasi-conjugate set of steeply dipping strike-slip faults that have a bisector oriented approximately 50° to the Kern Canyon fault (Figure 9a). Although there is considerable scatter in vein orientation, the average orientation of veins bisects the quasi-conjugate set of subsidiary strike-slip faults (Figure 9b). The fracture and subsidiary fault fabrics at Engineer Point indicate that the main phase of cataclastic faulting was right lateral, strike-slip. The phyllonite displays an S-C fabric with right-lateral C' surfaces (Figure 10). The nearly vertical intersection of surfaces and asymmetry indicate right-lateral strike-slip also dominated in the phyllonite zone.

Fracture orientations measured on two islands exposed on the east side of the fault zone display a strong preferred orientation (Figure 11). The preferred orientation is steeply dipping and striking

approximately N60E, consistent with the fault-related fracture fabric on Engineer Point (Figures 8 and 10). A second, much weaker set is similar to the secondary set of the regional fracture fabric (Figures 8 and10).

Microfracture Density on Western Side of Fault

Overall the density of microfractures on the western side of the fault increases towards the cataclastic zone. The relative occurrence of healed, sealed and open microfractures varies across the zone and appears to reflect damage associated with several distinct phases of faulting (Figure 12; Table 2). Preliminary data suggests that the open fractures increase in abundance with distance from the fault and that the healed fractures decrease in abundance with distance from the phyllonite zone suggesting a localized domain of diffusion-assisted healing during ductile shearing. In detail, microfracture density decreases near the phyllonite likely due to recrystallization of quartz associated with shearing in the phyllonite suggesting a large component of the microfracturing occurred prior to and during the ductile phase of deformation.

Trenching

Four preliminary, shallow trenches were dug with a bobcat, and eight additional trenches were dug with a backhoe between stations 44 and 49 (Figure 4). The trenches were cut perpendicular to fault strike along the eastern margin of Engineer Point. Trenching successfully exposed the eastern portion of the main cataclastic zone at Engineer Point (Figure 13). Exposures illustrate that the distribution of deformation across the fault zone is highly asymmetric. The damage zone on the western side of the fault is wider and displays distinct fault rock domains. The eastern side is characterized by a relatively abrupt boundary with highly fractured granodiorite and less alteration overall. Fracture density in the eastern granodiorite falls off rapidly with distance from the fault zone. Thin zones of concentrated shear that served as principal slip surfaces of the fault are present in the zone as evinced by juxtaposition of contrasting rock types and presence of ultracataclasite and gouge. Trench logs are being analyzed and compared to data of Treasher (1948).

CONCLUSIONS

Internal structure of the Kern Canyon fault is similar to other large displacement faults in that it consists of a broad zone of fractured and altered rock bounding a relatively narrow core of intense cataclasis. Majority of slip on the Kern Canyon fault occurred along several principal slip surfaces within the cataclastic fault zone. The fault was fluid saturated and the site of extensive synfaulting alteration reactions, neomineralization and fracture cementation. Structures suggest that fluid flow and mineralization was episodic and coupled with fault slip. The ductile phase of faulting initiated at brittle-plastic transition conditions to form a phyllonite shear zone. Structures and mineral reactions in the fault record evolving fluid chemistry, pressure and temperature conditions, possibly associated with progressive unroofing during faulting.

REFERENCES CITED

Busby-Spera, C.J. and Saleeby, J.B., 1990, Intra-arc strike-slip fault exposed at batholithic levels in the southern Sierra Nevada, California, Geology, 18, 255-259.

Chester, F.M., and Chester, J.S., 1998, Ultracataclasite structure and friction processes of the Punchbowl fault, San Andreas system, California, Tectonophysics, 295, p. 199-221.

Chester, F.M., Evans, J.P., and Biegel, R.L., 1993, Internal structure and weakening mechanisms of the San Andreas fault, JGR, 98, 771-786.

Hickman, S., Zoback, M., Younker, L., and Ellsworth, W., 1994, Deep scientific drilling in the San Andreas fault zone: Eos (American Geophysical Union Transactions), v. 75, p. 137-140.

Kistler, R.W., 1993, Mesozoic intrabatholothic faulting, Sierra Nevada, California, in Mesozoic Paleogeography of the Western United States – II, eds., Dunne, G.C. and McDougall, K.A., Pacific Section SEPM, Book 71, 247-262.

Moore, J.G., 1981, Geologic map of the Mount Whitney quadrangle, Inyo and Tulare County, California: U.S. Geological Survey Geologic Quadrangle Map GQ-1545.

Moore, J.G. and du Bray, E., 1978, Mapped offset on the right-lateral Kern Canyon fault, Sierra Nevada, California, Geology, 6, 205-208.

Moore, J.G. and Sisson, T.W., 1985, Geologic map of the Kern Peak quadrangle, Tulare County, California: U.S. Geological Survey Geologic Quadrangle Map GQ-1584.

Ross, D.C., 1986, Basement-rock correlations across the White Wolf-Breckenridge-southern Kern Canyon fault zone, southern Sierra Nevada, California, U.S.G.S. Bulletin, 1651, 25 pp.

Saleeby, J.B. and Busby-Spera, C., 1993, Paleogeographic and tectonic setting of axial and western metamorphic framework rocks of the southern Sierra Nevada, California, in Mesozoic Paleogeography of the Western United States – II, eds., Dunne, G.C. and McDougall, K.A., Pacific Section SEPM, Book 71, 197-226.

Scholz, C. H., 2000, Evidence for a strong San Andreas fault, Geology, 28, 163-166.

Shea, W.T. and Kronenberg, A.K., 1993, Strength and anisotropy of foliated rocks with varied mica contents, Journal of Structural Geology, 15, 1097-1121.

Snoke, W. A., Tullis, J., Todd, V. R., 1998, Fault-related rocks a photographic atlas, Princeton University Press, Princeton, New Jersey, 617 p., (read p. 3 - 18).

Webb, R.W., 1936, Kern Canyon fault, southern Sierra Nevada, Journal of Geology, 44, 631-638.

Wintsch, R.P., Christoffersen, R., and Kronenberg, A.K., 1995, Fluid-rock reaction weakening in fault zones: J. Geophysical Research, 100, p. 13,021-13,032.

Zoback, M. D., Zoback, M. L., Mount, V. S., Suppe, J., Eaton, J. P., Healy, J. H., Oppenheimer, D. H., Reasenberg, P. A., Jones, L. M., Raleigh, C. B., Wong, I. G., Scotti, O., and Wentworth, C. M., 1987, New evidence on the state of stress of the San Andreas fault system: Science, v. 238, no. 4830, p. 1105-1111.

ACKNOWLEDGMENTS

Robert Wintsch (Indiana University) and Ray Guillemette (Texas A & M University) participated in the microprobe analyses of the phylonite shear zone and interpretations of the synderfomation-alteration reactions. L. Neal participated in the mesoscopic and microscopic structural interpretation of the fault at Engineer Point and microprobe work as part of her M.S. Thesis at Texas A & M University. F. Chester (Texas A & M University) and D. Kirschner (Saint Louis University) participated in the collection of structural data in the field, and D. Kirschner also participated in trenching. A.K. Kronenberg participated in the TEM work and served on L. Neal's M.S. committee. TEM work was performed in the Microscopy and Imaging Center of Texas A&M University and Z. Luo is acknowledged for his assistance. This research was supported by the US Geological Survey (J.S.C.) under award numbers 00HQGR0029 and 00HQGR0056.

REPORTS PUBLISHED

Chester, J. S., Chester, F.M., Kronenberg, A.K., Fracture surface energy of the Punchbowl fault, San Andreas system, Nature , 437, 133-135, 2005.

Chester, J. S., Neal, L., Chester, F.M., Wintsch, R., Kirschner, D., Guillemette, R., Kronenberg, A.K., Structure and Petrology of the Kern Canyon Fault, California: A Deeply Exhumed Strike-slip Fault, Gordon Conference on Rock Deformation, Barga, Italy, May 19-24, 2002.

Chester, J. S., 2001, Structure and petrology of the Kern Canyon fault, California: A deeply exhumed strike-slip fault, Final Technical Report, USGS# 00-HQ-GR-0029, 2001.

Neal, L A., Chester, J. S., et al., Exhumation of a Large-displacement Strike-slip Fault: A View Through the Brittle-Ductile Transition, Manuscript in preparation for Journal of Structural Geology (see appendix of this report).

Neal, L.A., 2001, Internal structure of the Kern Canyon fault, California: A deeply exhumed strike-slip fault, M.S. Thesis, Texas A & M University, 2002.

Neal, L A., Chester, J. S., Chester, F. M., Wintsch, R. P., Internal structure of the Kern Canyon fault, California: A deeply exhumed strike-slip fault, EOS Trans. AGU, 81, p. F1145, 2000.

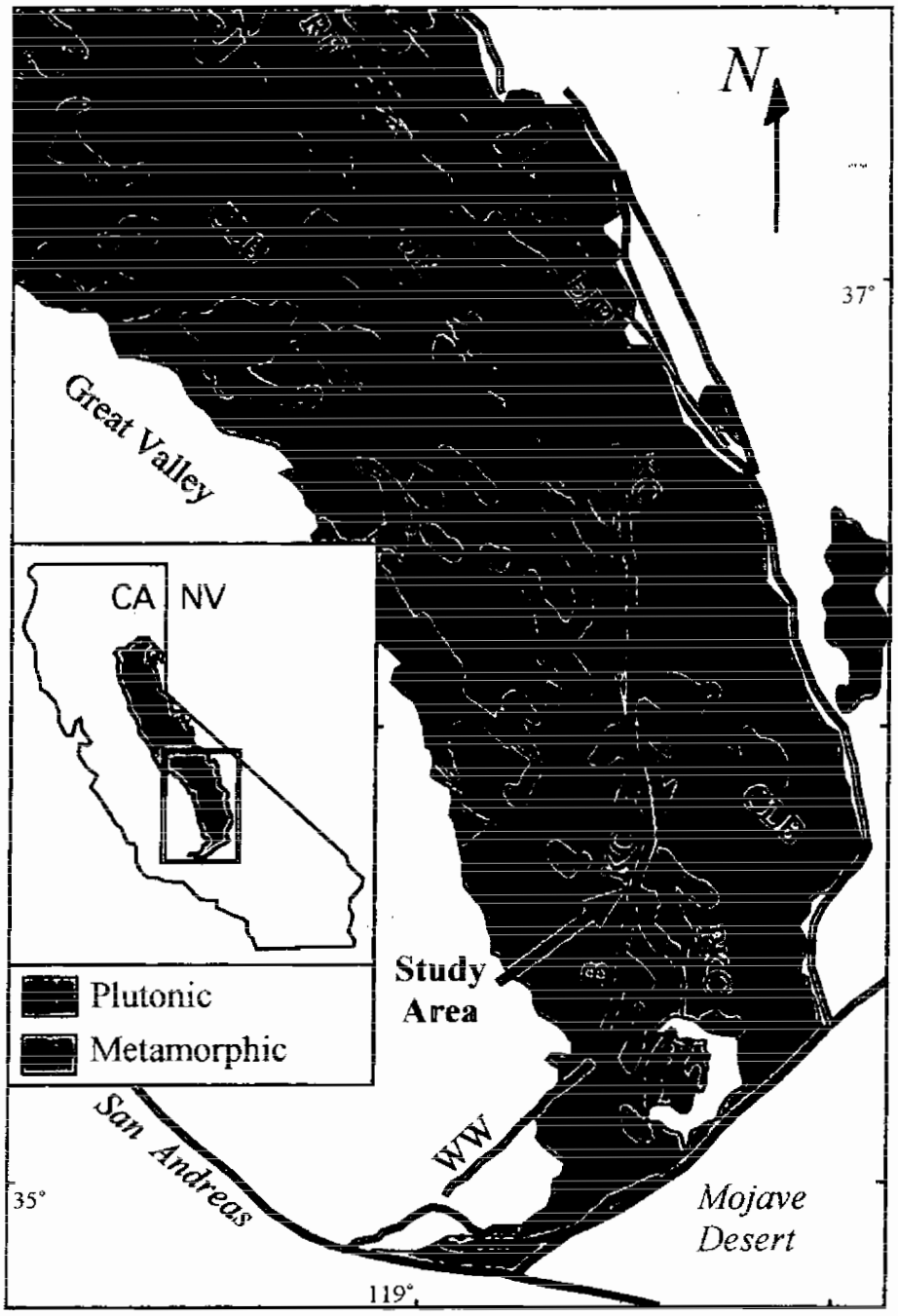

Figure 1. Southern Sierra Nevada batholith showing the Kern Canyon fault (KC), axial intrabatholithic break (AIB), cryptic lithospheric boundary (CLB), eastern intrabatholithic break (EIB), proto-Kern Canyon fault (PKC), Rosy Finch shear zone (RF), Breckenridge fault (B), and White Wolf fault (WW) (modified from Saleeby and Busby, 1993, and Kistler, 1993).

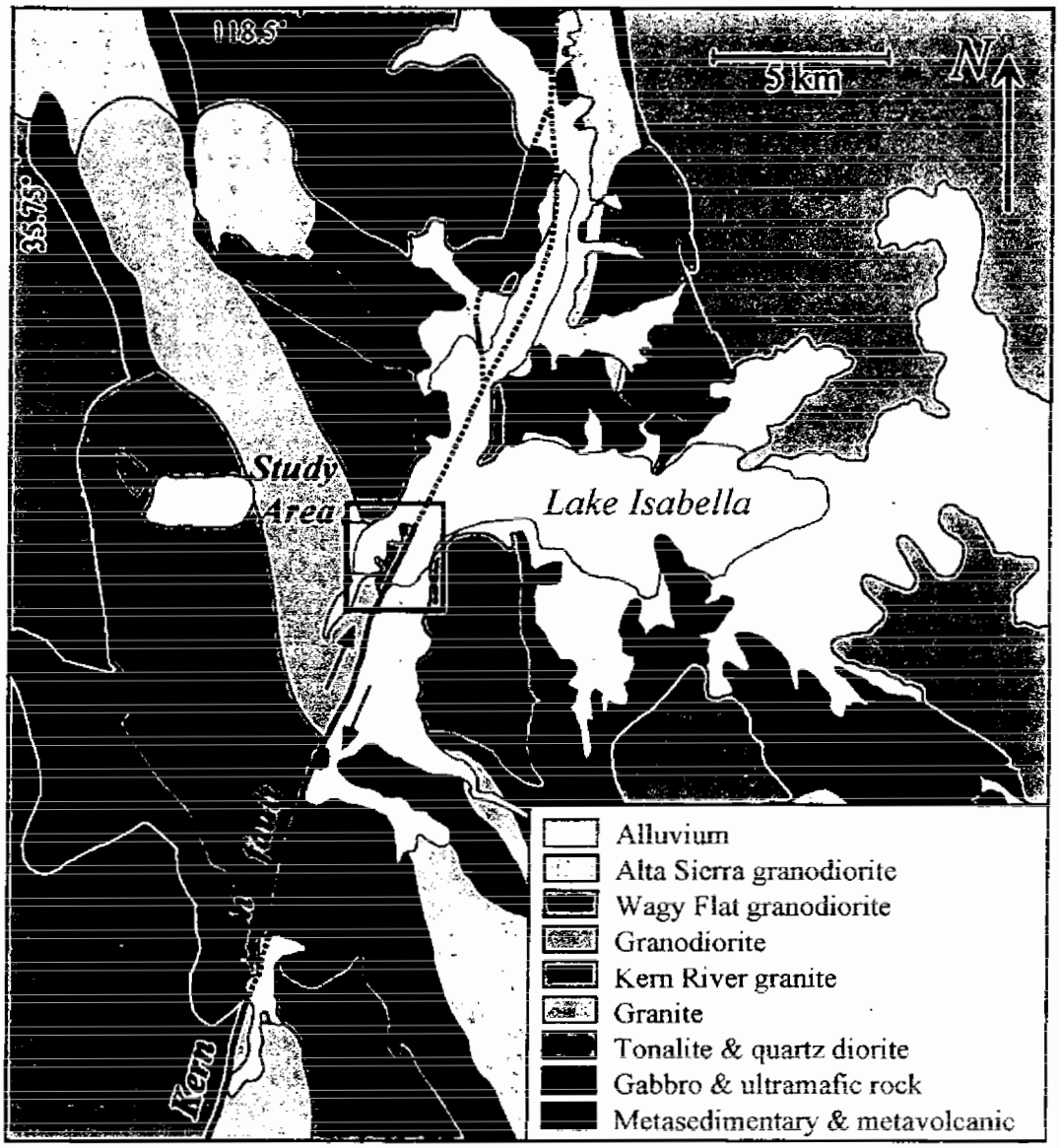

Figure 2. Geologic map of Lake Isabella region, California. Offsets of the Alta Sierra, Wagy Flat, and gabbroic and ultramafic rock units indicate approximately 15 km of right-lateral separation on the Kern Canyon fault. Fault is exposed at Engineer Point (peninsula within study area box) at the southern end of Lake Isabella. Map modified from Ross (1990).

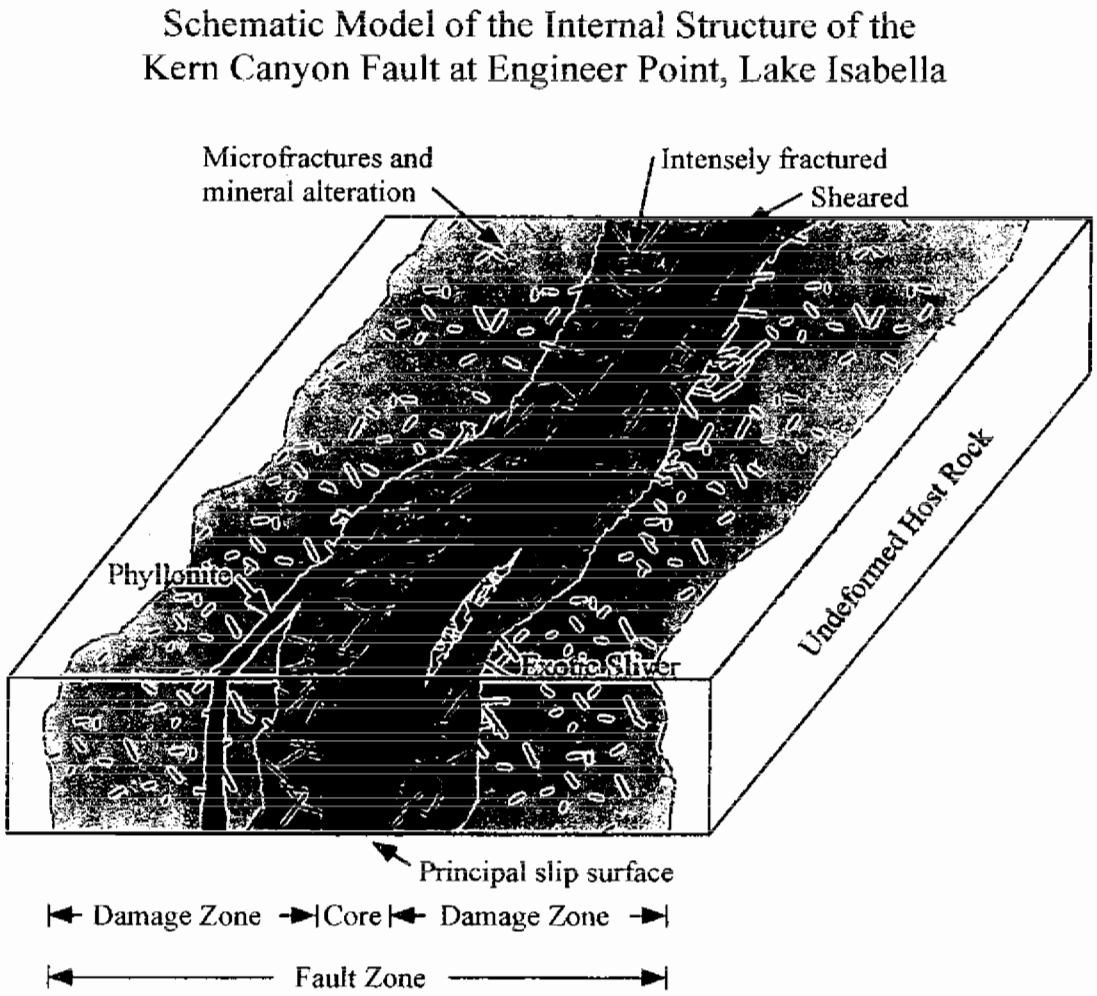

Figure 3. Schematic model of the internal structure of the Kern Canyon fault at Engineer Point. The core of the Kern Canyon fault contains multiple principal slip surfaces with relatively large displacements bounding slices of several different protoliths. The phyllonite occurs in the western side of the damage zone and is cut by the westernmost slip surface of the core.

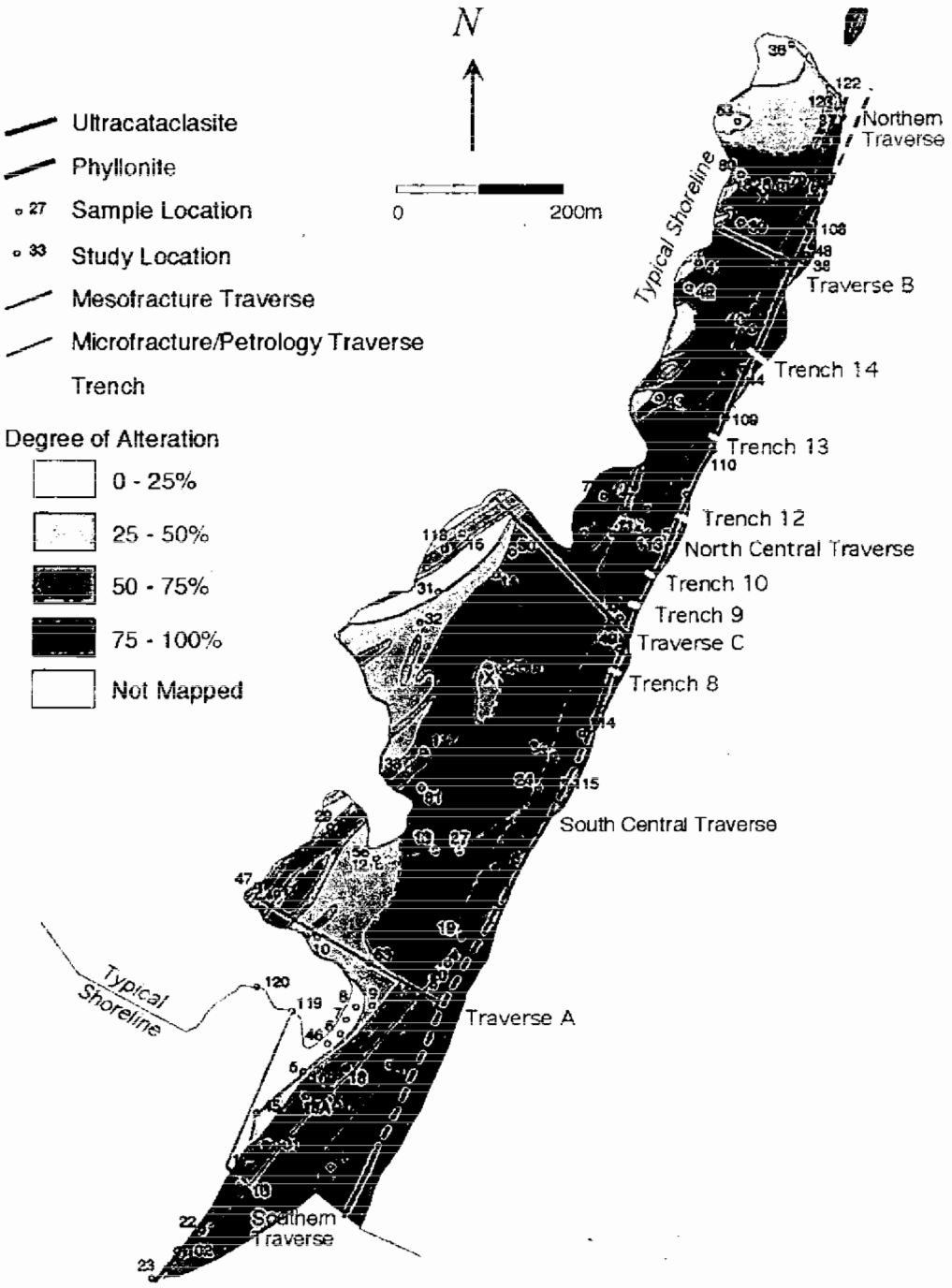

Figure 4. Map of Engineer Point showing faults, alteration intensity and trench locations.

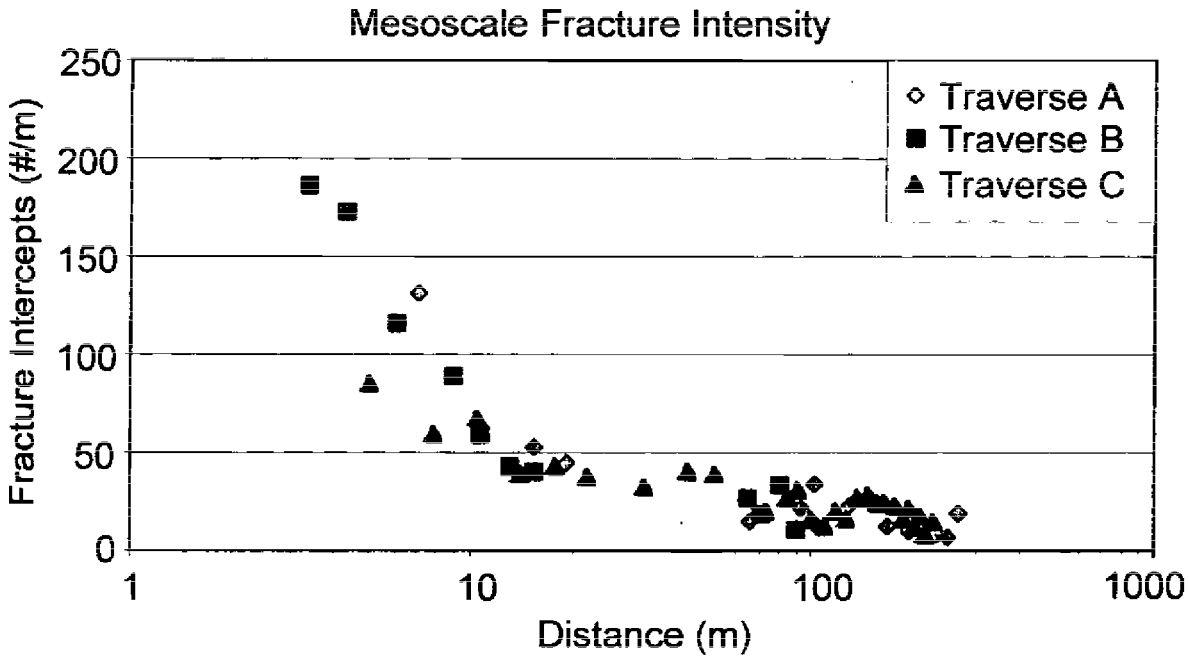

Figure 5. Intensity of open fractures, veins and subsidiary faults in the Wagy Flat granodiorite as a function of distance from the foliated cataclasite in the Kern Canyon fault (see Figure 5 for traverse locations). Intensity was determined by the average number of intercepts per meter length along two perpendicular count lines at each counting station. Deformation intensity increases gradually from regional levels at several hundred meters from the fault, then displays a marked increase in intensity at approximately 20 m from the westernmost boundary of the foliated cataclasite in the Kern Canyon fault.

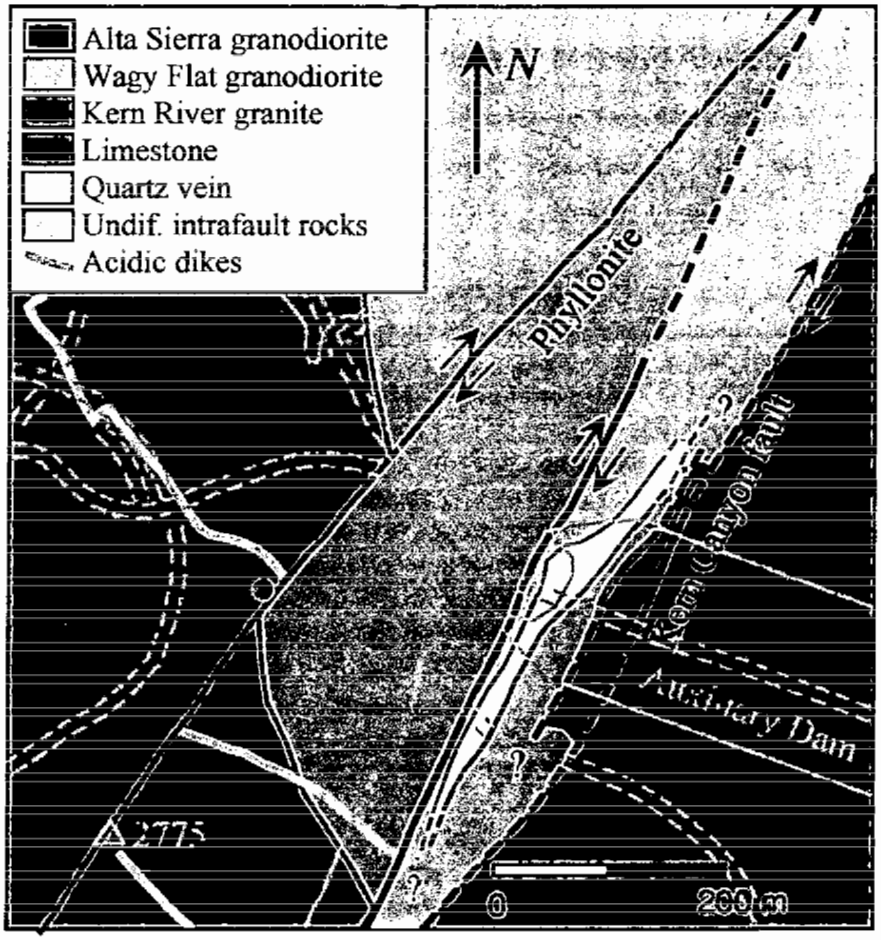

Figure 6. Bedrock geologic map at the western auxiliary dam abutment, Engineer Point, Lake Isabella. Approximately 200 m right-lateral separation is displayed across the phyllonite zone as indicated by offset of the Alta Sierra/Wagy Flat contact. Locally, the fault core contains slices of different protoliths indicating that the 15 km of separation on the Kern Canyon fault was accommodated along several principal slip surfaces within the cataclastic zone. Geology under dam site from Treasher (1948).

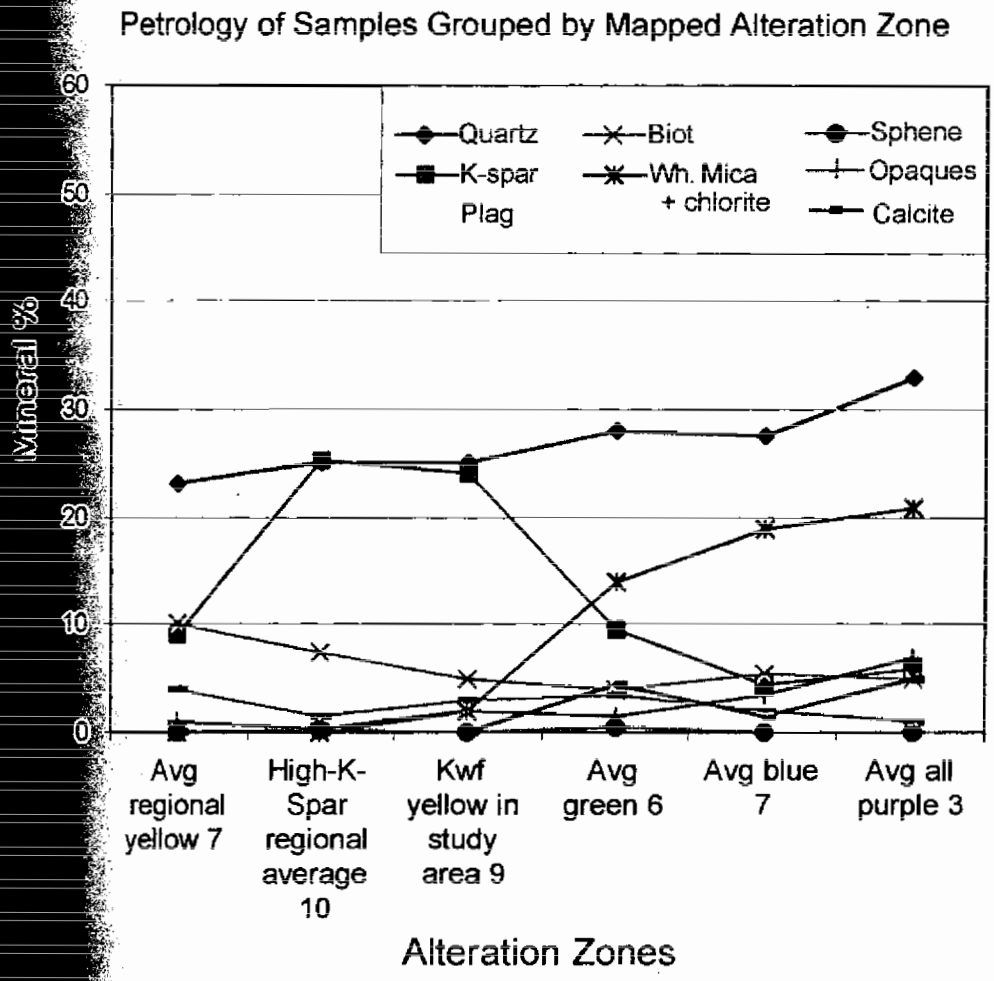

7. Plot of mineralogy as a function of mesoscale alteration index of samples
cted from the western side of the fault zone at Engineer Point and from the
outh west of Lake Isabella.

Regional Fracture Fabric

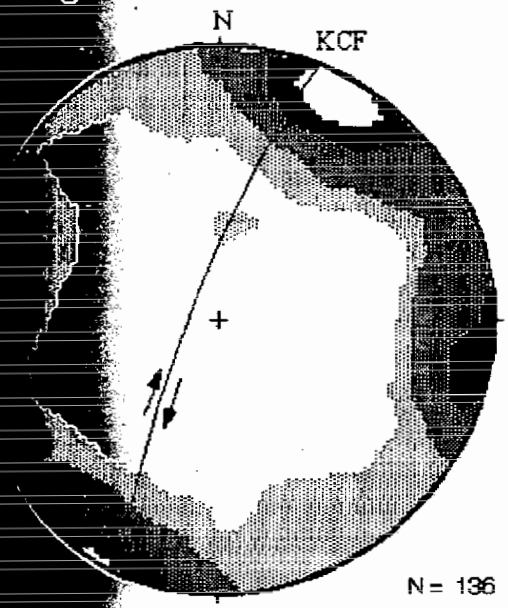

b. Engineer Point Fracture Fabric

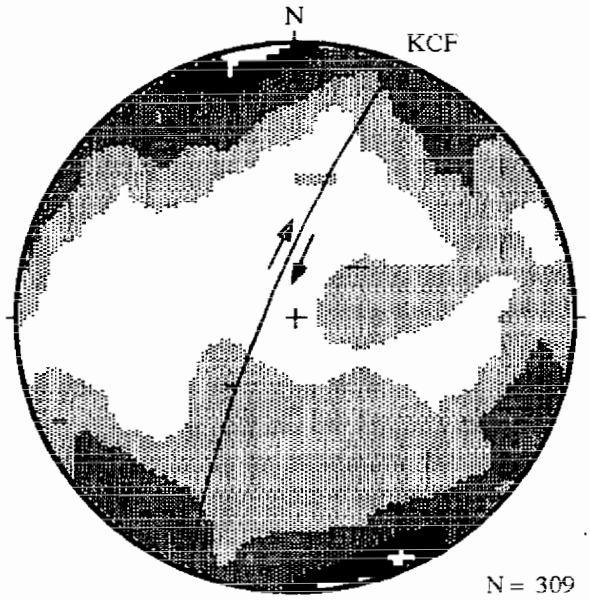

c. Engineer Point Vein Fabric

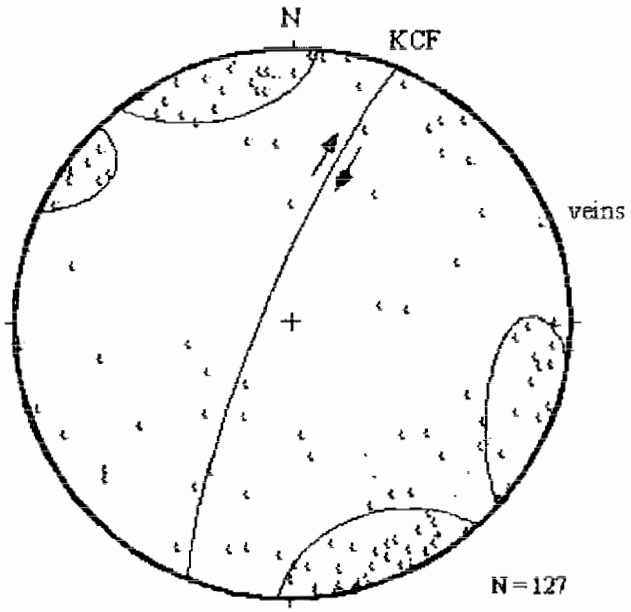

8. Contour and scatter plots of poles to fractures. (a) Open fractures and veins in host surrounding southern end of Lake Isabella, but not including data from Engineer Point. en fractures and veins at Engineer Point. (c) Veins only at Engineer Point. Plots are emisphere equal-area projections with north at the top. Kamb contours are shown at 2 ntervals. Also shown is the average orientation of the Kern Canyon Fault.

a.

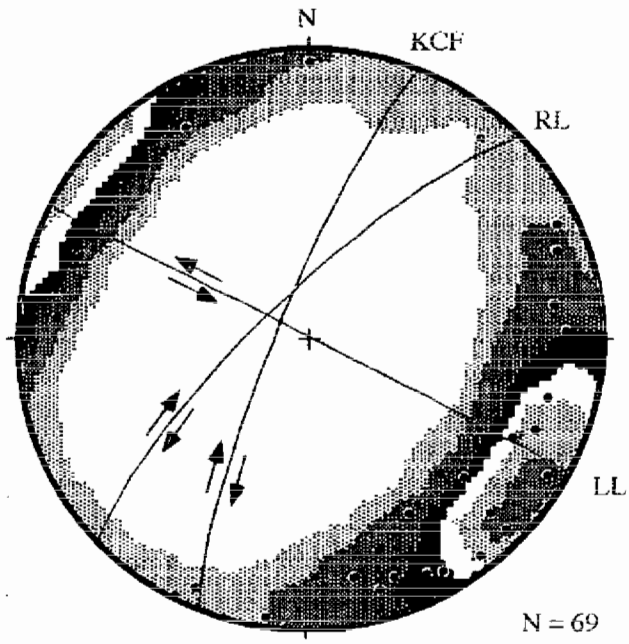

b.

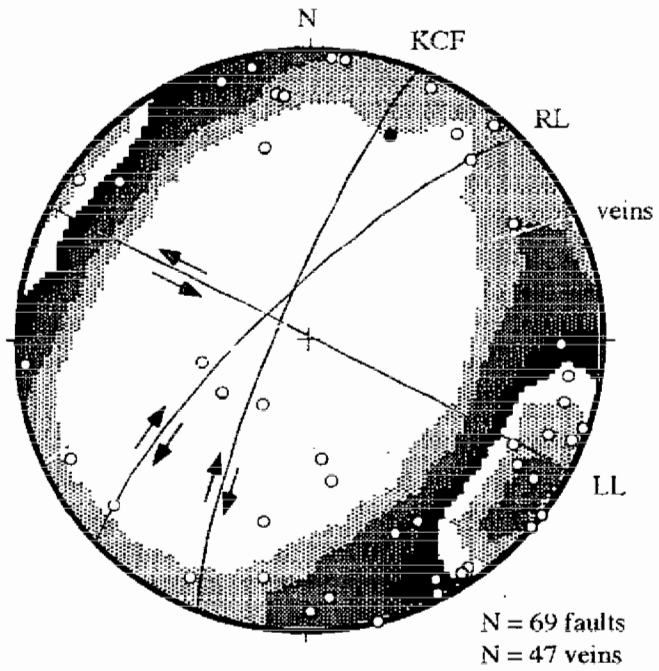

Contour plot of poles to all measured subsidiary faults in the intensely fractured zone st side of Engineer Point overlain by great circles representing average orientation of anyon Fault, average orientation of all faults with known right-lateral sense-of-shear average orientation of all faults with known left-lateral sense-of-shear (LL). Plot (a) s the poles to known right-lateral faults (red dots), and poles to known left-lateral en dots). Plot (b) shows poles to veins (yellow dots) and the average orientation of ts are lower hemisphere equal-area projections with north at the top. Kamb contours at 2 sigma intervals.

a. Phyllonite Fabric North of K18

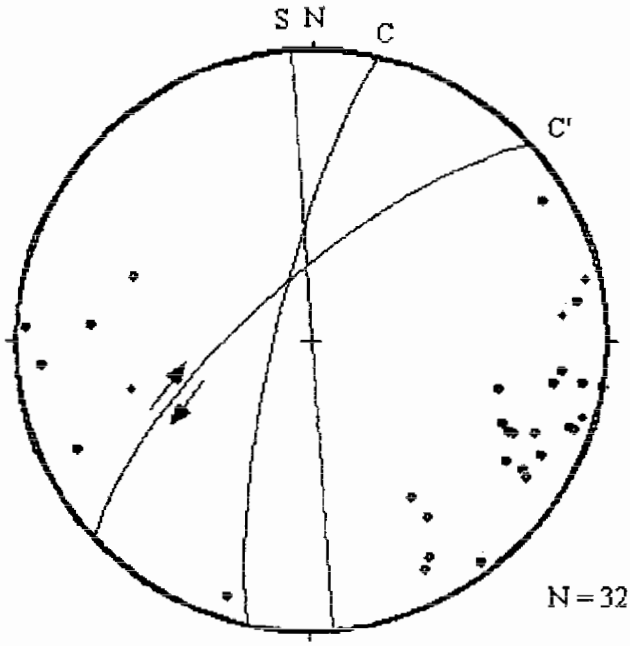

b. Phyllonite Fabric South of K18

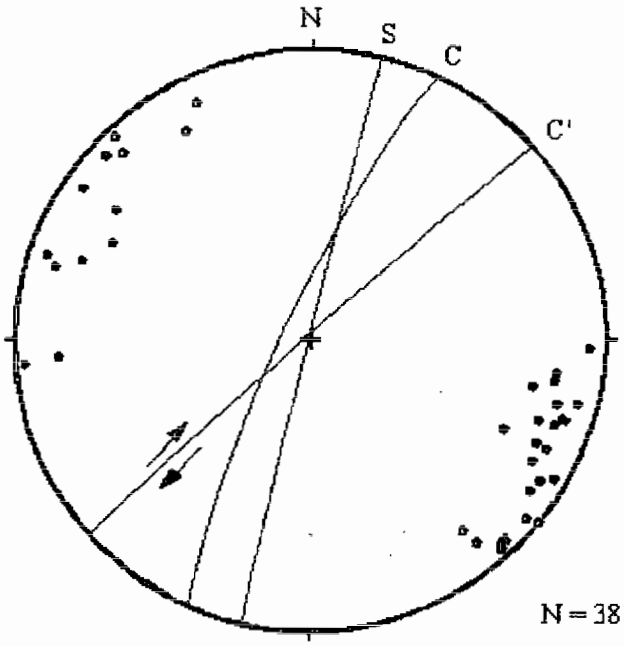

Figure 10. Orientations of poles to C, C', and S surfaces in the phyllonite plotted in lower hemisphere equal-area projections. Average orientation and sense-of-shear shown by great circles and arrows. (a) North of station K18; C surfaces are in red, N=21; C' surfaces are in black, N=7; S surfaces are in green, N=4. (b) South of station K18; C surfaces are in red, N=16; C' surfaces are in black, N=12; S surfaces are in green, N=10.

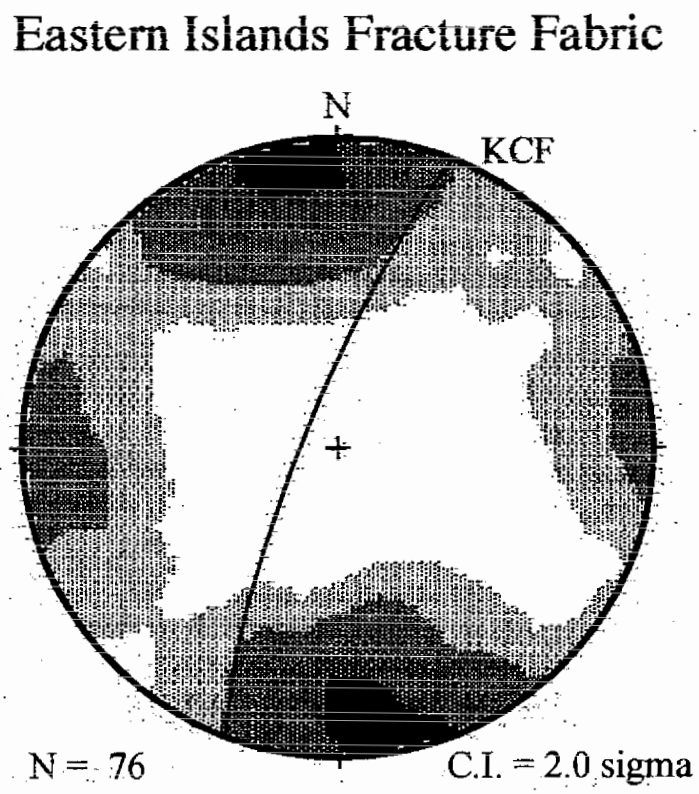

Figure 11. Contour plot of poles to fractures in rock exposed on the islands east of the Kern Canyon fault. Plot is lower hemisphere equal-area projection with north at the top. Kamb contours are shown at 2 sigma intervals. Also shown is the average orientation of the Kern Canyon Fault.

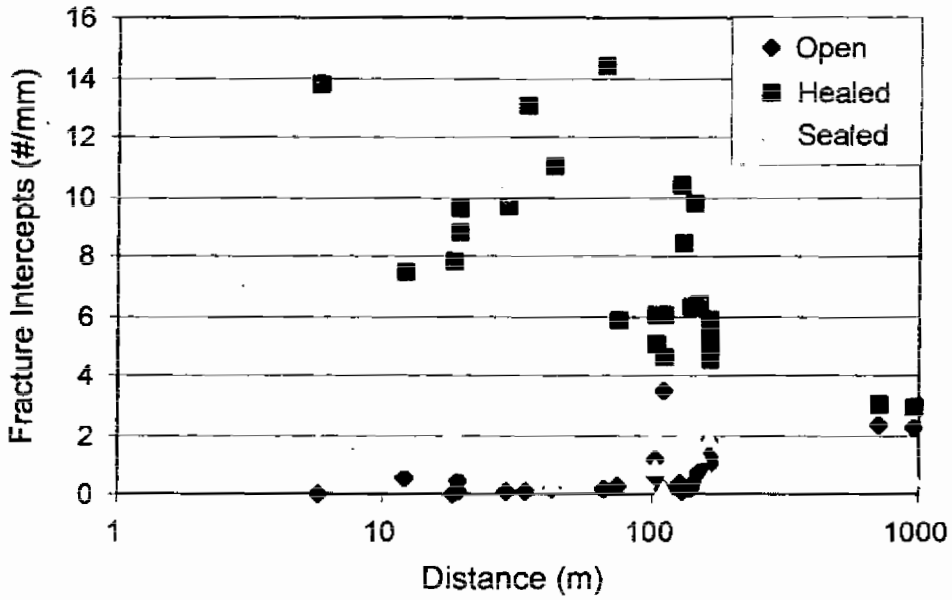

Figure 12. Intensity of open, sealed and healed microfractures as a function of distance from the foliated cataclasite in the Kern Canyon fault zone.

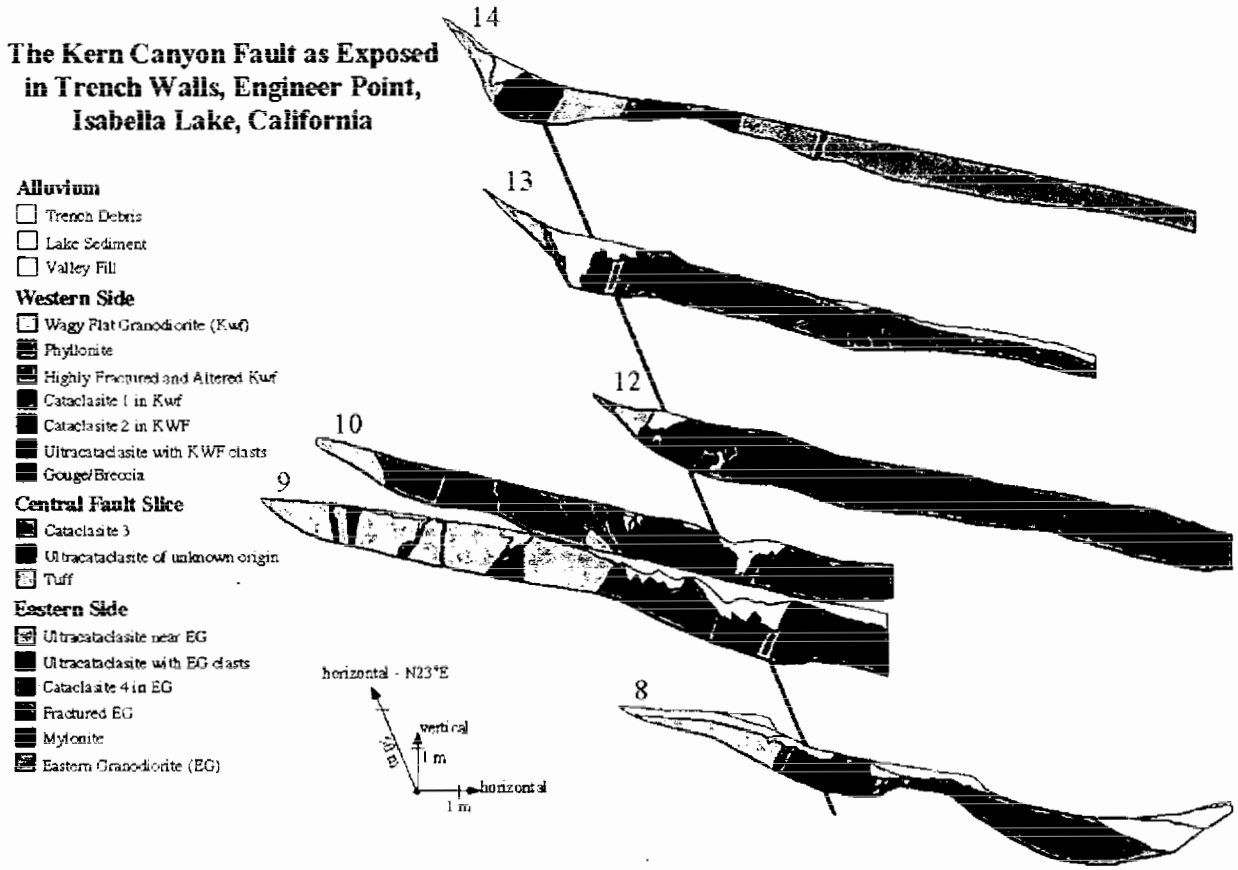

Figure 13. Simplified cross sectional views of trench walls.

Structure and Petrology of the Kern Canyon Fault: A Record of Faulting and Exhumation Through the Brittle-Ductile Transition

L. A. Neal, J. S. Chester, et al.
Department of Geology and Geophysics, Texas A & M University, College Station, Texas

(Manuscript in preparation for the Journal of Structural Geology)

INTRODUCTION

A long-standing problem in earthquake mechanics is our incomplete understanding of the physical and chemical processes that control earthquake nucleation and rupture propagation along mature faults, such as faults of the San Andreas system, California. To date, numerous hypotheses have been put forward to explain the apparent weakness of the San Andreas fault (e.g., Scholz, 2000; Hickman et al., 1994; Zoback et al., 1987). Similarly, a number of hypotheses have been proposed to explain observations of seismicity on faults, including the depth extent of seismogenesis, occurrence of aseismic creep, and complexity of earthquake rupture, such as heterogeneous moment release, and triggered slip. Critical to many of these hypotheses are specific assumptions about the structure, petrology, and fluid environment of fault zones. Although we have increased our understanding of these parameters significantly through detailed field studies of exhumed faults, there is a general lack of observations of large-displacement, strike-slip faults at depths greater than about 5 km, i.e., from the middle of the seismogenic zone in the continental crust. As such, too few data are available to constrain or test many of the existing hypotheses for fault weakening and earthquake mechanics. This study is the first part of a detailed structural and petrological investigation of the mechanics and mechanisms of seismic faulting from the mid- to lower-portion of the seismogenic regime to shallower depths. The goal is to provide critical information on the physical and chemical processes that operate within this zone over the earthquake cycle, using the Kern Canyon fault as an example fault zone that was active as it was exhumed across the brittle-ductile transition.

GEOLOGIC SETTING

The Kern Canyon fault zone is part of a deeply exhumed, large displacement, strike-slip fault system in batholithic, metasedimentary and metavolcanic rocks of the southern Sierra Nevada (Fig. 1; e.g., Moore and du Bray, 1978). The system is approximately 140 km in length and parallels the marginal faults of the Sierra Nevada (Moore, 1981; Moore and Sisson, 1984; Ross, 1986), extending from south of Isabella Lake northward towards Mt. Whitney. The fault zone generally is regarded as a narrow, brittle zone of Cenozoic age (Moore & du Bray, 1978; Ross, 1986). Along the central and northern portions of the fault there is evidence of an earlier, wider zone of ductile shearing referred to as the proto-Kern Canyon fault (e.g., Busby-Spera & Saleeby, 1990). The proto-Kern Canyon fault zone is a regionally extensive, synplutonic dextral shear zone that may be the southern continuation of the axial intrabatholithic break of the Sierra Nevada (Saleeby and Busby, 1993; Kistler, 1993).

The proto-Kern Canyon and Kern Canyon fault zones diverge at about Kernville. The Kern Canyon fault continues to the southwest through Engineer Point and the dam at Isabella Lake (Ross, 1986), and the proto-Kern Canyon fault continues southeast to the eastern end of the Tehachapi Mountains (e.g., Busby-Spera & Saleeby, 1990; Saleeby & Busby-Spera, 1993).

The proto-Kern Canyon fault zone is interpreted to represent a major, ancient intra-arc strike-slip fault associated with right-oblique convergence during subduction of the Farallon plate or possibly the northward component of convergence of the Kula plate from mid(?)- to Late Cretaceous time (Busby-Spera and Saleeby, 1990). Deformation associated with this phase of movement is characterized by a 0.5-3 km wide mylonite-phyllonite shear zone. S-C fabrics in the mylonitic rocks are consistent with right-lateral shear with a minor component of uplift of the east side relative to the west. Metamorphism and deformation are assumed to have occurred during emplacement of the mid-Cretaceous plutons, at a pressure of 3+ 0.5 kbar. About 8-10 km of structural relief across the fault zone is indicated by geobarometric data. The magnitude of lateral displacement is poorly constrained, however, field evidence for dominantly strike-slip separation and approximately 10 km of vertical separation at some localities suggests that at least 40 km of strike-slip separation may have occurred.

Along the central portion of the Kern Canyon fault, the intensity of mylonitization increases towards the fault suggesting that the Cenozoic fault trace coincides with the locus of maximum slip on the proto-Kern Canyon fault in this region. Most previous workers are in agreement regarding the existence and location of the Kern Canyon fault north of Kernville. However, the movement history and relation of the southern portion of the fault to the Breckenridge and the White Wolf faults are not entirely clear (Fig. 1; e.g., Ross, 1986; Saleeby, 1992). Geologic mapping shows that the Kern Canyon fault cuts granites as young as 80 Ma, but does not cut a 3.5 Ma overlying basalt flow. Thus, the fault may be associated with Cenozoic basin-and-range extension (Dellinger and Zilka, 1984). Although the fault trace often is mapped as continuous and relatively straight or smoothly curving, the limited number of exposures do not preclude a segmented character. Moore and du Bray (1978) demonstrated right-lateral, strike-slip separation of igneous and metamorphic rock units along the northern section of the fault, and Ross (1986) showed compatible offset of units further south. The mapped separation increases from several km at the northern end to about 13 km along the southernmost portion of the fault. Moore and du Bray note that the contacts of the offset units are variably and steeply dipping, and thus the offset patterns imply that the fault is dominantly strike-slip.

The Kern Canyon fault zone generally consists of a zone of brittle shear 100 m wide or less within a broader zone up to 1 km wide containing subparallel and secondary faults (Moore & du Bray, 1978; Ross, 1986). The smaller faults have sympathetic shear to the Kern Canyon fault zone. At the northern end of the Kern Canyon fault zone, displacements may be partly accommodated on a network of north-trending joints and sheared joints that occur over a broad region of the Sierra Nevada (Lockwood and Moore, 1979; Segall and Pollard, 1983). Several studies have noted the presence of cataclastically deformed, highly sheared and altered rocks within the fault. Probably the most complete study of the fault structure was that done by Treasher (1948) as part of the siting of the Isabella auxiliary dam. Surface study, trenching and drilling in the vicinity of the dam abutment at Engineer Point showed that the zone of faulting and hydrothermal alteration there is about 250 m wide, and that the fault contains a narrower zone of intense shear on the order of 90 m wide. As reported by Treasher (1948) and Ross (1986), fault rocks range from fault gouge and fault breccia to microbreccia and protomylonite. Optical microscopy reveals significant alteration to white mica, chlorite and calcite (Ross, 1986).

METHODS

At Engineer Point ductile and brittle shear zones, major subsidiary faults, relative degree of hydrothermal alteration, sample locations, and stations at which structural data were collected were mapped on a 1:12,000 topographic base. Additional large-scale maps (1:12 and 1:48) were constructed at key outcrops. Mesoscopic structural data collected included orientations of faults, joints, veins, foliations, and lineations. The orientation, length, amount and sense of displacement, and width and type of fill were recorded. All structural data were analyzed using Allmendinger's (1995) Stereonet software. The intensities of mesoscale joints, faults, and veins were measured along three traverses extending westward from highly deformed rocks of the brittle fault zone. Because the intensity of deformation has been found to increase with proximity to faults, as in studies of other fault zone (e.g., Chester et al., 1993; Wilson et al., 2003), the interval spacing of counting stations was decreased systematically with proximity to the fault. Intensities were recorded as the number of joints, fault and vein intercepts along a 1.2 m x 1.2 m counting cross. At each station, the counting cross was placed at a measured distance along the traverse and oriented randomly to obtain a directionally-unbiased representation of damage intensity. Intercepts of all structural features with the cross were counted. The number of intercepts were normalized against the length of the counting line to determine the intensity of counts per linear meter for each station and for each type of structural feature. These values were summed to yield a relative deformation intensity value for each station.

Oriented samples representative of the different types of protoliths and each type of fault rock were collected along four traverses spanning the western half of the fault zone where it was exposed above water level, and at some distance from the fault to determine the petrology of the protoliths relative to that of the fault rocks. Thin sections were cut in the horizontal plane, except in rocks with a strong LS fabric. The latter sections were cut perpendicular to the foliation and parallel to the lineation.

The intensity of microfractures in 20 of these samples, from 4 ordered traverses across the peninsula and into the surrounding region, were determined following the methods outlined by Wilson et al. (2003). In each section microfractures were counted in 30 to 50 quartz grains having a minimum dimension of 0.75 mm so as to target primary quartz grains versus fault-related neoblasts. Along a traverse the count line was oriented randomly at each grain and moved to span the greatest possible dimension within the grain. Data were recorded as counts per millimeter line length and the value for traverses within a sample were averaged to provide an intensity value. Microfractures were classified as open, healed, sealed, or recrystallized. Open fractures are those filled by epoxy with no indication of mineralization within the fracture or along the fracture edges. Healed fractures are defined as those that display bubble trains. Sealed fractures are those displaying any mineral-fill along the fracture surfaces; these usually were sealed along their entire length, but some also contained epoxy.

Thin sections used for mineral point counts were stained with barium chloride and rhodizonate for plagioclase identification, and with sodium cobaltinitrite for potassium feldspar identification (Bailey, 1960). Optical microscopy was used to determine mineral composition and secondary alteration as a function of position and relation to mesoscale alteration intensity. Point counts were completed on 21 samples (200 grains per section) taken from 4 traverses along the peninsula and on the 3 representative samples of the protolith; these data were compared to that of Ross (1987). Neo-crystalline plagioclase and primary plagioclase, and white micas and chlorite were not differentiated. EDS and WDS microprobe analyses were used to determine

major, minor, and trace element mineral composition of the fault rocks and mineral alteration fringes. Operating conditions for these analyses were 15 kV voltage, 10 nA current and 10 μm beam diameter for large grains and 3-5 μm beam diameter for finer-grains.

MACROSCOPIC STRUCTURE AND ALTERATION WITHIN THE FAULT ZONE

Macroscopic Structure

At Engineer Point the Kern Canyon fault zone is a broad zone of fractured, sheared and altered rock bounding a narrow zone of phyllonite and mylonite (Figs. 2 and 4), recording a ductile phase of faulting, and a linear zone of cataclastic rocks, that records a later phase of brittle faulting. At the southern end of the peninsula, the phyllonite zone trends N40E, is to the west of and spatially separate from the cataclasitic zone, and is relatively undisturbed by brittle faulting. To the north, the two zones converge (Fig. 3a) and the phyllonite is faulted-out for a short distance. Where the phyllonite zone reappears it is on the western side and roughly parallels or is caught-up within the cataclastic zone for a distance of several hundred meters. At water levels in the reservoir of about 785 m part of the cataclastic zone is offshore, particularly at the northern end of the peninsula, and the mylonite/phyllonite zone defines the shoreline on the east side of the peninsula. The mylonite is cut by thin (~1 mm wide) quartz veins and a single large, foliation-parallel quartz vein that is approximately 1 m wide and extends for ~100 m. Offset along the phyllonite zone of the contact between the Cretacous Waggy Flat and Alta Sierra granodiorites, and of acidic dikes at the southern end of the peninsula suggests that this zone experienced approximately 175 m of right-lateral separation (Fig. 7).

The cataclastic zone strikes N23E along the eastern edge of the peninsula and contains gouge, cataclasite, foliated cataclasite, and anastomozing zones of concentrated shear bordering slices of less deformed rock. The eastern portion of the cataclastic zone often is submerged under water. Fault-bounded slices of exotic rocks, including limestone (Treasher, 1948) and metavolcanics (between stations K38 and K48) are present within the cataclastic zone. These units probably correlate with the Fairview metasedimentary/metavolcanic units mapped on the west side of the fault by Ross (1986). Based on locations of outcropping Fairview pendant rocks (found 3 km to the north on the west side of the fault and 5 km to the south on the east side of the fault), Ross (1986) interpreted that the cataclasitc zone of the Kern Canyon fault experienced 8 km of right-lateral, strike-slip displacement.

Three igneous units are cut by the Kern Canyon fault in the immediate vicinity of Engineer Point (Ross, 1986). The Wagy Flat Granodiorite (Kwf), Alta Sierra Granodiorite (Kas), and Kern River Granite (Kkr) (Fig. 2, Tables 1 and 2). All are small plutonic bodies formed within the Sierra Nevada batholith and emplaced no later than the Late Cretaceous (Ross, 1990).

Wagy Flat granodiorite (Kwf) is the primary protolith outcropping on Engineer Point, covering all but the southern end of the peninsula. It is a medium-grained granodiorite consisting of plagioclase, quartz, biotite, potassium feldspar, and minor hornblende (Table 1; Ross, 1987, 1990). Radiometric dates are not available for the Wagy Flat granodiorite. The Alta Sierra (Kas) granodiorite and the Kern River granite (Kkr) are Late Cretaceous in age (Table 2; Evernden and Kistler, 1970). The Alta Sierra, which outcrops in the extreme southwestern portion of the study area, is compositionally similar to the Wagy Flat but is finer-grained with coarser biotite crystals (Table 1; Ross, 1987, 1990); it intrudes the Wagy Flat locally (Ross, 1990). The Kern River granite (Kkr) outcrops on the east side of Isabella Lake approximately 1

km to the east of the study area (Ross, 1990). The Kkr is also present on the western side of the fault between 7 and 15 km north of the study area, consistent with the 13 to 15 km right-lateral slip observed at other locations along this segment (Ross, 1986).

Petrology and Distribution of Alteration

A visual estimate of the volume percentage of rock outcropping on the peninsula that is noticeably discolored by alteration at the outcrop scale is represented by a qualitative mesoscale alteration intensity index (Fig. 3a). Alteration increases with proximity to both the cataclastic and phyllonite zones; it is moderate (25-75% of rock appears altered) across most of the peninsula but it approaches 100% near and within the cataclastic and phyllonite zones. Local increases occur around subsidiary faults and joints where altered zones range from cm to dm in width.

Petrologic data (Table 3, Fig. 3b) for samples collected at Engineer Point, including a representative, relatively unaltered protolith (K26A, Fig. 4), and data from Ross (1987, 1990) for more regional samples, were grouped and analyzed in two ways with respect to the alteration categories (Table 4). In the first analysis, samples are grouped by the overall mesoscale alteration index assigned to the sampled region. The petrologic data of all samples within a particular zone were averaged to obtain a representative petrology for each mesoscale alteration zone (Table 4 and Fig. 5a). However, since alteration intensity is not homogenous at the mesoscale, and some hand samples display a greater or lesser degree of alteration than shown on the map (Fig. 3a) the second analysis is based on a visual alteration index assigned to the hand sample, which shifts some samples into a new alteration category (Table 4; Fig. 5b).

The group of samples with the lowest alteration index (0-25%) are further subdivided into (1) representative of "unaltered" protolith, sampled off peninsula, and (2) those from the peninsula. The unaltered Kwf protolith modal composition is taken as an average of 59 samples: K26A from this study (Fig. 4) and 58 samples from Ross (1987, 1990). Regional sampling indicates that the distribution of potassium feldspar is heterogeneous across the Kwf pluton. Of the 58 samples, 20 have less than 6% potassium feldspar, and 3 samples have greater than 21% potassium feldspar. Potassium feldspar ranges from 0% to 30%, with a mean of 9% and a standard deviation of 6% (Neal, 2004; Ross, 1987, 1990). Review of Ross's (1987, 1990) data indicates that an increase in potassium feldspar tends to be associated with a decrease in plagioclase and biotite.

With respect to the mesoscale grouping, K36A represents the lowest alteration level. This sample is characterized by a relatively high potassium feldspar content (24%). All potassium feldspar observed is igneous in nature. Sample K12A also has a relatively high potassium feldspar content (13%). Even a heavily altered sample on Engineer Point (K113E), in which potassium feldspar is partly altered, reflects a higher than average potassium feldspar content. These observations suggest that the Kwf exposed along the peninsula is located within a region of the intrusion characterized by high potassium feldspar content (Table 3). An average of the 3 regional samples with the greatest potassium feldspar content ($\geq$ 22%) is included to represent an average protolith composition for the peninsula that is consistent with the samples described above (Figs. 8a and 8b). The visual characterization of increasing alteration at the hand sample scale is consistent with a progression in alteration noted at the microscopic scale (Table 4, Figs 8a and 8b). The mineralogy of samples in the lowest alteration zone is similar to an average protolith with a high potassium feldspar content. In general, white mica/chlorite, quartz, calcite,

and opaque mineral percentages increase with alteration index, whereas plagioclase, potassium feldspar, and biotite decrease.

Of the minerals that increase in quantity with increasing alteration, the greatest increase is in the white mica/chlorite category (Table 4, Fig. 5b). White mica/chlorite content increases from 0% in the "unaltered" protolith to 24% within the 75-100% alteration zone. This increase is most dramatic between the 50-75% (10%) and the 75-100% (24%) zones. Quartz increases from 23% in the protolith to 32% within the highest alteration zone. Calcite increases from 0% to 5%, and opaque minerals increase from 1% to 7% (Fig. 5b). Of the minerals that decrease in quantity with increasing alteration, the change in plagioclase is most notable (Table 4, Fig. 5b). Plagioclase drops from an average of 54% in the protolith to 23%, with a sharp decrease from 35% in the 50-75% alteration zone. Potassium feldspar drops to 5% in the most altered zone, and biotite decreases somewhat irregularly from 10% in the protolith to 4% when most altered in the 75-100% alteration zone, with a spike to 10% in the intermediate (50-75%) zone.

Representative alteration at the outcrop scale was mapped at station K13 (Figs. 9 and 10). Alteration rinds occur along primary- and cross-joint-sets to form a blocky character in outcrop typical of the mesoscale heterogeneity within the 50-75% altered zone (Figs. 4, 9 and 10). A progressive increase in alteration intensity towards fracture faces is displayed and alteration at the hand-sample-scale ranges from 0% within the centers of blocks up to 100% within the rinds (Fig. 3a). Average fracture spacing at this location is less than 1 m (Fig. 9). Within an alteration rind, the altered rock grades first into a dark gray, then into an orange-hue, and with further alteration, into gray-white. Rock within the orange region often is more resistant than surrounding rock of greater or lesser degree of alteration. The most intensely altered rock has a chalky, friable texture. In some blocks, alteration rinds extend to the interiors. Few fractures are open; most are filled with calcite, and a few (<5%) with quartz. No shear parallel to the fracture walls is visible at the outcrop scale. Calcite fill is usually less than 5 mm thick but can be up to 3 cm. Quartz veins tend to be wider, ranging from 3 to 5 cm in width. One vein contains both quartz and calcite fill distributed in layers parallel to the vein margin. All veins and nearly all fractures have alteration rinds around them. There does not appear to be any correlation between the extent or width of alteration rinds and the mineralogy or width of fracture fill. Modal analysis of rinds (e.g., from sample K13F) representative of the 50-75% alteration zone suggests that only minor petrologic changes are associated with the local alteration relative to the modal composition of the K26A protolith sample (Table 3). The rind has 3% more white mica/chlorite counts than the Kwf protolith (Table 3).

Alteration and Mesoscale Fractures

The spacing, length, width, and alteration of fractures are plotted according to the alteration index at the location where the data were collected (Fig. 3a) and averaged by alteration zone (Table 5, Fig. 6). These data represent only a small percentage of all fractures, as only those fractures belonging to the one or two dominant fracture sets at each station are described; minor fractures are not considered. The dominant fracture set at each station is the set with greatest fracture length. Within the 75-100% alteration zone, fracturing and alteration are so intense that fracture sets are difficult to discern. Consequently, data from within the most altered zone may be less accurate than data from less altered zones. Too few data were collected within the 25-50% alteration zone to be statistically reliable at this point (Table 5).

Average apparent fracture length decreases steadily from 5 m in the least altered zone to 3.1 m in the most altered zone. The decrease in fracture length reflects the increase in fracture intensity, as fractures are truncated by increasingly dense cross-cutting sets. Vein width does not appear to be tied to alteration intensity; veins are narrow within the most and least altered zones but broaden within the intermediate alteration zones (25-75%). As alteration increases, spacing between fractures decreases significantly (Table 5, Fig. 6). In the least altered zone, spacing between fractures in the major fracture sets is approximately 1 m. This is reduced to 0.4 m in the 50-75% alteration zone and to 0.2 m in the 75-100% alteration zone. The average width of alteration halos increases dramatically within the most altered zone (Table 5, Fig. 6). The combined effect of decreasing fracture spacing and broadening halos with increased alteration effectively reduces the amount of unaltered rock within each fracture-bounded block and accounts for the changes in mesoscale alteration intensity visible on the alteration map.

Orientation and Intensity of Regional and Fault-Related Fractures

The regional fracture fabric is characterized by two steeply dipping joint sets that strike approximately N05E and N60W (Fig. 8a). In contrast to this regional pattern, the fractures at Engineer Point display a strong preferred orientation characterized by steeply dipping fractures striking N60E superposed over a weaker set that reflects the regional fracture fabric (Fig. 8b). Fractures filled with quartz and calcite display two diffuse sets, a fault-parallel set and a set that is oriented at approximately 45° to the Kern Canyon fault (Fig. 8c).

Three traverses across the peninsula are used to characterize mesoscale damage intensity (Fig. 3a). Traverse A originates within a yellow-brown clay (probably a hematite-rich gouge) of indeterminate protolith. Granodiorite surrounding the gouge is heavily fractured, cut by veins, and covered with patchy caliche. It contains pods of less deformed granodiorite, which appear to be Kwf. Granodiorite is exposed to the east of the traverse starting point for at least several meters, beyond which it is covered by sand. Traverse B begins at the midpoint of a 3 m wide zone of extremely fractured rock. West of this region is a resistant zone of mylonite cutting Kwf protolith. East of the Traverse B starting point are: 1) 1.5 m of crushed rock, 2) several meters of sand cover, 3) an outcrop of volcanic or metavolcanic rock (station K38) with partial sand cover which extends to the waterline. Traverse C begins within heavily fractured rock in which fractures bound pods of hydrothermally altered Kwf. A zone of clay gouge is offshore at this location but comes onshore a short distance to the south, near station K49.

Although locally variable in width and deformation intensity, the rock exposed on the peninsula generally displays an ordered progression of mesoscale structures recording an increase in deformation intensity towards the brittle fault (Fig. 9). Regional damage intensity is in the range of 10 to 20 fractures per meter. Between ~500 meters and 15 meters from the fault, deformation intensity steadily increases approximately 50 fractures per meter. At approximately 15 meters from the brittle fault, fracture intensities range from 150 to 300 fractures per meter and even greater in regions too intensely fractured and sheared to be quantified at the mesoscopic scale.

Phyllonite Zone

To determine the composition of the phyllonite, samples were collected along four traverses on the west side of the Kern Canyon fault at Engineer Point (Fig. 3b). The southern traverse

begins within the phyllonite zone; the south-central traverse originates in a highly fractured granodiorite of indeterminate protolith that is 3 m to the east of a set of small hematite gouge surfaces; the north-central traverse begins within heavily fractured Kwf, ~6 m west of the cataclastic zone; the northernmost traverse begins within fractured mylonite, ~18 m to the west of the estimated location of the western boundary of the cataclastic zone (submerged offshore during this study).

The phyllonite is darker in color and finer in grain size than the surrounding rock. It consists of a quartz-dominated matrix, relict quartz and feldspar augen, mica fish, and microscopic shear zones of chlorite, muscovite, and phengite (Table 3). Accessory minerals identified through qualitative EDS microprobe analyses include apatite, calcite, ilmenite, limonite, magnetite, monazite, rutile, sphene, tourmaline, and zircon. The proto-phyllonite bordering the phyllonite zone is characterized by a reduction in grain size for quartz and feldspar, from that of the protolith, development of a mica-rich matrix, and the inception of through-going mica-rich, microscopic shear zones. The center of the phyllonite zone contains well-developed, fine-grained, mica-rich shear zones that separate regions of coarser grained augen and mica fish. The phyllonite matrix is dominated by quartz but also contains feldspar, white mica, and chlorite. Minerals within the matrix are recrystallized, as indicated by their very fine grain size, lack of undulatory extinction, grain shape, and lack of microfractures.

Within the altered rock bounding the phyllonite, three spatial domains defined at the microscale by the distribution of petrologic alteration and shear strain magnitude display distinct chemical reaction products and deformation characteristics. Within these domains, there is a progression of alteration towards the phyllonite. Preliminary quantitative microprobe analyses of the outermost domain show that this zone is characterized, in part, by the pseudomorphic replacement reactions of anorthite to albite (An02-00) + muscovite + calcite; biotite to vermiculite, and sphene to rutile + quartz. In the higher-strained domains, vermiculite has altered to chlorite, potassium feldspar has altered to sericite + plagioclase + quartz, and albite has altered to sericite + quartz. Consequently, white mica/chlorite, less than 2% of the protolith, together comprise at least 30% of rock volume within the phyllonite zone (Fig. 10d). Microscopic zones of phyllosilicates appear along albite-albite grain boundaries and along boundaries between different phases. These zones are composed of phengitic mica and display strong lattice preferred orientation and well-developed mica contiguity. An additional domain displays an increasing degree of phyllonite development and increasing deformation, sealing, recrystallization of quartz (Fig. 10b), and consumption of feldspars, with total feldspar counts plummeting to 50% or less of regional values (Fig. 10c).

Fabric and Kinematics. The phyllonite zone is on the order of 10 m wide with gradational deformation boundaries. S-C' fabric, reduced grain size and darker rock color were used to define the boundaries. The average orientation and sense of shear were determined for each foliation surface (C, C', and S) (Fig. 11). Phyllonite foliation (S) averages N4W to N13E and is near vertical (Fig. 11). The nearly vertical intersection of surfaces and the asymmetry are consistent with right-lateral shear. S-C' fabric intensity and orientation varies within and across the phyllonite zone. The acute angle between the S and C' surfaces is greatest and the fabric weakest at the boundaries of the zone; fabric strengthens and the angle narrows within the center of the zone. This is consistent with an increase in shear strain inward (Goodwin and Wenk, 1995). Increasing shear strain is also associated with decreased porphyroclast grain size and number and decreased spacing between C surfaces.

Microstructures and Deformation Mechanisms. Quartz and feldspar augen within the phyllonite are fractured, display undulose extinction, and are extensively recrystallized. Some quartz grains are recrystallized along microfractures and subgrain boundaries, and dissolution fringes are present along quartz grain boundaries. Augen are elongate and asymmetric, and a fluxion structure exists in the matrix surrounding many augen. Both mica fish and asymmetric pressure shadows around augen in the phyllonite are sigma-type porphyroclasts (Simpson and Schmid, 1983) and imply right lateral shear consistent with the S-C' fabric.

Healed and sealed microfractures are common within the phyllonite zone (Table 6). Some bubble trains show discoloration indicative of mineralization along the fracture surface; this suggests that some healed microfractures may have been sealed prior to healing. Within the center of the phyllonite zone, many fractures are recrystallized (Fig. 10b); the drop in healed fracture counts within the center of the phyllonite suggests that recrystallization eradicated pre-existing healed microfractures and that recrystallization may have been contemporaneous with healing and occurred preferentially within the phyllonite (Table 6, Fig. 10b). Total microfracture intensities increase towards the phyllonite zone from a minimum observed value of ~6 microfractures per mm at a distance of 700 m for the Kas protolith (K25A) and 950 m for the Kwf protolith (Fig. 12); however, this broad trend of increased healed microfracture intensity may reflect healing that occurred after phyllonite faulting rather than prior to or during phyllonite faulting. In the regional protolith samples, approximately 40% of the microfractures are open, 50% are healed, and the remaining 10% are sealed (Table 6, Fig. 12). Few open microfractures are observed within the center of the phyllonite zone (Fig. 10a).

Cataclastic Zone

The rock within the cataclastic zone is composed of extensively fractured Kwf and Kas granodiorite, phyllonite, secondary alteration products, and vein minerals. Three distinct classes of fault rocks are present within the cataclastic zone: 1) a cohesive hematite gouge, 2) a foliated cataclasite, and 3) slivers of exotic rocks bounded by zones of shear. Narrow hematite gouge zones are noted at and along the western boundary of the fault zone. The cohesive hematite gouge is dark brown and consolidated, yet friable, ranges in width from one to several centimeters, is laminated internally having dark brown laminae 1-3 mm in width separating zones of lighter brown matrix, and is lined with thin layers of hematite-cement. It is present intermittently within the highly fractured Kwf, west of the cataclastic zone, particularly between stations K20 and K24 (Fig.3a). At station K20, the hematite gouge zone is approximately 20 m west of the western fractured rock/foliated cataclasite boundary of the cataclastic fault. Hematite gouge segments typically are less than 10 m in length. The intermittent presence of the hematite gouge, its discontinuous character at the outcrop-scale, and the lack of visible offset of either igneous units or the main shear zone suggest that it represents late-stage, minor faulting which overprints the earlier-formed cataclastic zone. Gouge orientations are variable; orientations of measured surfaces include N28E, 41NW, rake 45SW; N64E, 15NW, rake 12SW; and N45E, 30NW.

A representative sample, (K20A) of the hematite gouge taken from a several cm-wide gouge zone consists of quartz-feldspar porphyroclasts of older cataclasites surrounded by extremely fine grained matrix. The porphyroclasts are composed of quartz, feldspar, and mica grains. Clasts often consist of more than one mineral, with fractured grains that are sutured along boundaries and often recrystallized. The matrix is extremely fine-grained. Microprobe imaging

of the sample reveals that this gouge is zoned, with regions of varying matrix, texture and composition.

An incohesive, chalky, foliated cataclasite also was noted at several stations (K48, K49, and K113). The foliated cataclasite is variable in color along strike, ranging from green and blue-gray to orange and maroon. It outcrops in zones up to 1 meter wide with irregular boundaries defined by distinct variations in texture and color between the gouge and surrounding cataclastic rock.

Internally, the unconsolidated gouge is heterogeneous, with irregular and undulatory contacts between regions of different color. Parent rocks for the foliated cataclasite have not been determined and could include multiple rock types transported and mixed along the fault. Possible parent rocks include the regional granodiorites (Kwf, Kas, Kkr), metasedimentary rocks, and metavolcanic rocks, as well as the phyllonite.

As described by Treasher (1948), a limestone sliver occurs within the fault zone at the auxiliary dam's western abutment. A wedge of gray to black volcanic or metavolcanic rock also outcrops within the fault zone intermittently showing through sand cover over a length of approximately 300 m between stations K38 and K48 (Fig.3a). The largest outcrop is 75 m long and 10 m high consisting of layered volcanic beds of varying composition (station K48, Fig. 5). The volcanic rocks rest in direct contact with and to the west of highly weathered granitic rock Within the volcanic sliver, the lowermost exposed rock is a friable, light gray, fine-grained tuff. Above it is a more thickly bedded, well-lithified, light gray welded tuff that is broken into blocks that are hexagonal in cross section. The blocks plunge 5° to 10° toward the shoreline. Internal bedding is visible within the welded tuff as variably shaded light gray bands; layers are up to a 30 cm thick and are oriented N32E 78NW to N36E 76NW. Pervasive vesicles of 1-3 mm length and 0.5 mm width form a layer-parallel texture; some vesicles are filled by a fine-grained crystalline mineral (probably quartz), especially near the upper portion of the outcrop. The welded tuff is up to 9 m thick and is capped by an extremely fine-grained black rock of ~0.5 m thickness. The black rock is glassy in texture in some areas and dull black to gray in others; it may be an altered or metamorphosed obsidian. The black volcanic rock has trails of fine, layer-parallel vesicles similar to those of the welded tuff. In the western quarter of the mapped region (Fig. 5), the welded tuff is capped by a light-colored ash-breccia consisting of numerous angular clasts. It appears to be volcanic breccia, however its position beside the foliated cataclasite suggests that it may be a fault breccia instead. The volcanic sliver is bounded on its upper surface by a foliated cataclasite 3 to 5 m in width that is usually sand-covered. West of the sand cover, there is a 9 m wide zone of heavily fractured Kwf mylonite. The fractured rock consists of multiple anastomozing bands of rust-colored gouge interspersed with a light gray, highly brecciated mylonite which grades westward into progressively less fractured mylonite.

Primary minerals within the cataclastic zone include quartz, plagioclase, potassium feldspar, biotite, hornblende, sphene, and accessory minerals (Table 3). Optically identifiable alteration products of these minerals include chlorite, white mica, calcite, new grains of quartz, new grains of plagioclase, and opaque minerals. Near the cataclastic zone, biotite frequently is altered to white mica, chlorite, and quartz; the reaction products either pseudomorphically replace the biotite (e.g., chlorite) or form within (001) cleavage separations within biotite grains. Plagioclase grains are heavily sericitized within 50 to 100 m of the cataclastic zone (Fig. 13b). White micas and chlorite produced by the phyllonite sericitization of feldspars increase from 2% in the protolith to 33% near the cataclastic zone (Table 3, Fig. 13b). Sericitization of plagioclase is also observed to increase locally within altered zones surrounding subsidiary fractures. A

sample collected from within an altered zone bounding a fracture at station K12 (K12B in Table 3) was compared to one collected from within a nearby unaltered block (K12A in Table 3). Comparison of these samples shows increased white mica/chlorite content and decreased plagioclase content (Table 3); this suggests that plagioclase sericitization was ongoing during cataclastic faulting.

In addition to the deformation-related sericitization of feldspars, feldspar grains also exhibit evidence of brittle deformation. Fractures are commonly seen in feldspar grains that have limited sericite development. With further fracturing, sericite appears to occur in close association with the microfractures. This suggests that the microfractures may have aided in the progression of sericitization by providing a fluid conduit and/or formed preferentially in regions of the grain already weakened by sericite development.

Quartz and calcite veins are common, and veins with thicknesses of up to several decimeters are present near the cataclastic fault. Quartz is localized in large, decimeter to meter scale veins within or near the cataclastic zone. Calcite occurs in centimeter to decimeter scale veins but also is present as microfracture fill and as dispersed, grain-scale cement. Individual veins often have many layers of mineralization precipitated parallel to the fracture surface; cathodoluminescence indicates multiple generations of calcite in veins and vugs. Some microveins are partially filled. Veins and cataclastic shears are mutually cross-cutting; calcite veins always postdate quartz veins.

Fracture Fabric of Cataclasitc Zone. Fabric data representing 69 subsidiary faults and 47 veins were collected on the east side of Engineer Point (Figs. 14a and b). Within the cataclastic zone, the veins and narrow zones of localized right-lateral shear are steeply-dipping to vertical and have a preferred NE strike forming acute angles with the main cataclastic zone (Figs.14a and b). Both right-lateral and left-lateral subsidiary faults exist; right-lateral subsidiary faults are much more abundant than left-lateral faults. The average orientation of right-lateral faults is N45E. Left lateral faults average S62E, and veins average N65E.

The right and left-lateral faults form a quasi-conjugate set (Fig. 14a); its bisector is oriented N82E, which is approximately 60° from the cataclastic zone. Additionally, the average vein orientation is N65E (Fig. 14b); which approximately bisects the quasi-conjugate fault set. The near-vertical intersection of the average orientations of the right-lateral and left-lateral faults (Fig. 14a) with the average vein orientation (Fig. 14b) is indicative of strike-slip displacement. Combined, the shear indicators suggest right-lateral strike-slip separation along the cataclastic zone. Right-lateral subsidiary faulting within the Kern Canyon cataclastic zone at 24° from the main fault is consistent with R-shears of a Riedel array (1929). Left-lateral shear zones are, on average, 98° from the main fault; their orientation and antithetic displacement are consistent with R'-shears. Yet the angles measured between the subsidiary shears and the cataclastic zone are wider than are typical of Riedel arrays.

Overprinting of the Phyllonite Zone. The phyllonite zone is cut by the brittle fault in the central portion of the study area; therefore, it is possible to follow the phyllonite northward from the southern end of the study area and observe the progressive effects associated with cataclastic overprinting. Two grid maps at a scale of 1:12 were constructed at stations K4 and K19 in the region where the two faults intersect to illustrate the outcrop-scale character of overprinting. This region consists of extensively fractured phyllonite and proto-phyllonite. The resulting rock consists of fractured and rotated chunks of phyllonite in which the crystal plastic microstructures (e.g., the S-C' fabric, mica fish, and ductily-deformed augen) are overprinted by brittle microstructures. Brittle deformation of the phyllonite is progressive from the edge of the

cataclastic zone, beginning with a phyllonite proto-breccia progressing to a breccia and finally a gouge. Ribbons of gouge locally cross-cut the brecciated phyllonite, and the gouge orientation is roughly parallel to the phyllonite S foliation, suggesting that at outcrop scale, the phyllonite foliation influences late-stage localization of slip. Within the study area, the two zones are not coincident for any great distance; the phyllonite tends to intersect the cataclastic zone at a low angle and is intermittently faulted out in the central portion of the study area (Fig.3a).

Microstructures. Near the cataclastic zone, biotite grains are kinked and sheared. Quartz grains show strong undulatory extinction. Within the most intensely sheared samples, relict quartz and feldspar grains are crushed and rotated, and narrow zones of microbreccia and gouge are common in thin section. Few open microfractures are observed near the cataclastic zone; most fractures are sealed or healed (North Central and South Central traverses, Table 6). Healed fractures increase toward the cataclastic zone (Fig. 12). Sealed fractures increase slightly toward the cataclastic zone (Fig. 12). Calcite and iron-rich minerals (limonite, hematite) are the dominant microfracture seals near the cataclastic zone (Table 6). Twinned calcite occurs within sealed microfractures and vugs in many samples near the cataclastic zone, and the frequency of calcite-filled microfractures increases toward the cataclastic zone (Table 6). Calcite-sealed microfractures account for 50% of all sealed fractures at station K113C at 6 m from the cataclastic zone while calcite-sealed microfractures are absent in protolith samples (Table 6).

Coincident with and likely due to the increase in calcite and iron-oxide/hydride microfracture fill, the intensity of open microfractures decreases steadily from regional values (2.2 microfractures per mm) toward the cataclastic zone (Fig. 10d, Table 6). Within 100 m of the cataclastic zone, nearly all open microfractures have been mineral-filled. At station K113C, the nearest sample to the cataclastic zone at a distance of 6 m, no open fractures exist; all have been mineral sealed (Fig. 10d, Table 6).

DISCUSSION

Relative Timing of Deformation

Thermochronometry has been used in the central Sierra Nevada to describe the uplift and exhumation history of the range from emplacement through the Cenozoic (House et al., 1997). House et al (1997) propose a model in which the Sierra Nevada experienced initial, rapid magmatic cooling after emplacement at ~80-100 Ma followed by a period of relatively stable temperatures in the range of ~62-46°C from ~60 to ~15 Ma. At ~15 Ma, uplift and westward tilting of the Sierran range resulted in rapid cooling to a present-day geothermal gradient of ~13.8°C/km (House et al., 1997). This implies that the batholith underwent two major phases of cooling (ca 80-100 Ma and ca 15 Ma) as well as at least one major stage of uplift/exhumation beginning ~15 Ma.

Thermal stresses probably would have been generated during both stages of cooling reported in House et al. (1997), and both stages could have generated in cooling joints and microfractures (e.g., Kranz, 1983). Uplift and exhumation of the Sierran block beginning at ~15 Ma also potentially contributed to the development of stress-release regional joints and microfractures (e.g., Wang and Simmons, 1978). These events would have contributed to the formation of micrfractures over a regional scale and suggests that the relatively low intensity (~6 total mf/mm) of open, healed, and sealed microfractures is present at a distance of approximately 1

km from the Kern Canyon fault (Fig. 12) may represent the background, regional microfracture intensity.

Healed microfracture intensities drop within the phyllonite (Fig. 10a) while recrystallization along microfractures increases by the same magnitude (Fig. 10b). The timing and nature of the formation of the pre-existing microfractures has not yet been established. They could have been open microfractures created by batholithic cooling that pre-dated the phyllonite fault or they could have formed, and perhaps healed, contemporaneously with phyllonite formation.

The distribution of microfractures within quartz grains around the cataclastic zone (Fig. 12) suggests that many microfractures formed in association with cataclastic faulting. The rise in healed microfracture intensities toward the cataclastic fault (Fig. 12) suggests that open microfractures were created in the region surrounding the fault which were then healed. Similarly, a slight rise in sealed microfractures toward the fault (Fig. 12) suggests that open fractures were created and then sealed with increasing frequency toward the cataclastic zone. The decrease in open microfracture intensities within quartz grains, as the cataclastic fault is approached (Fig. 12 and 13d) indicates that very few open microfractures persisted near the cataclastic fault, as they were healed or sealed. Offset sealed veins indicate that numerous fluid rock reactions occurred at this depth during the phyllonite phase of faulting. Experimental work by Brantley et al. (1990) suggests that open microfractures in quartz in a stagnant fluid at lithostatic pressure have predicted healing times of 4 hours at 600°C and 30 days to 90 years at 200°C. Thus, healing along the cataclastic zone could have been geologically rapid so that open microfractures did not persist for long near the fault. The open fractures that remain, might then be attributed to shallower phases of displacement along the fault or exhumation.

Mesoscale fracturing is ubiquitous in the Sierra Nevada and has been described by several workers studying areas north of Engineer Point (e.g., Lockwood and Moore, 1979; Segall and Pollard, 1983; Martel, 1990). Lockwood and Moore (1979) examined regional lineaments and conjugate strike-slip faults and concluded that throughout the eastern Sierra Nevada there was pervasive deformation along narrow, subvertical zones of joints and shears, and along crush zones of unknown displacement (lineaments). The average orientation of lineaments changes from approximately N24E in the northern Sierra Nevada to N61E near Mount Whitney, ~145 km north of the present study area. The microfaults tend to occur in conjugate sets and record both right- and left-lateral offset. They attributed the microfaulting to Late Cenozoic Basin and Range extension which they hypothesized allowed the Sierran block to extend in the direction of N61W by up to 2.3%. Left-lateral microfaults change orientaion from approximately N30E to N60-70E from the central to the southern portions of the region studied. Right-lateral faults change similarly, averaging ~N25W in the central portion of the region to N20-40E in the southern portion. In the Mount Whitney quadrangle, the two southernmost stations nearest to the Kern Canyon fault lineament average N26E for right-lateral faults and N60E for left-lateral faults (Lockwood and Moore, 1979). Lockwood and Moore (1979) note that the Kern Canyon fault is sub-parallel to the dominant right-lateral microfault set in the southern portion of their study area.

The subsidiary fault fabric recorded near the cataclastic zone (Fig. 14) in the present study shows that right-lateral faults strike N45E while left-lateral faults strike S62E. If these small faults are comparable to the microfaults observed by Lockwood and Moore (1979), it suggests a continued progression of clockwise rotation of microfaults southward along the Kern Canyon fault. The fracture fabric measured within the present study area (Fig. 8b) appears to be superposed over a weaker regional fracture fabric (Fig. 8a). The spatial distribution (Fig. 9) and

orientation (Fig. 14) of mesoscale fractures surrounding the cataclastic zone suggest a genetic relationship to the cataclastic fault; therefore, mesoscale fracturing must largely post-date the phyllonite. Furthermore, the fact that the fractures on the peninsula frequently are surrounded by alteration (Fig. 6, Table 5) implies that the heterogeneous mesoscale alteration surrounding the fault-related fractures also post-dates the phyllonite and fluid-rock reactions associated with the shallower cataclastic phase.

Deformation Conditions

New grains of chlorite and white mica that are aligned with the foliation of the phyllonite indicate syntectonic mineralization. The mineral assemblage present (chlorite + muscovite + albite) in the phyllonite shear zone reflects lower-greenschist grade conditions during faulting (Yardley, 1994). The relation of the lower-greenschist grade phyllonitic ductile shearing at Engineer Point to the medium to high-grade ductile shearing (Saleeby and Busby, 1993) along the Proto-Kern Canyon fault zone (PKCFZ) is uncertain. The phyllonite zone may be a distant, minor subsidiary shear zone contemporaneous with proto-Kern Canyon fault zone fault slip of as early as ~85 Ma, or the phyllonite zone may represent a shearing event that postdates the PKCFZ yet predates the Cenozoic faulting. Phyllonite foliation data observed in this study (Fig. 11) are similar to the foliations reported for the PKCFZ further to the north (Busby-Spera and Saleeby, 1990); this suggests a genetic relationship between the phyllonite zone and the PKCFZ. Geochronological work will be required to resolve timing of the ductile shear zones.

Rates of uplift and exhumation are available for the southern Sierras (Chase and Wallace, 1988; House et al., 1997). Deformation mechanisms and mineral reactions provide some insight about conditions during faulting. The lower greenschist-grade mineral assemblage within the phyllonite zone suggests temperatures of 350 to 400° C (Yardley, 1994). Phyllonite deformation mechanisms include crystal plastic flow accompanied by dynamic recrystallization and minor cataclasis, consistent with Sibson's (1983) fault model suggesting phyllonite deformation temperatures of ~300-350° C and pressures of ~3-4 kb. These conditions would be present at perhaps 10-13 km burial depth in quartzo-feldspathic crust of average thermal gradient (Sibson, 1983).

Temperatures along the Kern Canyon fault were elevated relative to those of Sibson's model (1983) during igneous emplacement along the Sierra Nevada; consequently, burial depth and pressure of phyllonite formation could be shallower than predicted by the model. However, starting at ~10 Ma, the geothermal gradient is thought to have been low and the lithospheric strength correspondingly high (Chase and Wallace, 1988). House et al. (1997) tie the low heat flow to batholithic cooling associated with uplift and tilting of the Sierras. The current average geothermal gradient in the central Sierra Nevada is 13.8°C/km (House et al., 1997). At some point after igneous emplacement, the high geothermal gradient associated with plutonism cooled sufficiently to produce an unusually low geothermal gradient. Determining the timing of the change in heat flow will be significant for determining deformation conditions along the fault.

Shear Zone Widths

The widths of the ductile and brittle shear zones depend upon the parameter measured (Schulz and Evans, 2000). In this study, different widths can be defined for both the brittle and

ductile shear zones based on petrologic data, microfracture intensities, and mesoscale fracture intensities.

Field observations show a sharp increase in alteration intensity to 75-100% at ~15 m from the center of the phyllonite zone that corresponds with the mapped boundary of proto-phyllonite rock texture. The proto-phyllonite zone consists of a narrow zone (10-15 m half-width) of sheared and altered rock with a well-defined S-C' fabric; the S-C' fabric, sericitization of feldspars, and recrystallization of microfractures is restricted to a 2 m-wide phyllonite zone in the center of the proto-phyllonite. This localization of alteration and microstructures suggests that nearly all of the fault's 175 m of displacement was confined to the phyllonite and proto-phyllonite rather than being distributed over a broader zone. Wintsch et al. (1995) argue that sericitization of feldspars is an effective reaction-weakening process. It seems plausible then that slip along the phyllonite zone was facilitated by sericitization reactions. Fault weakening processes during sericitization include shearing within ever more continuous mica bands (Kronenberg et al., 1990; Mares and Kronenberg, 1993; Wintsch et al., 1995) and syntectonic dissolution of feldspars and crystallization of quartz, feldspars, chlorite, and micas (Simpson, 1985). Microstructures suggestive of all of these processes are observed along the phyllonite zone within the study area. Thus, alteration reactions, mineral reorientation, and discontinuous dissolution-precipitation processes may have facilitated slip along the phyllonite zone.

The width of the cataclastic zone can be defined based on mesoscale fracture intensity (Fig. 9) and the distribution of mesoscale alteration on the peninsula (Fig.3a). Near the cataclastic zone, average mesoscale alteration intensity increases, and a threshold of 75-100% alteration is achieved at a distance of approximately 20 to 40 m from the cataclastic zone (Fig.3a). This zone of increased alteration extends along the length of the study area and varies in width. There is a broader zone of less altered rock that includes nearly all of the study area; this region extends at least 350 m from the western foliated cataclasite boundary of the cataclastic zone. The distribution of alteration around the cataclastic zone (Fig. 3a), and local perturbations around subsidiary faults and fractures (Fig. 3a) indicate that most macroscopically observed alteration is associated with the cataclastic fault rather than the phyllonite zone. The distribution of alteration across the peninsula (Fig. 3a) is particularly interesting. It shows reduced alteration of the rock in regions where the phyllonite zone is located between the cataclastic fault and the low-alteration host rock to the west, as at the northern and southern termini of the peninsula. This suggests that the phyllonite zone may have interrupted fluid access to the rock west of it.

Mesoscale fracture intensity defines a zone of increased fracturing and faulting relative to the protolith over a distance of ~500 m from the western foliated cataclasite boundary (Fig. 9). Within ~500 m zone, two additional zones can be defined: one in which fracture intensity rises to 50 fractures/m at about 15 m and another, interior zone in which fracture intensity abruptly rises to exceed measurable levels (Fig. 9). Microfractures show a similar pattern of gradually increasing intensity towards the cataclastic zone over a distance of at least 200 m (Fig. 12).

The presence of the phyllonite zone in close proximity to the cataclastic fault may have affected the mechanical properties of the cataclastic fault. Petrography of the phyllonite reveals high white mica and chlorite counts (Fig. 10) which are generally contiguous and oriented at low angles to the shear zone boundary. Shea and Kronenberg (1992) show that mica-rich rock is weaker than other common silicates at mid-crustal conditions; they infer that phyllosilicate-producing retrograde reactions may contribute to fault localization. Based on this, the later cataclastic fault might be expected to localize directly along the mica-rich phyllonite zone. However, field observations of phyllonite outcrops indicate that the phyllonite zone is apparently

resistant to erosion and tends to form a ridge that stands above the surrounding rock, as shown in Fig. 3a.

These observations are paradoxical; how can the phyllonite zone be both weak (with its extensive sericitization) and strong (by outcrop character)? Wibberly (1999) suggests that quartz released locally by feldspar sericitization may produce enough free quartz to locally cement and thus reaction-harden shear zones. Within the study area, an increase in quartz content occurs near the center of the phyllonite shear zone (Table 3), consistent with Wibberley's observations. If this is the case in the phyllonite, there may have been an initial stage of reaction weakening caused by sericitization of feldspars which facilitated slip followed by a later stage (perhaps following cessation of slip) of quartz precipitation which hardened the rock. An alternate explanation for the apparent relative strengthening of the phyllonite zone as compared to the rock surrounding it is that phyllonite zone weakness, because of phyllosilicate/chlorite enrichment, may have been transient, present only during high temperature and pressure crystal-plastic deformation. Relative strengthening of the center of the phyllonite zone could explain the tendency of the cataclastic zone to run along the eastern flank of the phyllonite (Fig. 3a) rather than to directly overprint it.

Fault Structure

The internal structure of the cataclastic zone is similar to that of other large-displacement faults (e.g., Wallace and Morris, 1986; Chester et al., 1993; Chester and Chester, 1998) in that it consists of a broad zone of faulted and fractured rock to the west of a relatively narrow zone of highly sheared and comminuted fault rocks. Chester and Logan (1986), introduce terminology to describe the structural zones of the Punchbowl fault, in which the broad region of faulted and fractured rock is the damage zone and the inner zone is the fault core. Recent work on the Punchbowl fault (Wilson et al., 2002) suggests that a damage zone may have internal layers. Preferred orientations of microfractures in an arkosic sandstone around the Punchbowl fault define several fabric domains within the damage zone: an inner damaged zone (IDZ) within 2.5 m of the fault core, a middle damaged zone between 2.5 and 14.2 m, and an outer damaged zone (ODZ) extending from 14.2 to ~100 m from the core. The cataclastic Kern Canyon fault appears to have a structure similar to that of other large-displacement faults. A zone of increased mesoscale fracture intensity ~500 m in half-width from the western foliated cataclasite boundary (Fig. 9) delimits the damage zone. The width of the cataclastic damaged zone (~500 m) is on the order of 10^{-2} of fault displacement (13-15 km). The cataclastic fault core is not well exposed, and its width is unknown. Mesoscale fracture intensities (Fig. 9) suggest that the damage zone has a three-part internal structure, including 1) a zone of extremely high fracture intensity within ~3 m of the core (>350 fractures/m), 2) a zone of less intense but still elevated intensity between 3 and 15 m, and 3) a zone of gradually diminishing intensity from 15 to ~500 m.

The phyllonite zone is similarly surrounded by a deformed and chemically altered zone extending approximately 10-15 m from the center of the phyllonite. The phyllonite zone half-width (10-15 m) is on the order of 10^{-1} of fault displacement (~175 m); this compares favorably with the thickness to displacement ratios observed by Hull (1998) for mylonite zones.

Fluids and Faulting

The alteration within and around the phyllonite zone clearly is associated with phyllonite-phase faulting (Fig. 10). The heterogeneous, mesoscale alteration that surrounds fractures in the cataclastic damage zone is associated with brittle-phase faulting; the altered zones surrounding fractures are marked by increased feldspar sericitization. Thus, sericitization of feldspars likely occurred during both the ductile and the brittle phases of faulting. It is known that the retrograde reactions responsible for the sericitization of feldspar require the presence of fluids (Wintsch et al., 1995; Wibberley, 1999). Therefore, we can infer that fluids probably were present during both phases of faulting.

Alteration occurs in some areas but not in others, suggesting that fluids might not have had access to certain regions or that fluids may have been in equilibrium with rocks in unaltered regions. In the northern and southern portions of the study area, the rock west of the phyllonite/mylonite zone appears to be less altered than rock in the central portion of the study area, where much of the phyllonite zone is faulted out. This alteration distribution suggests that the peninsula-wide, homogenous alteration (as shown in Fig. 3a) was associated with cataclastic faulting rather than phyllonite-phase faulting. Furthermore, it suggests that the phyllonite may act as an impermeable barrier to fluid flow, isolating the rock to its west from fluids along the cataclastic zone to the east.

The character of alteration observed on the peninsula appears to have changed through time. The earliest alteration may have been restricted to a zone as narrow as 15 m around the phyllonite zone. Later alteration associated with the cataclastic deformation is either broad and approximately homogenous across the peninsula (Fig. 3a) or highly heterogeneous and restricted to narrow zones around subsidiary fractures and faults. These observations suggest that there was a change in fluid-flow character through time; flow appears to have been fairly restricted during phyllonite faulting and more extensive during cataclastic faulting. The intersection of major, open fracture zones with the cataclastic zone may have provided permeability pathways for fluid movement along the fault plane.

Cross-cutting relations between veins and variations in vein mineralogy indicate that multiple generations of fluid of evolving chemistry were present within and around the Kern Canyon fault at Engineer Point; quartz precipitation always appears to have preceded calcite. Very fine quartz veins are present within the phyllonite. Wibberley (1997) shows that silica-rich fluid is generated on a local scale from the sericitization of feldspar. If Wibberley's observations (1997) are applicable to the phyllonite zone at Engineer Point, then the fine veins present within the phyllonite may indicate the presence of locally-sourced silicic fluids during phyllonite deformation.

Within the fractured rock west of the cataclastic zone, the presence of mutually cross-cutting veins and cataclastic shears indicates that fracture and cementation occurred syntectonically. Large and laterally extensive quartz veins are present near and within the cataclastic zone. Treasher (1948) observed a particularly large quartz vein at the site of the auxiliary dam; the size of the vein suggests significant syntectonic silica precipitation and suggests extensive fluid flow during cataclastic faulting.

Many veins have textures indicative of crack-seal vein precipitation. Crack-seal veins are thought to form by incremental precipitation of minerals (Sibson et al., 1975). Two theories for the origin of crack-seal vein textures are precipitation from the cyclic passage of fluid through a fault zone (e.g., seismic pumping; (Sibson et al., 1975)) or advective mass transport of fluid

present within a saturated fault zone (Etheridge et al., 1984). Either theory may explain the presence of apparently episodic calcite and quartz cementation within the cataclastic fault zone.

Quartz Volume

Quartz content remains relatively constant within the phyllonite zone, while feldspar content decreases and white mica/chlorite content increases (Fig. 10). While the cation compositions of the feldspars undergoing reactions are not end-members, nor are resulting phyllosilicate phases simple in composition, the general form of the sericitization reaction is:

$$3\ NaAlSi_3O_8 + K^+(aq) + 2\ H^+(aq) \rightarrow KAl_3Si_3O_{10}(OH)_2 + 6\ SiO_2 + 3\ Na^+(aq) \quad (1)$$

3 plagioclase — muscovite — 6 quartz

3(100.07 cm^3/mol) — (140.71 cm^3/mol) — 6(22.6 cm^3/mol)

For the albite end-member composition of (1), mass balance of the feldspar sericitization reaction indicates that for every 3 moles of plagioclase (300.2 g) consumed, 6 moles of quartz are produced (135.6 g). Volumetrically, for every 1% volume of feldspar altered in the rock, normalized by the total rock volume, 0.45% total rock volume of quartz is generated. Therefore, for the 18% rock volume of plagioclase feldspar altered within the phyllonite zone, there should be a corresponding 8% rise in quartz. However, the average observed quartz content rises by only 1-3% within the mylonite/phyllonite zone. While quartz does show a minor increase in volume within the phyllonite zone, the increase is not as much as expected from mass-balance calculations assuming a cloased system.

In addition to the sericitization of feldspar, there is evidence for several other quartz-producing reactions in association with the phyllonite zone: 1) potassium feldspar altering to muscovite + quartz and 2) biotite/vermiculite altering to chlorite + quartz. These quartz-producing reactions further compound the observed deficiency of quartz within the phyllonite zone. The observation of significant silica loss from the phyllonite, considering this deforming rock as a system, has important implications for 1) volumetric change within the fault zone, 2) whether the system is open or closed, and 3) advective fluid transport.

The hydration reactions of plagioclase and potassium feldspar result in volume loss (Wintsch et al., 1995). Plagioclase, volumetrically the most significant reaction, results in an 8% volume loss per volume plagioclase reacted if all of the quartz is precipitated locally and a 53% volume loss per volume plagioclase reacted if the quartz is removed aqueously (Wintsch et al., 1995). The nearly constant quartz content across the phyllonite zone (Fig. 10, Table 3) appears to indicate that nearly all of the quartz was removed aqueously. If we focus only on the plagioclase alteration and assume a 50% volume loss in plagioclase due to silica removal, then there would be a 9% decrease in total rock volume within the phyllonite zone (assuming altered feldspar accounts for 18% of the total rock volume within the phyllonite). The volume loss estimate could be refined by considering additional fluid-rock reactions, but the reaction progress and the smaller volumes of reaction make these modifications minor in comparison to the change in volume of reaction (1).

Thus, superposed on the simple shear documented by fabric development, the phyllonite underwent volumetric strain by reaction that would tend to relieve internally stored strains, promote local dilation, and allow further fluid infiltration. The much lower than expected quartz content within the phyllonite zone suggests that advective flow of fluids removed silica from the

zone, and that fluids entering the fault zone were under-saturated in silica. Given silica solubility relations, fluids under-saturated in silica with respect to quartz could 1) come from lower pressure regions, 2) come from lower temperature regions, and/or 3) be introduced in such large volumes relative to the rock volume that only small degrees of under-saturation lead to significant losses in silica from the phyllonite (Fyfe et al., 1978; Wintsch, personal comm.). If the Kern Canyon fault was an open system, with large volumes of fluid passing through during phyllonite faulting, it is likely that the system was a water-dominated. Water-dominated systems are defined as those in which water composition is largely unaffected by fluid-rock reaction (Wintsch et al., 1995). In granitic rock, water-dominated systems are characterized by dissolution of feldspars and precipitation of phyllosilicates (Wintsch et al., 1995). The sericitization of feldspars observed within the phyllonite zone suggests that the Kern Canyon fault was a water-dominated system.

How much quartz is "missing" from the phyllonite zone? The total volume of quartz lost is unknown but can be approximated through back-of-the-envelope calculations. Using a conservative estimate of 8% loss in total rock mass due to aqueous silica leaving the phyllonite zone during the plagioclase hydration reaction, the volume of a discrete, tabular segment of the phyllonite zone 15 m wide by 2 km long and 1 km deep yields a total rock volume of 30×10^6 m^3. If 8% of this volume was removed as aqueous silica, the total volume of quartz removed from the system would be 2.4×10^6 m^3. This estimate is probably fairly conservative, in that it only includes quartz released by plagioclase alteration and ignores any additional quartz released through potassium feldspar and biotite/vermiculite alteration

The large volume of "missing" quartz suggests that advective fluids transported silica out of the phyllonite system to be precipitated elsewhere. A wide vein of quartz is observed at the northern end of the mylonite within the area studied. However, volume calculations for the vein (estimated dimensions of 1 m wide, 100 m long, 100 m deep) suggest that it can account for only 1×10^4 m^3 of quartz, which is less than 1% of the missing quartz by volume. If the silica did not precipitate as quartz within the phyllonite zone, it could have been transported vertically through the fault system or laterally to neighboring rocks or may have precipitated within the cataclastic zone. The massive quartz vein observed by Treasher (1948) could account for some of the missing quartz. Assuming a tabular geometry of 30 m width, 200 m length, and 200 m depth, yields a volume of 1.2×10^6 m^3 for the quartz vein. However, the quartz vein observed by Treasher (1948) is atypical of the cataclastic zone; no other quartz veins of similar size are observed, and that one vein alone could only account for a fraction of the missing silica. Similarly, the volume of quartz distributed along subsidiary fractures within the damage zone of the cataclastic fault would likely account for only a portion the quartz produced by phyllonite reactions. This further supports the hypothesis that the phyllonite zone was an open system over a length scale larger than the study area and that aqueous silica was removed from the fault zone by large distances. These combined considerations suggest that incoming fluids may have been meteoric in origin. Fluids that entered the phyllonite from lower pressure and/or lower temperature conditions do not suggest deep sources, and large advective volumes suggest influx from the Earth's surface as well.

Similar quartz-producing hydration reactions are observed in association with the cataclasite zone. Quartz remains relatively constant toward the cataclastic fault while feldspar counts decrease and white mica/chlorite counts increase suggesting that the cataclastic zone also may have experienced silica-los. However, this suggestion is complicated by the apparent change in fluid chemistry from a quartz-dominated to calcite-dominated system at some point during

cataclastic faulting. Because of this uncertainty, mass balance estimates are icomplete at this time; yet similar advection of fluid, loss of silica, and volume change are suggested for the cataclastic zone.

Comparison to Other Fault Zones

Data for the Kern Canyon fault can be compared to known or suspected seismogenic faults, both active and inactive. Recent studies range from those of shallow faults in the 2 to 6 km depth range (e.g., the Punchbowl, San Gabriel, Nojima, and Awatere faults) to deeper faults near the base of the seismogenic zone (e.g., Great Glen fault zone).

The Punchbowl and San Gabriel faults are both inactive traces of the San Andreas fault exhumed from depths of 2-5 km; their structures consist of broad damaged zones bounding one or several narrow fault cores (Chester et al., 2004). The Nojima fault is an active, right-lateral reverse fault observed by means of 3 boreholes (at 500, 800, and 1800 m depth) located near the epicenter of the 1995 Kobe earthquake; the boreholes traverse the damaged zone and core of the fault (e.g., Ohtani et al., 2000). The Awatere fault is an active, right-lateral reverse fault that displays an exhumed hanging wall from an estimated depth of 6 km; field study indicates that it consists of a damaged zone (~50 m in width) bounding a narrow core of ultracataclasite and gouge (Little, 1995). The Great Glen fault zone is a dominantly left-lateral strike-slip fault exhumed from a depth of 9-16 km; displacement was accommodated along contemporaneous mylonite and cataclastic shear zones located within an extensively altered zone ~3 km wide (Stewart et al., 1999).

The internal structure of the Kern Canyon fault's cataclastic zone is similar to the structure described by Chester and Logan (1986) for the Punchbowl fault and later observed for other shallow faults, including the San Gabriel (Chester et al., 2004), Nojima (Ohtani et al., 2000), and Awatere (Little, 1995). It is unlike that of the Great Glen fault zone, in which cataclastic faulting is broadly distributed and occurred contemporaneously with ductile shearing (Stewart et al., 1999). The extensive fluid-assisted alteration observed to the west of the Kern Canyon fault (to a distance of >300 m) is unlike the alteration observed around shallow fault zones such as the Punchbowl, San Gabriel, and Nojima faults. In these shallow zones, nearly all fluid-assisted alteration is restricted either within the core or to a very narrow zone (<100 m) around the core (Ohtani et al., 2000; Chester et al., 2004). The Kern Canyon fault's alteration pattern more closely resembles that of the Great Glen fault zone; the extensive, greenschist-grade alteration of rock within and around the Great Glen fault zone is thought to have facilitated mylonite shearing and allowed it to occur contemporaneously with brittle faulting (Stewart et al., 1999).

These observations suggest that the internal structure of the cataclastic zone of the Kern Canyon fault is similar to that of shallow fault zones. However, the broad alteration observed around the cataclastic zone of the Kern Canyon fault is probably more typical of deeper faults, such as the Great Glen fault zone. The combination of structure and alteration characteristics along the Kern Canyon fault suggests that the Kern Canyon fault represents faulting that initiated at an intermediate depth within the seismogenic zone and was reactivated as it was exhumed.

CONCLUSIONS

Based on field and laboratory study of the Kern Canyon fault at Isabella Lake, California, the following conclusions can be drawn:

1) The internal structure of the Kern Canyon fault is similar to other large displacement faults in that it consists of a broad zone of fractured and altered rock to the west of a relatively narrow core of intense cataclasis. At the study area, the majority of slip on the Kern Canyon fault occurred within the cataclastic zone; a minor component of displacement was accommodated by the phyllonite zone.
2) Cross-cutting field relations and inferred temperature-pressure conditions indicate that phyllonite faulting predates cataclastic faulting. The ductile deformation occurred in a narrow zone (10-15 m in width) under lower greenschist grade conditions. Structures and mineral reactions in the fault record evolving fluid chemistry, pressure, and temperature conditions, probably associated with progressive cooling during faulting. The phyllonite may be genetically related to the proto-Kern Canyon fault which shares similar foliation and lineation.
3) Fracture, vein, and subsidiary fault fabric of the Kern Canyon fault indicate right-lateral strike-slip movement throughout faulting history, with a minor dip-slip component during the latest stage of brittle faulting.
4) The fault was fluid-saturated and the site of extensive synfaulting alteration reactions, mineralization, and fracture cementation. Pore fluids were present during both ductile and brittle phases. Structures suggest that fluid flow and mineralization were episodic and coupled with fault slip. Pore fluids provided free ions necessary for chemical reactions associated with phyllonite development to proceed. Pore fluids were also necessary for alteration reactions that occurred during cataclastic faulting. Dilatancy during faulting provided paths for fluid migration through the fault zone.
5) Episodic calcite and quartz cementation occurred within the fault zone. Both types of cement are present within the cataclastic zone as vein and void fill. Quartz is also present in fine veins within the phyllonite shear zone. Cathodoluminescence and cross-cutting relations in the cataclastic zone indicate that multiple episodes of cementation occurred, and that calcite cementation always appears to post-date quartz cementation. Mechanical twinning of calcite cement indicates that calcite cementation was syntectonic.

REFERENCES

Allmendinger, R.W., 1995. Stereonet v. 4.9.6, http://www.geo.cornell.edu/pub/rwa. Department of Geological Sciences, Cornell University, Ithaca, NY.

Anders, M.H., Wiltschko, D.V., 1994. Microfracturing, paleostress and the growth of faults. Journal of Structural Geology 16(6), 795-815.

Atkinson, B.K., 1984. Geophysical aspects of subcritical crack growth in rocks. In: Henderson, C.M.B. (Ed.), Progress in Experimental Petrology 6, 1981-1984. Natural Environment Research Council, London, pp. 234-236.

Bailey, E.H., Stevens, R.E., 1960. Selective staining of K-feldspar and plagioclase on rock slabs and thin sections. American Mineralogist 45(9-10), 1020-1025.

Brace, W.F., Kohlstedt, D.L., 1980. Limits on lithospheric stress imposed by laboratory experiments. Journal of Geophysical Research B85(11), 6248-6252.

Brantley, S.L., Evans, E., Hickman, S.H., Crerar, D.A., 1990. Healing of microcracks in quartz: implications for fluid flow. Geology 18, 136-139.

Bruhn, R.L., Yonkee, W.A., Parry, W. T., 1990. Structural and fluid-chemical properties of seismogenic normal faults. In: Das, S., Ohnaka, M. (Eds.), Earthquake Source Processes. Tectonophysics 175. Elsevier, Amsterdam, Netherlands, pp. 139-157.

Busby-Spera, C.J., Saleeby, J.B., 1990. Intra-arc strike-slip fault exposed at batholithic levels in the southern Sierra Nevada, California. Geology 18(3), 255-259.

Byerlee, J.D., Wyss, M., 1978. Friction of rocks. In: Rock Friction and Earthquake Prediction. Birkhaeuser Verlag, Basel, Switzerland, pp. 615-626.

Caine, J.S., Evans, J.P., Forster, C.B., 1996. Fault zone architecture and permeability structure. Geology 24(11), 1025-1028.

Chase, G.C., Wallace, T.C., 1988. Flexural isostasy and uplift of the Sierra Nevada of California. Journal of Geophysical Research B93(4), 2795-2802.

Chester, F.M., 1983. Mechanical properties and fabric of the Punchbowl fault zone, California. M.S. thesis, Texas A&M University, College Station, TX.

Chester, F.M., Chester, J.S., 1998. Ultracataclasite structure and friction processes of the Punchbowl Fault, San Andreas System, California. Tectonophysics 295(1-2), 199-221.

Chester, F.M., Chester, J.S., Evans, J.P., Kirschner, D.L., Schulz, S.E., 2002. Internal fault structure of large-displacement faults in the continental crust. In: Rupturing the Lithosphere, Vol. 1, MARGINS Theoretical Institute. Columbia University Press, accepted.

Chester, F.M., Evans, J.P., Biegel, R.L., 1993. Internal structure and weakening mechanisms of the San Andreas Fault. Journal of Geophysical Research B98(1), 771-786.

Chester, F.M., Logan, J.M., 1986. Implications for mechanical properties of brittle faults from observations of the Punchbowl fault zone, California. In: Wang, C.Y. (Ed.), International Structure of Fault Zones. Pure and Applied Geophysics 124. Birkhaeuser Verlag, Basel, Switzerland, pp. 79-106.

Chester, F.M., Logan, J.M., 1987. Composite planar fabric of gouge from the Punchbowl Fault, California. In: Cobbold, P.R., Gapais, D., Means, W.D., Treagus, S.H. (Eds.), Shear Criteria in Rocks. Journal of Structural Geology 9. Pergamon, Oxford-New York, pp. 621-634.

Cowan, D.S., 1999. Do faults preserve a record of seismic slip? A field geologist's opinion. Journal of Structural Geology 21, 2703-2719.

Dalrymple, G.B., 1963. Potassium-argon dates of some Cenozoic rocks in the Sierra Nevada, California. Geological Society of America Bulletin 74, 379-390.

Dellinger, D.A., Zilka, N.T., 1984. Golden Trout Wilderness, California. In: Wilderness Mineral Potential; Assessment of Mineral Resource Potential in U.S. Forest Service Lands Studied 1964-1984. U.S. Geological Survey, Menlo Park, CA, pp. 251-254.

Etheridge, M.A., Wall, J.V., Cox, S.F., Vernon, R.H., 1984. High fluid pressures during regional metamorphism and deformation: Implications for mass transport and deformation mechanisms. Journal of Geophysical Research B89, 4344-4358.

Evans, J.P., 1990. Textures, deformation mechanisms, and the role of fluids in the cataclastic deformation of granitic rocks. Geological Society Special Publications 54, 29-39.

Evans, J.P., Chester, F.M., 1995. Fluid-rock interaction in faults of the San Andreas system: Inferences from San Gabriel fault rock geochemistry and microstructures. Journal of Geophysical Research B100(7), 13,007-13,020.

Evernden, J.F., Kistler, R.W., 1970. Chronology of emplacement of Mesozoic batholithic complexes in California and western Nevada. U. S. Geological Survey, Reston, VA, 42.

Flinn, D., 1977. Transcurrent faults and associated cataclasis in Shetland. Journal of the Geological Society of London 133(Part 3), 231-248.

Forbes, H., 1930. Geological report on Isabella, Borel, and Ant Hill Damsites on Kern River. State of California, Division of Water Resources, Bakersfield, CA, 27.

Friedman, M., 1969. Structural analysis of fractures in cores from the Saticoy Field, Ventura Co., California. American Society of Petroleum Geology Bulletin 53, 367-389.

Fyfe, W.S., Price, N.J., Thompson, A.B., 1978. Fluids in the Earth's Crust. Elsevier, Amsterdam, 383 pp.

Gay, N.C., Ortlepp, W.D., 1979. Anatomy of a mining-induced fault zone. Geological Society of America Bulletin 90(1), 47-58.

Goodwin, L.B., Wenk, H.R., 1995. Development of phyllonite from granodiorite: mechanisms of grain-size reduction in the Santa Rosa mylonite zone, California. Journal of Structural Geology 17(5), 689-707.

Groshong, R.H., 1988. Low-temperature deformation mechanisms and their interpretation. Geological Society of America Bulletin 100(9), 1329-1360.

Hadizadeh, J., Babaie, H.A., Babaie, A., 1991. Development of interlaced mylonites, cataclasites and breccias; Example from the Towaliga Fault, south central Appalachians. Journal of Structural Geology 13(1), 63-70.

Hadley, K., 1976. Comparison of calculated and observed crack densities and seismic velocities in Westerly Granite. Journal of Geophysical Research B81(11), 3484-3494.

Hickman, S., Zoback, M., Younker, L., Ellsworth, W., 1994. Deep scientific drilling in the San Andreas fault zone. Eos, Transactions, American Geophysical Union 75(12), 137-142.

Hill, M.L., 1955. Nature of movements on active faults in southern California. In: Oakeshott, G.B., (Ed.), Earthquakes in Kern County, California, during 1952. California Division of Mines Bulletin 171, pp. 37-40.

Hobbs, B.E., Ord, A., Teyssier, C., 1986. Earthquakes in the ductile regime? In: Wang, C.Y. (Ed.), International Structure of Fault Zones. Pure and Applied Geophysics 124. Birkhaeuser Verlag, Basel, Switzerland, 309-336.

House, M.A., Wernicke, B.P., Farley, K.A., Dumitru, T.A., 1997. Cenozoic thermal evolution of the central Sierra Nevada, California, from (U-Th)/He thermochronometry. Earth and Planetary Science Letters 151, 167-179.

House, W.M., Gray, D.R., 1982. Cataclasites along the Saltville Thrust, USA and their implications for thrust-sheet emplacement. Journal of Structural Geology 4(3), 257-269.

Hull, J., 1988. Thickness-displacement relationships for deformation zones. Journal of Structural Geology 10(4), 431-435.

Janecke, S.U., Evans, J.P., 1988. Feldspar-influenced rock rheologies. Geology 16, 1064-1067.

Kirby, S.H., 1980. Tectonic stresses in the lithosphere: constraints provided by the experimental deformation of rocks. Journal of Geophysical Research B85(11), 6353-6363.

Kistler, R.W., 1993. Mesozoic intrabatholithic faulting, Sierra Nevada, California. In: Dunne, G.C., McDougall, K.A. (Eds.), Mesozoic Paleogeography of the Western United States; II. Field Trip Guidebook. Society of Economic Paleontologists and Mineralogists, Pacific Section, Los Angeles, CA, pp. 247-261.

Kohlstedt, D.L., Evans, B., Mackwell, S.J., 1995. Strength of the lithosphere: Constraints imposed by laboratory experiments. Journal of Geophysical Research B100(9), 17,587-17,602.

Kranz, R.L., 1983. Microcracks in rocks: A review. Tectonophysics 100, 449-480.

Kronenberg, A.K., Segall, P., Wolf, G.H., 1990. Hydrolytic weakening and penetrative deformation within a natural shear zone. In: Duba, A.G., Durham, W.B., Handin, J.W., Wang, H.F. (Eds.), The Brittle-Ductile Transition in Rocks. Geophysical Monograph 56. American Geophysical Union, Washington, DC, pp. 21-36.

Lawson, A., 1904. The geomorphogeny of the upper Kern Basin. University of California Department of Geological Sciences Bulletin 3, 291-386.

Lister, G.S., Snoke, A., 1984. S-C mylonites. Journal of Structural Geology 6, 617-638.

Little, T.A., 1995. Brittle deformation adjacent to the Awatere strike-slip fault in New Zealand: Faulting patterns, scaling relationships, and displacement partitioning. Geological Society of America Bulletin 107(11), 1255-1271.

Lockner, D.A., Byerlee, J.D., 1995. An earthquake instability model based on faults containing high fluid-pressure compartments. In: Wang, R., Aki, K. (Eds.), Mechanics Problems in Geodynamics, Part 1. Pure and Applied Geophysics 145. Birkhaeuser Verlag, Basel, Switzerland, pp. 717-745.

Lockwood, J.P., Moore, J.G., 1979. Regional deformation of the Sierra Nevada, California, on conjugate microfault sets. Journal of Geophysical Research B84(11), 6041-6049.

Louderback, G.D., 1920. Geology for the Reservoir Site, Water Resources of Kern River and Adjacent Streams and their Utilization. State of California, Department of Engineering, Sacramento, CA, pp. 134-137.

Magloughlin, J.F., Spray, J.G., 1992. Frictional melting processes and products in geological materials: Introduction and discussion. Tectonophysics 204, 197-206.

Mares, V.M., Kronenberg, A.K., 1993. Experimental deformation of muscovite. Journal of Structural Geology 15(9/10), 1061-1075.

Marliave, C., 1938. Geological Reconnaissance Report on Isabella Dam Sites Situated on Kern River in Kern County. State of California, Department of Public Works, Division of Water Resources, Sacramento, CA.

Martel, S.J., 1990. Formation of compound strike-slip fault zones, Mount Abbot quadrangle, California. Journal of Structural Geology 12(7), 869-882.

Menendez, B., Zhu, W., Wong, T.F., 1996. Micromechanics of brittle faulting and cataclastic flow in Berea Sandstone. Journal of Structural Geology 18(1), 1-16.

Moore, D.E., Hickman, S., Lockner, D.A., Dobson, P. F., 2001. Hydrothermal minerals and microstructures in the Silangkitang geothermal field along the Great Sumatran fault zone, Sumatra, Indonesia. Geological Society of America Bulletin 113(9), 1179-1192.

Moore, J.G., 1981. Geologic map of the Mount Whitney Quadrangle, Inyo and Tulare counties, California. U. S. Geological Survey, Reston, VA.

Moore, J.G., du Bray, E., 1978. Mapped offset on the right-lateral Kern Canyon fault, southern Sierra Nevada, California. Geology 6, 205-208.

Ohtani, T., Fujimoto, K., Ito, H., Tanaka, H., Tomida, N., Higuchi, T., 2000. Fault rocks and past to recent fluid characteristics from the borehole survey of the Nojima fault ruptured in the 1995 Kobe earthquake, southwest Japan. Journal of Geophysical Research B105(7), 16161-16171.

Passchier, C.W., 1982. Pseudotachylyte and the development of ultramylonite bands in the Saint-Barthelemy Massif, French Pyrenees. Journal of Structural Geology 4(1), 69-79.

Paterson, M.S., 1995. A theory for granular flow accommodated by material transfer via an intergranular fluid. In: Spiers, C.J., Takeshita, T. (Eds.), Influence of Fluids on Deformation Processes in Rocks. Tectonophysics 245. Elsevier, Amsterdam, pp. 135-151.

Riedel, W., 1929. Zur mechanik geologischer brucherscheinungen. Zentralblatt fur Mineralogie, Geologie und Paleontologie B, 354-368.

Robertson, E.C., 1983. Relationship of fault displacement to gouge and breccia thickness. Mining Engineering 35(10), 1426-1432.

Ross, D.C., 1986. Basement-rock correlations across the White Wolf-Breckenridge-southern Kern Canyon fault zone, southern Sierra Nevada, California. U. S. Geological Survey, Reston, VA.

Ross, D.C., 1987. Granitic rock modal data from the southern Sierra Nevada, California. U.S. Geological Survey, Menlo Park, CA.

Ross, D.C., 1990. Reconnaissance geologic map of the southern Sierra Nevada, Kern, Tulare, and Inyo Counties, California. U.S. Geological Survey, Menlo Park, CA.

Saleeby, J.B., Busby, C., 1993. Paleogeographic and tectonic setting of axial and western metamorphic framework rocks of the southern Sierra Nevada, California. In: Dunne, G.C., McDouball, K.A. (Eds.), Mesozoic Paleogeography of the Western United States, II. Society of Economic Paleontologists and Mineralogists, Pacific Section, Los Angeles, CA, pp. 197-225.

Scholz, C.H., 1990. The mechanics of earthquakes and faulting. Cambridge University Press, Cambridge, United Kingdom.

Scholz, C.H., Dawers, N.H., Yu, J.Z., Anders, M.H., 1993. Fault growth and fault scaling laws: Preliminary results. Journal of Geophysical Research B98(12), 21951-21961.

Schulz, S.E., Evans, P.E., 2000. Mesoscopic structure of the Punchbowl Fault, Southern California and the geologic and geophysical structure of active strike-slip faults. Journal of Structural Geology 22, 913-930.

Segall, P., Pollard, D.D., 1983. Nucleation and growth of strike slip faults in granite. Journal of Geophysical Research B88(1), 555-568.

Shea, W.T., Kronenbreg, A.K., 1992. Rheology and deformation mechanisms of an isotropic mica schist. Journal of Geophysical Research B97(11), 15201-15237.

Shimamoto, T., 1989. The origin of S-C mylonites and a new fault-zone model. Journal of Structural Geology 11(1-2), 51-64.

Sibson, R.H., 1977. Fault rocks and fault mechanisms. Journal of the Geological Society of London 133(Part 3), 191-213.

Sibson, R.H., 1980. Transient discontinuities in ductile shear zones. In: Carreras, J., Cobbold, P.R., Ramsay, J.G., White, S.H. (Eds.), Shear Zones in Rocks. Journal of Structural Geology 2. Pergamon, Oxford, pp. 165-171.

Sibson, R.H., 1983. Continental fault structure and the shallow earthquake source. Journal of the Geological Society of London 140, 741-767.

Sibson, R.H., 1986. Brecciation processes in fault zones: Inferences from earthquake rupturing. Pure and Applied Geophysics 124(1-2), 159-175.

Sibson, R.H., 1989. Earthquake faulting as a structural process. Journal of Structural Geology 11(1/2), 1-14.

Sibson, R.H., 1992. Implications of fault-valve behavior for rupture nucleation and recurrence. Tectonophysics 211, 283-293.

Sibson, R.H., Moore, J.M., Rankin, A.H., 1975. Seismic pumping - a hydrothermal fluid transport mechanism. Journal of the Geological Society of London 131, 653-659.

Sibson, R.H., Robert, F., Poulsen, K.H., 1988. High-angle reverse faults, fluid-pressure cycling, and mesothermal gold-quartz deposits. Geology 16, 551-555.

Simpson, C., 1985. Deformation of granitic rocks across the brittle-ductile transition. Journal of Structural Geology 7(5), 503-511.

Simpson, C., Schmid, S. M., 1983. An evaluation of criteria to deduce the sense of movement in sheared rocks. Geological Society of America Bulletin 94, 1281-1288.

Sisson, T.W., Moore, J.G., 1984. Geology of Giant Forest-Lodgepole area, Sequoia National Park, California. U. S. Geological Survey, Reston, VA.

Stewart, M., Strachan, R.A., Holdsworth, R.E., 1999. Structure and early kinematic history of the Great Glen fault zone, Scotland. Tectonics 18(2), 326-342.

Swanson, M.T., 1992. Fault structure, wear mechanisms and rupture processes in pseudotachylyte generation. Tectonophysics 204, 223-242.

Treasher, R.C., 1948. Definite Project Report, Isabella Project, Kern River, California: Part IV, Dam and Appurtenances, Appendix A Geology. U.S. Corps of Engineers, Department of the Army, Sacramento, CA.

Wallace, R.E., Morris, H.T., 1986. Characteristics of faults and shear zones in deep mines. Pure and Applied Geophysics 124(1-2), 107-125.

Wang, H.F., Simmons, G., 1978. Microcracks in crystalline rock from 5.3-km depth in the Michigan Basin. Journal of Geophysical Research A83, 5849-5856.

Webb, R.W., 1936. Kern Canyon fault, southern Sierra Nevada. Journal of Geology 44(5), 631-638.

Wibberley, C., 1999. Are feldspar-to-mica reactions necessarily reaction-softening processes in fault zones? Journal of Structural Geology 21, 1219-1227.

Wilson, J.E., 1999. Microfracture fabric of the Punchbowl fault zone, San Andreas system, California. M.S. thesis. Texas A&M University, College Station, TX.

Wilson, J.E., Chester, J.S., Chester, F.M., 1999. Microfracture fabric of the Punchbowl fault zone, San Andreas system, California. In: 1999 AGU Fall Meeting, San Francisco, CA.

Wilson, J.E., Chester, J.S., Chester, F.M., 2002. Microfracture analysis of fault growth and wear processes, Punchbowl fault, San Andreas system, California. Journal of Structural Geology, in review.

Wintsch, R.P., 1975. Feldspathization as a result of deformation. Geological Society of America Bulletin 86(1), 35-38.

Wintsch, R.P., Christoffersen, R., Kronenberg, A.K., 1995. Fluid-rock reaction weakening of fault zones. Journal of Geophysical Research B100(7), pp 13021-13032.

Yardley, B.W.D., 1994. An Introduction for Metamorphic Petrology. Longman Scienific & Technical, New York.

Zoback, M.D., Hickman, S.H., Ellsworth, W.L., 1998. Scientific Drilling into the San Andreas Fault at Parkfield, CA: Project Overview and Operational Plan. U.S. Geological Survey, Reston, VA.

Table 1. Average Modal Compositions[1] of Kern Canyon Fault Protoliths

Unit	Abbr.	# Samples	Plagioclase	K-Feldspar	Quartz	Biotite	Hornblende
Wagy Flat	K_{wf}	58	53.5 ± 6.7	9 ± 6.3	22.5 ± 3.6	10.5 ± 3	4 ± 1.7
Alta Sierra	K_{as}	32	56 ± 5.1	11 ± 6.4	24 ± 4.4	8 ± 1.8	1 ± 1.0
Kern River	K_{kr}	54	40 ± 5.7	24 ± 5.8	26 ± 5.3	8 ± 3.1	2 ± 2.4

[1] Data from Ross, 1990

Table 2. Summary of Radiometric Dates of Kern Canyon Fault Protoliths

Unit	Date	Method	Reference
K_{as}	89.0 ±2.1 Ma	K-Ar of biotite	Data from Evernden (1970) (Ross, 1990)
K_{kr}	86.8, 87.2, and 88.8 Ma	K-Ar of biotite	Data from Evernden (1970) (Ross, 1990)
K_{kr}	80 ±3 Ma	U-Pb of zircon	Data from Saleeby (1986) (Ross, 1990)
K_{kr}	81.1 ±11.1 Ma	Rb/Sr whole-rock	Data from Kistler (1986) (Ross, 1990)

Table 3. Mineralogy of the Kern Canyon Fault Rocks

Sample[1]	Description	Dist. from Cataclastic Zone[2] (m)	Dist. from Phyllonite Zone[3] (m)	Quartz	K-spar	Plag	Biotite	White Mica/ Chlorite[4]	Sphene	Opaques	Calcite	Other[5]
Northern Traverse												
K26A	host	950	950	33%	18%	38%	10%	2%	0%	0%	0%	0%
K36A	fractured host	110	69	25%	24%	41%	5%	2%	0%	2%	0%	3%
K122B	proto-mylonite	34	9	32%	12%	26%	13%	13%	0%	4%	0%	0%
K123A	proto-mylonite	29	5	36%	13%	19%	5%	22%	0%	6%	0%	0%
	mylonite zone	18	0									
K37C	mylonite	18	(2)	29%	0%	19%	1%	38%	0%	13%	0%	0%
Southern Traverse												
K26A	K_{wf} host	950	950	33%	18%	38%	10%	2%	0%	0%	0%	0%
K25A	K_{as} host	700	560	27%	15%	44%	11%	2%	0%	1%	0%	1%
K119A	fractured K_{as} host	164	94	27%	16%	46%	6%	3%	1%	1%	0%	1%
K119B	fractured K_{as} host	164	94	25%	3%	54%	9%	3%	0%	4%	0%	1%
K16E	proto-phyllonite	144	4	29%	1%	40%	7%	21%	0%	2%	0%	1%
	phyllonite zone	140	0									
K16C	proto-phyllonite	138	(2)	29%	2%	31%	1%	29%	0%	8%	0%	0%
K16B	proto-phyllonite	130	(10)	35%	6%	24%	0%	23%	0%	2%	9%	1%
K16A	fractured K_{wf} host	128	(12)	28%	5%	42%	9%	16%	0%	0%	0%	0%
North Central Traverse												
K26A	host	950	--	33%	18%	38%	10%	2%	0%	0%	0%	0%
K113G	fractured host	67	--	37%	5%	31%	6%	12%	0%	6%	0%	3%
K113E	fractured host	43	--	37%	19%	9%	1%	14%	0%	17%	4%	1%
K113D	fractured host	19	--	31%	7%	25%	17%	11%	1%	9%	0%	1%
K113C	fractured host	6	--	35%	6%	21%	1%	18%	0%	7%	12%	0%

Table 3. Continued

Sample[1]	Description	Dist. from Cataclastic Zone (m)[2]	Dist. from Phyllonite Zone (m)[3]	Quartz	K-spar	Plag	Biotite	White Mica/ Chlorite[4]	Sphene	Opaques	Calcite	Other[5]
South Central Traverse												
K26A	host	950	950	33%	18%	38%	10%	2%	0%	0%	0%	0%
K12A	fractured host	151	154	26%	13%	43%	7%	5%	1%	0%	2%	4%
K12B	fractured host	151	154	30%	6%	27%	1%	23%	0%	3%	7%	3%
K13F	fractured host	102	95	26%	9%	47%	10%	5%	0%	1%	0%	2%
K27A	fractured host	74	72	29%	0%	26%	1%	33%	0%	6%	3%	2%
K24C	fractured host	12	12	32%	0%	20%	2%	29%	0%	4%	11%	2%
K24B	fractured host	10	10	29%	0%	19%	5%	20%	0%	14%	12%	2%
K24A	fractured host	8	8	30%	0%	14%	5%	33%	0%	5%	12%	1%
	phyllonite zone	0	0									

1. All samples are from the Engineer Point peninsula except K25A (K_{as} protolith) and K26A (K_{wf} protolith).
2. Distances are measured in meters west of the western foliated cataclasite / fractured rock boundary.
3. Distances are measured in meters perpendicular from the center of the trace of the nearest phyllonite zone.
4. Counts are the sum of white mica (muscovite, phengite) and chlorite.
5. Other minerals primarily include hornblende and iron-opaque minerals.

Table 4. Petrology by Alteration Zone

A. Petrology[1] Based on Sample Location

	Quartz	Potassium Feldspar	Plagioclase	Biotite	White Mica / Chlorite	Sphene	Opaques	Calcite	Other
Average regional 0-25% alteration[2]	23	9	53	10	0	0	1	0	4
Average regional 0-25% alteration (high potassium feldspar)[3]	25	25	41	7	0	0	0	0	2
Average 0-25% alteration on peninsula[4]	25	24	41	5	2	0	2	0	3
Average 25-50% alteration zone[5]	28	10	35	4	14	1	2	5	4
Average 50-75% alteration zone[6]	28	5	37	6	19	0	4	2	2
Average 75-100% alteration zone[7]	33	6	23	5	21	0	7	5	1

1. Mineralogy determined by point count of 200 grains per sample and given in percentage by volume
2. Average of K26A and Ross (1990) data for K_{wf}
3. Average of Ross (1990) regional Kwf data in which potassium feldspar content is >21% (samples 4745A, 4795, A-5-1 in Appendix A)
4. Sample K36A only
5. Average of samples K12A and K12B
6. Average of samples K13F and K27A
7. Average of samples K113C, K113D, K113E, K113G, K24A, K24B, K24C, K122A, K122B, K16A, K16B, K16C, and K37C

Table 4. Petrology by Alteration Zone (Continued)

B. Petrology[1] Based on Hand Sample Visual Alteration Index

	Quartz	Potassium Feldspar	Plagioclase	Biotite	White Mica / Chlorite	Sphene	Opaques	Calcite	Other
Average regional 0-25% alteration[2]	23	9	53	10	0	0	1	0	4
Average regional 0-25% alteration (high potassium feldspar)[3]	25	25	41	7	0	0	0	0	2
Average 0-25% alteration on peninsula[4]	26	18	42	6	3	0	1	1	3
Average 25-50% alteration zone[5]	--	--	--	--	--	--	--	--	--
Average 50-75% alteration zone[6]	32	9	35	10	10	0	4	0	2
Average 75-100% alteration zone[7]	32	5	23	4	24	0	7	5	1

1. Mineralogy determined by point count of 200 grains per sample and given in percentage by volume
2. Average of K26A and Ross (1990) data for K_{wr}
3. Average of Ross (1990) regional K_{wr} data in which potassium feldspar content is >21% (samples 4745A, 4795, A-5-1 in Appendix A)
4. Average of samples K36A and K12A
5. No samples fall within the 25-50% alteration zone when classified by hand sample alteration index.
6. Average of samples K113G, K122B, and K13F
7. Average of samples K113C, K113D, K113E, K24A, K24B, K24C, K123A, K16A, K16B, K16C, K37C, K27A, and K12B

Table 5. Fracture Character by Alteration Zone

Alteration Zone		# Stations	# Measurements	Spacing	Length	Vein Width	% with Halo	Halo Half-width
				(m)	(m)	(mm)		(cm)
0-25%	yellow	6	57	1.0	5.0	12.1	61%	1.5
25-50%	green	1	5	1.1	4.2	26.8	100%	1.3
50-75%	blue	4	46	0.4	3.7	21.2	41%	1.3
75-100%	purple	7	81	0.2	3.1	15.3	9%	30.3

Table 6. Microfracture Intensities near the Kern Canyon fault (counts/mm)

Sample[1]	Sample Description	Dist. from Cataclastic Zone[2] (m)	Dist. from Phyllonite Zone[3] (m)	Open	Sealed[4]				Healed	Re-xtl[5]		Sum of all but open
					p	fe	c	u		s	f	
Northern Traverse of overprinted cataclasite and phyllonite												
K26A	host	950	950	2.2	0.5	0.1	0.0	0.0	3.0	0.0	0.0	3.5
K36A	fractured host	110	69	3.5	0.2	0.0	0.0	0.1	4.6	0.7	0.1	5.7
K122B	proto-mylonite	34	9	0.1	1.1	0.1	0.0	0.0	13.0	0.6	0.2	15.0
K123A	proto-mylonite	29	5	0.1	1.0	0.2	0.0	0.0	9.7	0.9	1.9	13.8
	mylonite zone	18	0									
K37C	mylonite	18	(2)	0.0	1.4	0.8	0.0	0.0	7.8	1.2	4.9	16.2
Southern Traverse across phyllonite zone at margin of cataclastic zone												
K26A	K_{wf} host	950	950	2.2	0.5	0.1	0.0	0.0	3.0	0.0	0.0	3.5
K25A	K_{as} host	700	560	2.3	0.9	0.1	0.0	0.0	3.0	0.0	0.0	3.9
K119A	K_{as} fractured host	164	94	1.0	1.3	0.5	0.0	0.4	5.2	0.1	0.0	7.7
K119B	K_{as} fractured host	164	94	1.7	0.4	0.2	0.0	0.1	5.9	0.1	0.0	6.6
K16E	proto-phyllonite	144	4	0.4	1.5	0.4	0.0	0.3	9.8	0.6	0.0	12.6
	phyllonite zone	140	0									
K16C	proto-phyllonite	138	(2)	0.2	0.9	0.8	0.1	0.1	6.3	1.8	2.5	12.5
K16B	proto-phyllonite	130	(10)	0.1	1.2	0.2	0.4	0.1	8.4	0.6	0.4	11.3
K16A	K_{wf} fractured host	128	(12)	0.4	1.0	0.5	0.0	0.1	10.4	1.1	0.0	13.1
North Central Traverse near the cataclastic zone												
K26A	host	950	--	2.2	0.5	0.1	0.0	0.0	3.0	0.0	0.0	3.5
K113F	fractured host	67	--	0.1	0.3	0.1	0.8	0.4	14.4	0.4	0.0	16.4
K113E	fractured host	43	--	0.2	0.1	0.0	0.3	0.1	11.0	0.5	0.0	12.0
K113D	fractured host	19	--	0.1	0.1	0.3	0.6	0.7	9.6	0.6	0.0	11.8
K113C	fractured host	6	--	0.0	0.3	0.8	0.5	0.6	13.8	0.6	0.0	16.7

Table 6. Continued

Sample[1]	Sample Description	Dist. from Cataclastic Zone[2] (m)	Dist. from Phyllonite Zone[3] (m)	Open	Sealed[4]				Healed	Re-xtl[5]		Sum of all but open
					p	fe	c	u		s	f	
South Central Traverse near the cataclastic zone												
K26A	host	950	950	2.2	0.5	0.1	0.0	0.0	3.0	0.0	0.0	3.5
K12A	fractured host	151	154	0.7	0.5	0.0	0.8	0.3	6.4	0.3	0.1	8.4
K13F	fractured host	102	95	0.6	0.9	1.0	0.0	0.7	6.1	0.3	0.0	8.9
K27A	fractured host	74	72	0.3	0.3	0.1	0.5	0.1	5.9	0.5	0.0	7.4
K24C	fractured host	12	12	0.5	0.6	0.0	0.5	0.1	7.4	0.8	0.1	9.4
	phyllonite zone	0	0									

1. All samples are from the Engineer Point peninsula except K25A (K_{as} protolith) and K26A (K_{wf} protolith).
2. Distances are measured in meters west of the western foliated cataclasite / fractured rock boundary.
3. Distances are measured in meters perpendicular from the center of the trace of the nearest phyllonite zone.
4. Sealed fractures are classified as phyllosilicate (p), iron/opaque (fe), calcite (c), or unknown (u).
5. Recrystallization occurs either along subgrain boundaries (s) or fractures (f).

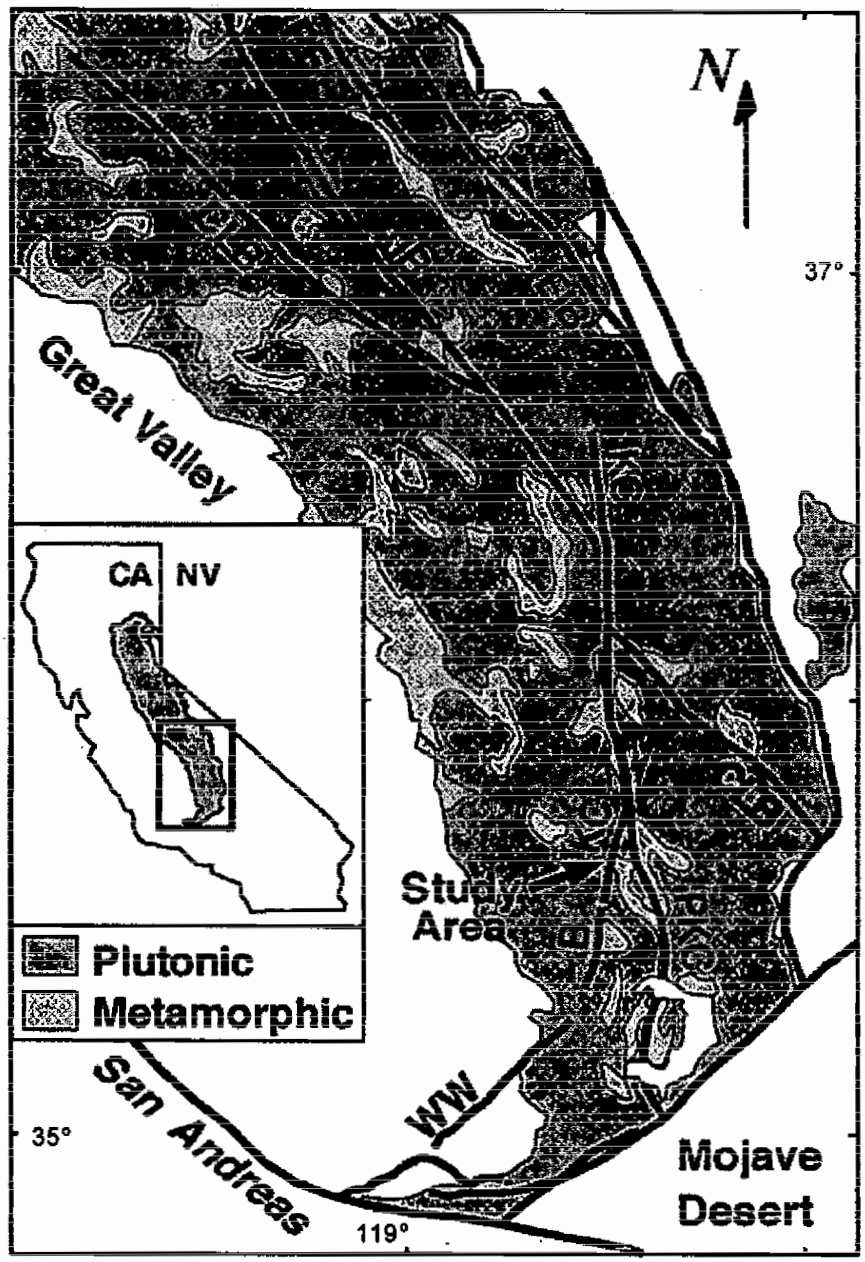

Figure 1. Map of the southern Sierra Nevada batholith. Map shows the location of the Kern Canyon fault zone (KC) relative to other tectonic features, including the axial intrabatholithic break (AIB), cryptic lithospheric boundary (CLB), eastern intrabatholithic break (EIB), proto-Kern Canyon fault (PKC), Rosy Finch shear zone (RF), Breckenridge fault (B), and White Wolf fault (WW) (Map provided by J. Chester, modified from Saleeby and Busby, 1993, and Kistler, 1993).

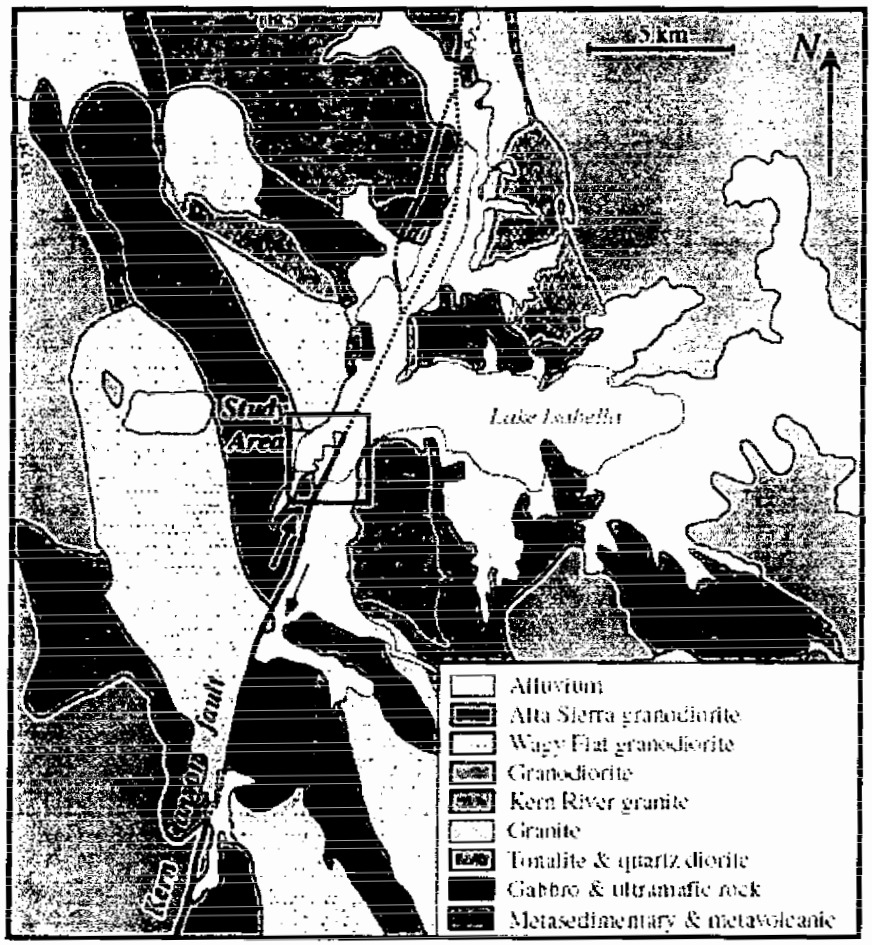

Figure 2. Geologic map of the Lake Isabella region, California. Offsets of the Alta Sierra, Wagy Flat, and gabbroic and ultramafic rock units indicate approximately 15 km of right-lateral separation on the Kern Canyon fault. Fault is well exposed at Engineer Point (peninsula within study area box) at the southern end of Lake Isabella. Map provided by J. Chester, modified from Ross (1990).

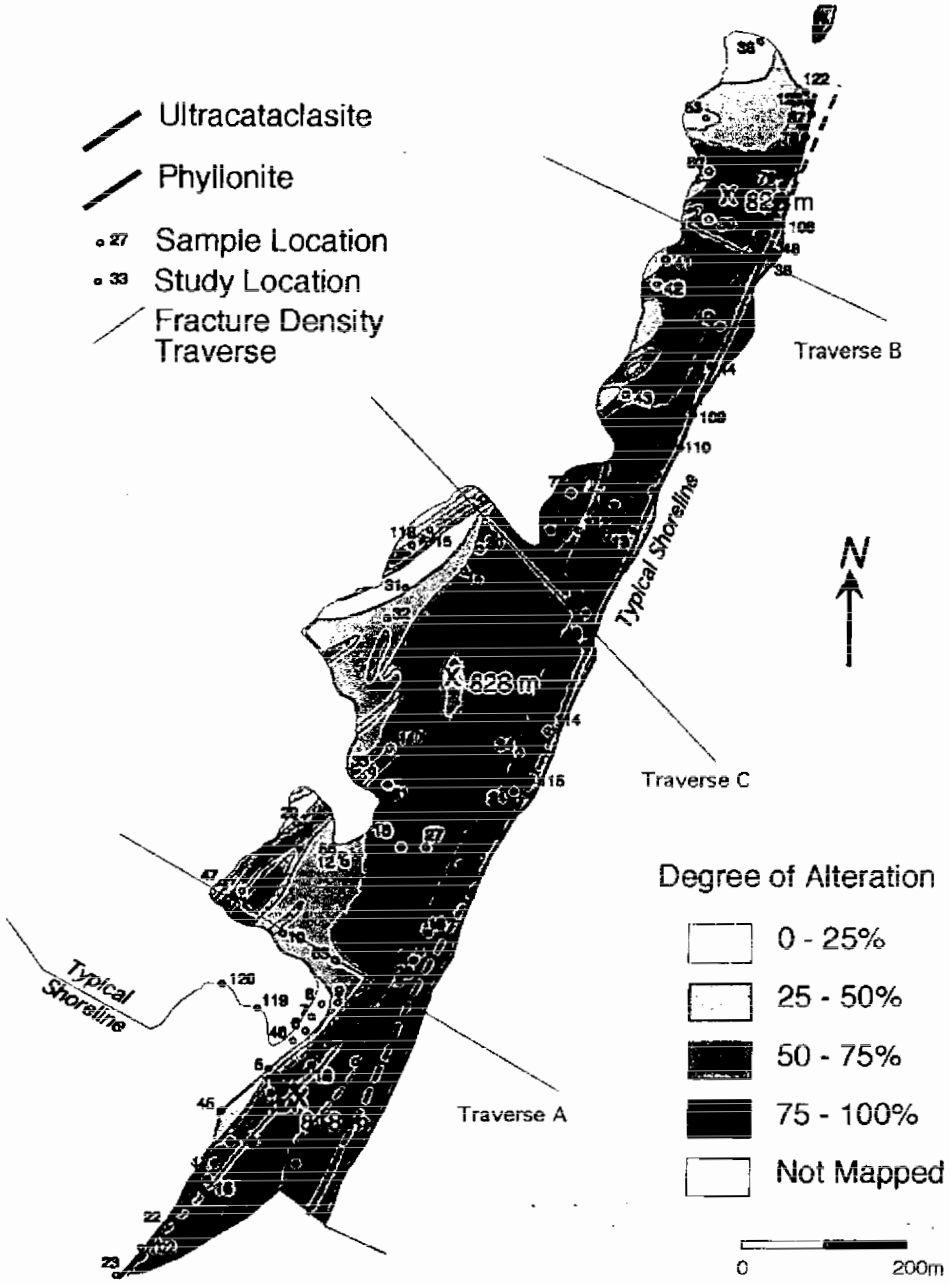

Figure 3a. Map of faults, alteration intensity, and study locations at Engineer Point. Alteration intensity defined by visual estimation of the volume of rock that is noticeably altered at the outcrop scale. Locations of the three mesoscale fracture intensity traverses are indicated. Typical shoreline elevation is 789 m. Cataclastic fault trace at southern end of study area is mapped based on the location of Treasher (1948).

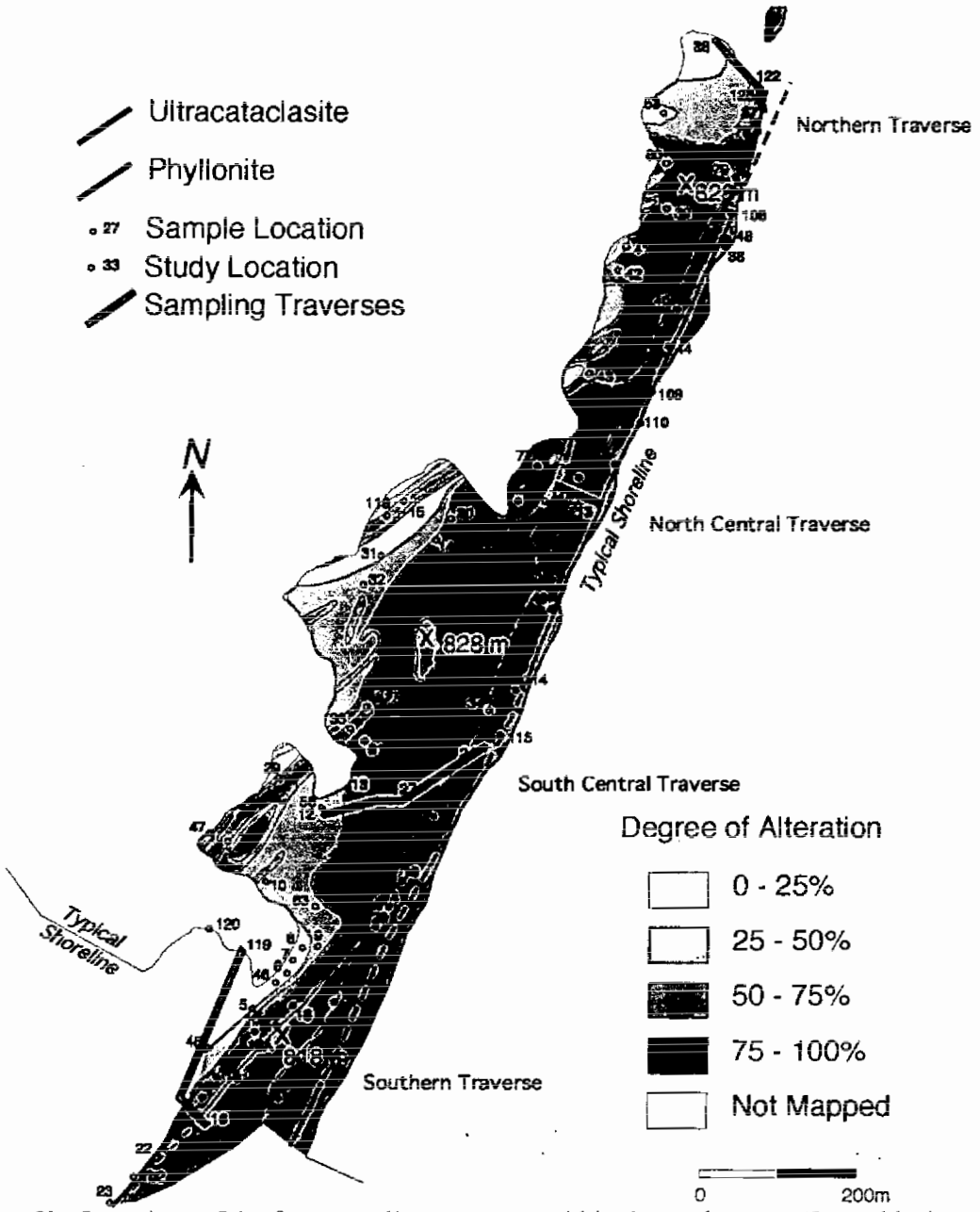

Figure 3b. Locations of the four sampling traverses within the study area. Heavy black lines indicate sampling traverse locations. Protolith sample locations are shown on Figure 5. Sample K26A served as the Wagy Flat granodiorite sample for all traverses. Sample K25A was the Alta Sierra granodiorite protolith sample for the Southern Traverse. Typical shoreline elevation is 789 m. Southern cataclastic fault trace (east of station K28) is mapped based on the location of Treasher (1948).

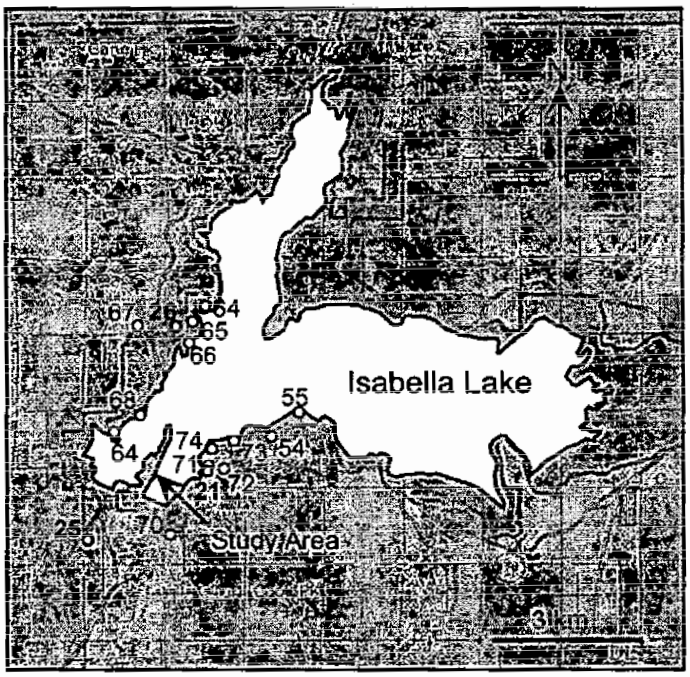

Figure 4. Map of region surrounding Engineer Point, showing study locations and protolith sample locations (bold).

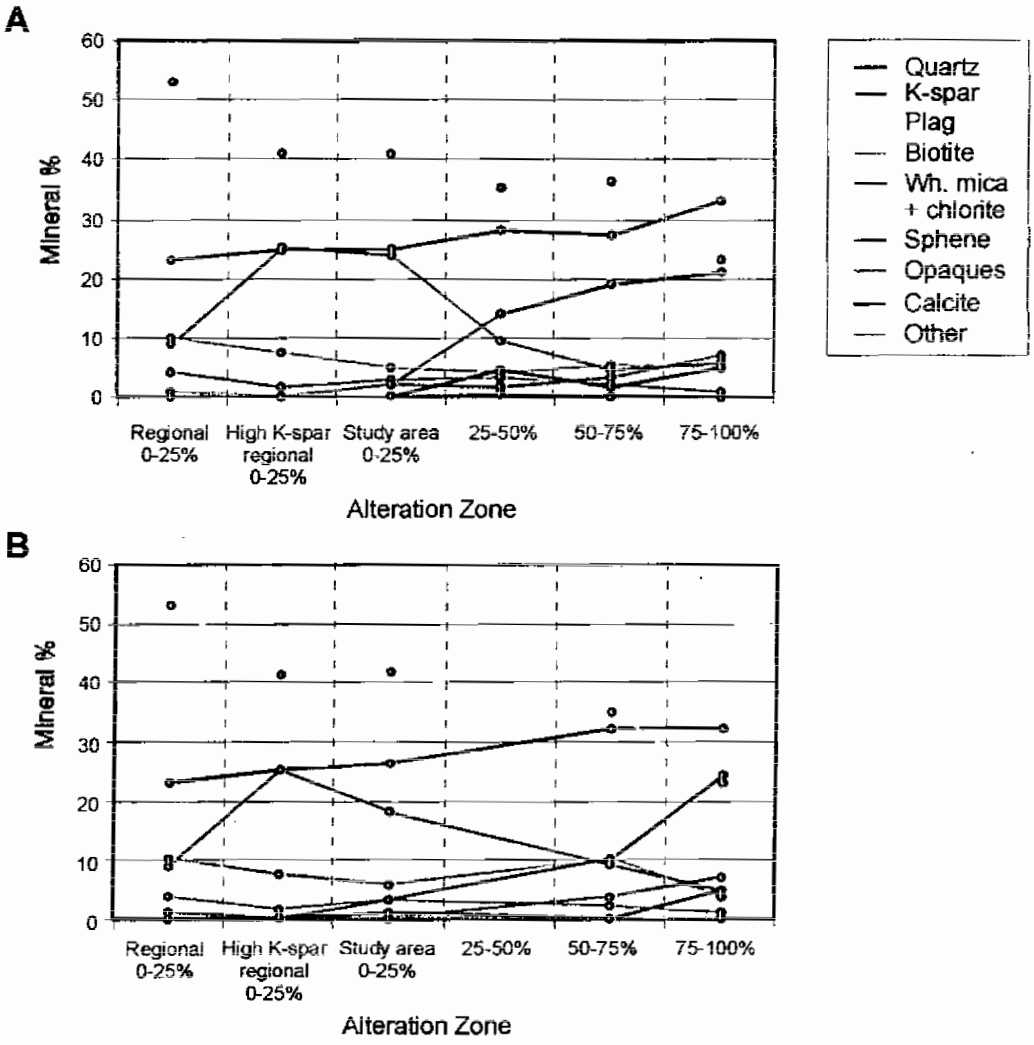

Figure 5. Petrology as a function of alteration zone. The regional 0-25% alteration zone data consist of an average of 59 samples (K26A from this study and 58 Kwf samples from Ross (1987,1990)). The 0-25% zone data within the study area are higher in potassium feldspar content than is typical of the Wagy Flat (Ross, 1990). Thus for comparison, the average of 3 samples of high potassium feldspar content (>=22%) from the Ross study also are shown.

a) Petrology by alteration zone based on sample location relative to the alteration zones mapped in Figure 4.

b) Petrology by alteration zone based on hand sample visual alteration index.

Figure 6. Mesoscale fracture character by alteration zone. The number of fractures characterized in each zone varies: 57 fractures within the 0-25% zone, 5 fractures within the 25-50% zone, 46 fractures within the 50-75% zone, and 81 fractures within the 75-100% zone. Data from the 25-50% alteration zone may be anomalous due to a paucity of data.

a) Fracture spacing decreases with increasing alteration intensity.

b) Fracture length decreases with increasing alteration intensity,

c) Percentage of fractures with alteration rinds generally decreases with increasing alteration.

d) Half-width of alteration rinds is greatest within the 75-100% alteration zone, averaging 30 cm. In the less-altered zones, halo half-widths average 1 to 1.5 cm.

e) Vein width is greatest within the moderately altered zones (25-75%). Veins are narrower in both the least altered and most altered zones.

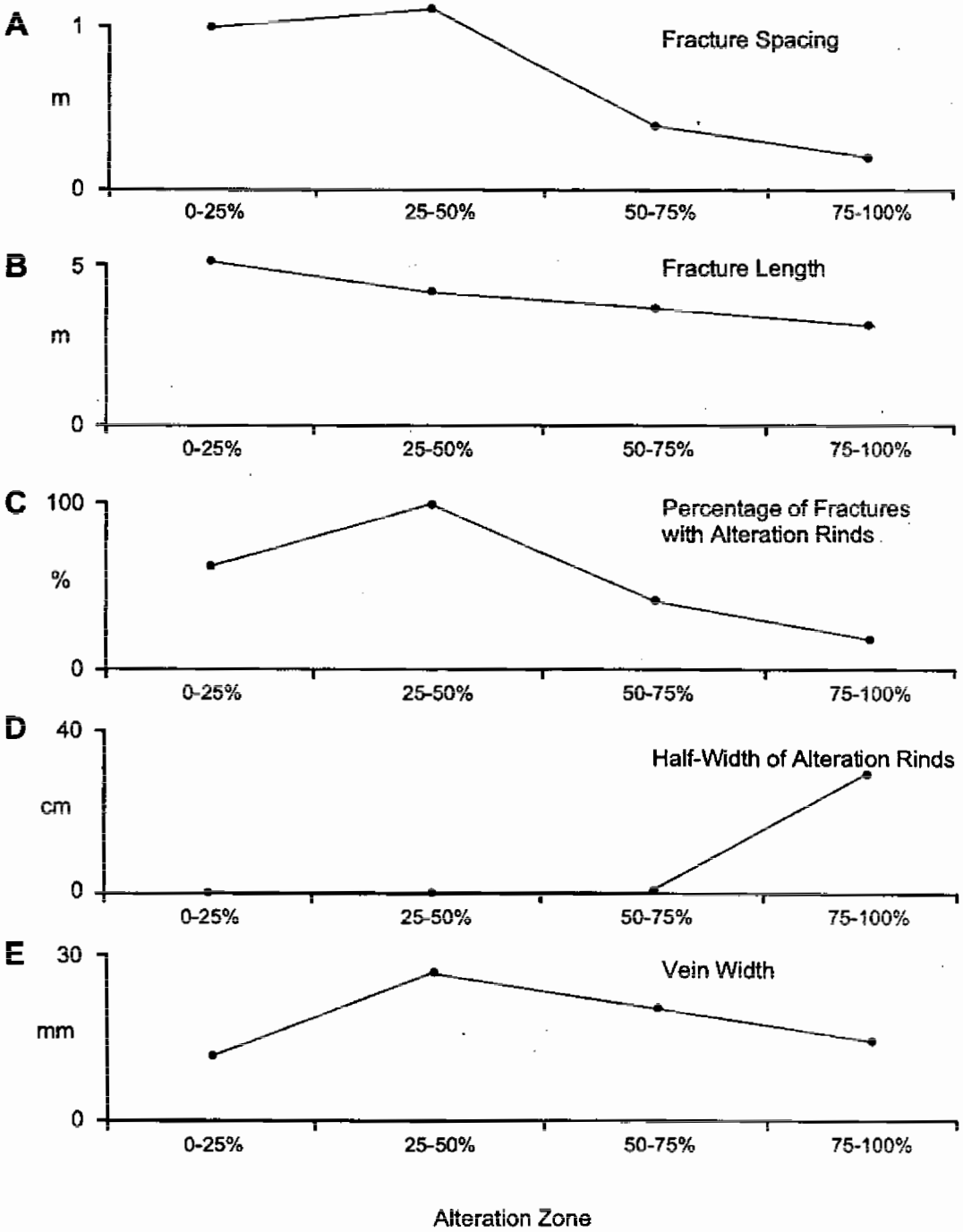
A
1
m
0
Fracture Spacing
0-25%
25-50%
50-75%
75-100%
B
5
m
0
Fracture Length
0-25%
25-50%
50-75%
75-100%
C
100
%
0
Percentage of Fractures with Alteration Rinds
0-25%
25-50%
50-75%
75-100%
D
40
cm
0
Half-Width of Alteration Rinds
0-25%
25-50%
50-75%
75-100%
E
30
mm
0
Vein Width
0-25%
25-50%
50-75%
75-100%
Alteration Zone

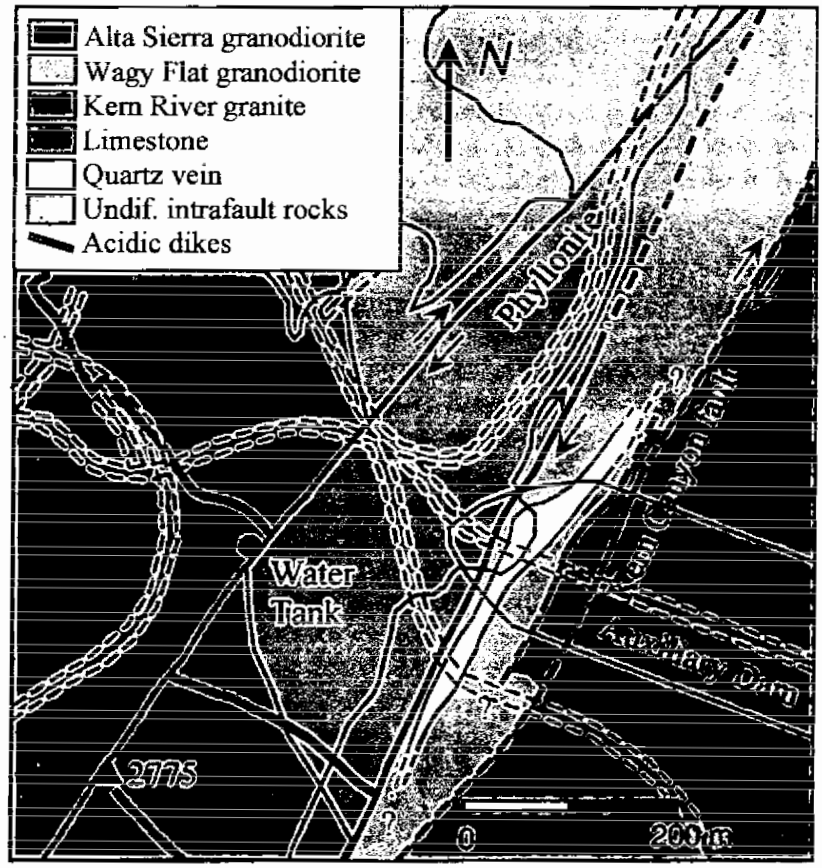

Figure 7. Bedrock geologic map at the western auxiliary dam abutment. Offset of the K_{wf}/K_{as} igneous contact suggests ~175 m of right-lateral separation. (Map provided by J. Chester, includes data from Treasher, 1948).

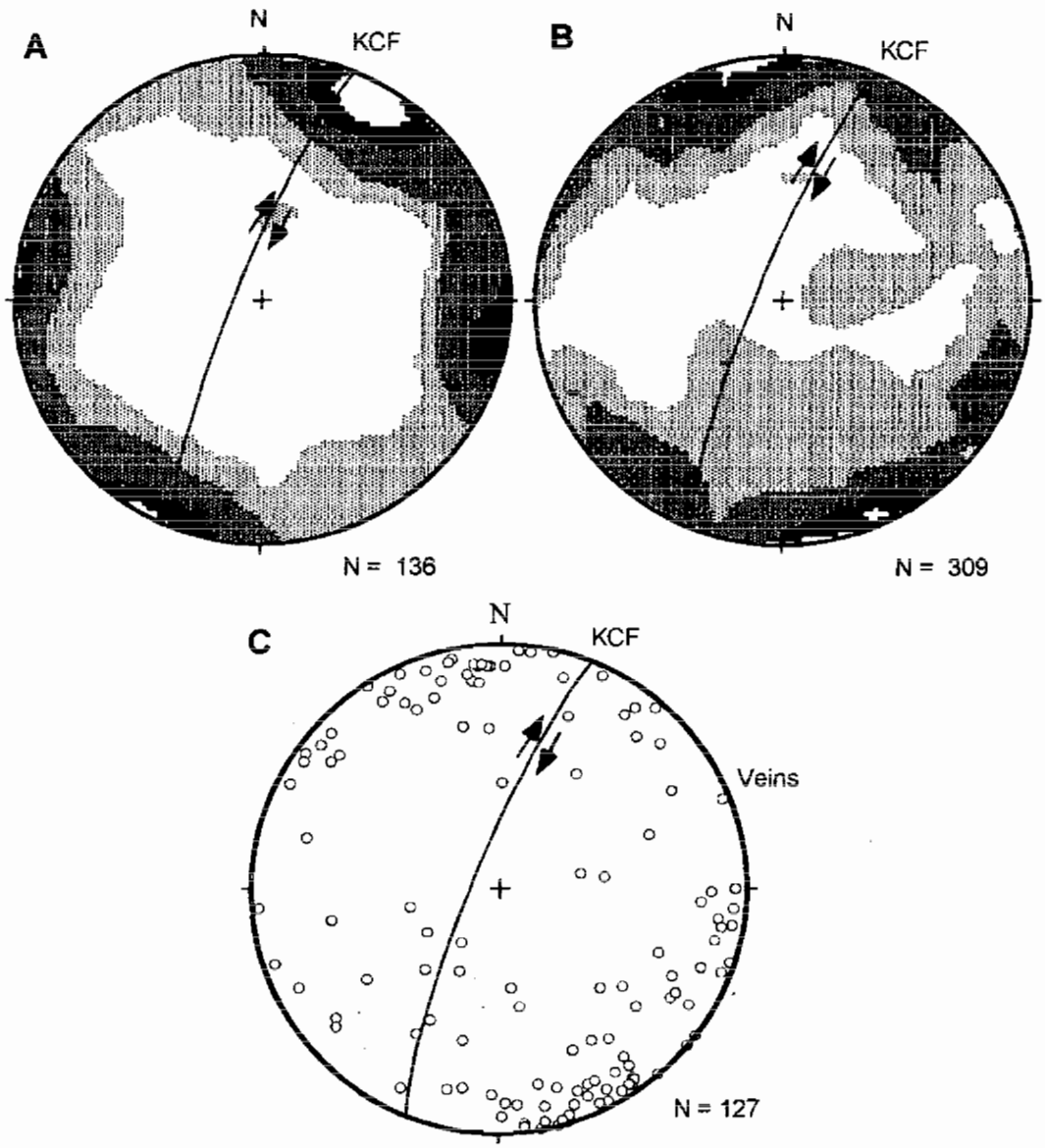

Figure 8. Regional and peninsula fracture and vein fabric. (a) Open fractures and veins in host rock surrounding southern end of Lake Isabella, but not including data from Engineer Point. (b) Open fractures and veins at Engineer Point. (c) Veins only at Engineer Point. Plots are lower hemisphere equal-area projections with north at the top. Kamb contours are shown at 2 sigma intervals. Also shown is the average orientation of the Kern Canyon Fault (KCF).

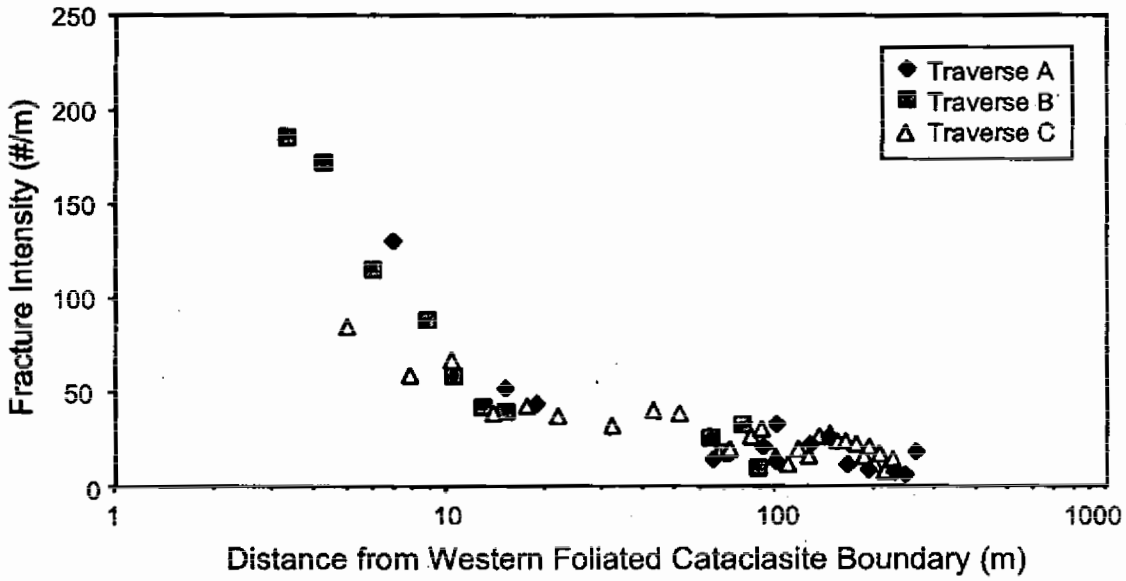

Figure 9. Intensity of open fractures, veins, and subsidiary faults in the Wagy Flat granodiorite. Intensity is plotted as a function of distance west of the western foliated cataclasite boundary (see Figure 4 for traverse locations). Intensity was determined by the average number of intercepts per meter length along two perpendicular count lines at each counting station. Deformation intensity increases gradually from regional levels at several hundred meters from the fault, then displays a marked increase in intensity at approximately 15-20 m from the western foliated cataclasite boundary.

Figure 10. Phyllonite zone characterization. Changes in deformational microstructures in quartz and petrology as a function of distance across the phyllonite zone along the South Traverse. Mineral percentages determined by point count of 200 grains per thin section. Microfracture counts represent the average liner microfracture intensity within 30-50 quartz grains per section. The dashed line represents the position of the center of the phyllonite zone as mapped in Figure 4; negative numbers represent distances east of the phyllonite zone, and positive numbers represent distances west of the phyllonite zone.

a) Healed and open microfracture intensities. Healed microfracture intensities increase toward the phyllonite zone but decrease within the zone. East of the phyllonite, healed microfractures increase toward the cataclastic zone. Open microfracture intensities decrease toward the phyllonite zone.

b) Recrystallization along subgrain boundaries vs recrystallization along microfractures. Recrystallization along microfractures is restricted to the center of the phyllonite zone and likely accounts for the decrease in healed microfractures seen in Figure 19a. Subgrain boundary recrystallization is observed over a slightly broader zone than microfracture recrystallization.

c) Total feldspar and quartz content. Combined plagioclase and potassium feldspar content diminishes gradually toward the phyllonite zone and decreases significantly within the zone. Quartz content remains relatively constant across the traverse with a minor increase within the phyllonite zone.

d) White mica/chlorite content. Combined white mica and chlorite content increases gradually toward the phyllonite zone and increases markedly within the zone.

e) Biotite/vermiculite content. Biotite/vermiculite content plummets within the phyllonite zone as biotite is replaced first by vermiculite and then by chlorite.

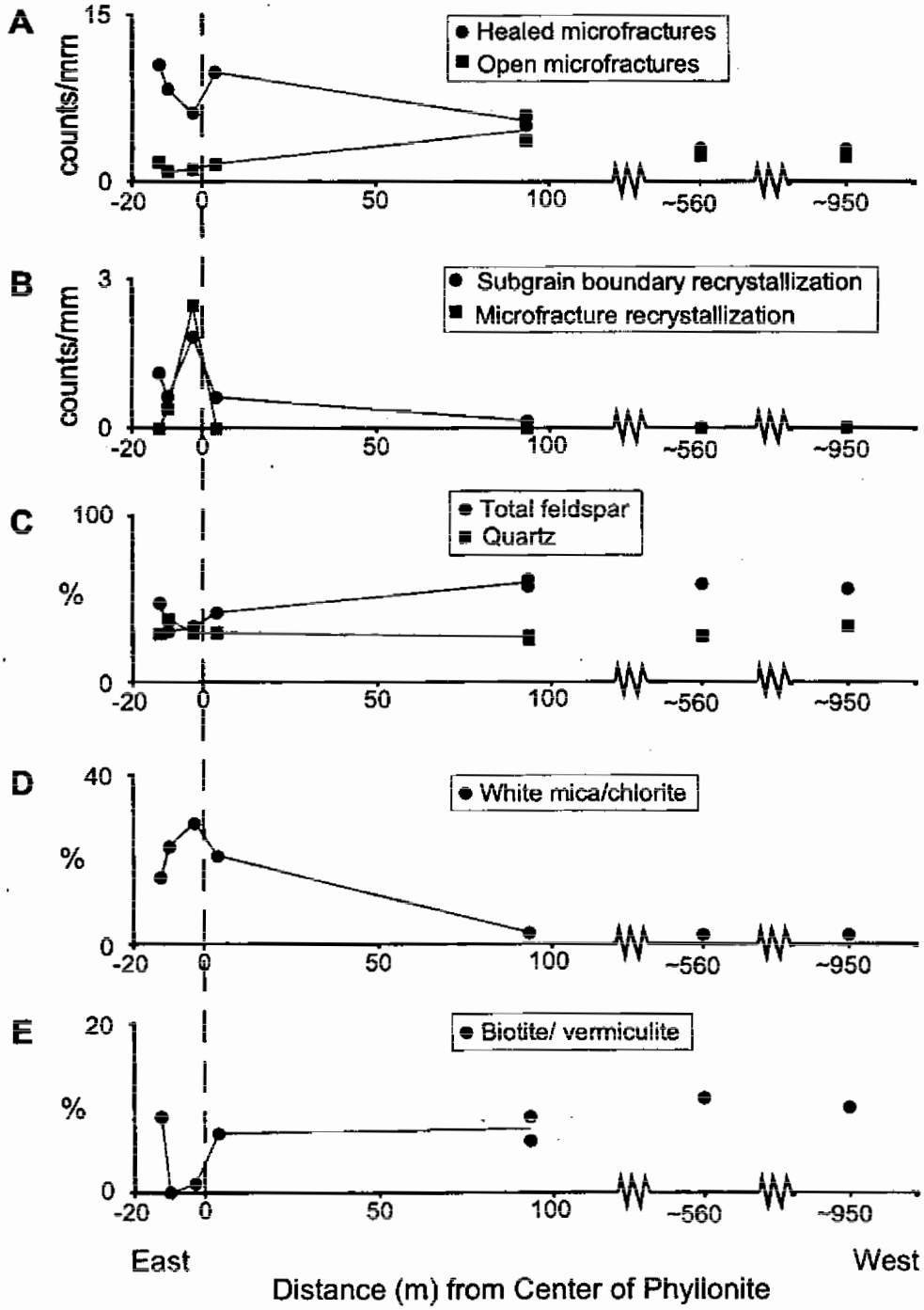
A
15
counts/mm
0
Healed microfractures
Open microfractures
-20
0
50
100
~560
~950
B
3
counts/mm
0
Subgrain boundary recrystallization
Microfracture recrystallization
-20
0
50
100
~560
~950
C
100
%
0
Total feldspar
Quartz
-20
0
50
100
~560
~950
D
40
%
0
White mica/chlorite
-20
0
50
100
~560
~950
E
20
%
0
Biotite/ vermiculite
-20
0
50
100
~560
~950
East
West
Distance (m) from Center of Phyllonite

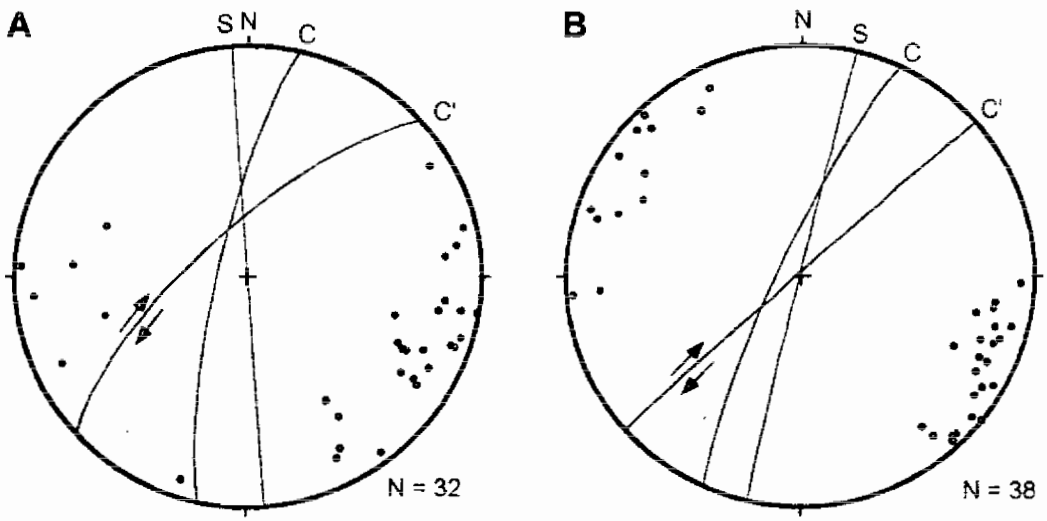

Figure 11. Orientations of poles to C, C', and S surfaces in the phyllonite. Plots are lower hemisphere equal-area projections with north at the top. Average orientation and sense-of-shear shown by great circles and arrows. (a) North of station K18; C surfaces are in red, N=21; C' surfaces are in black, N=7; S surfaces are in green, N=4. (b) South of station K18; C surfaces are in red, N=16; C' surfaces are in black, N=12; S surfaces are in green, N=10. Data provided by J. Chester and F. Chester.

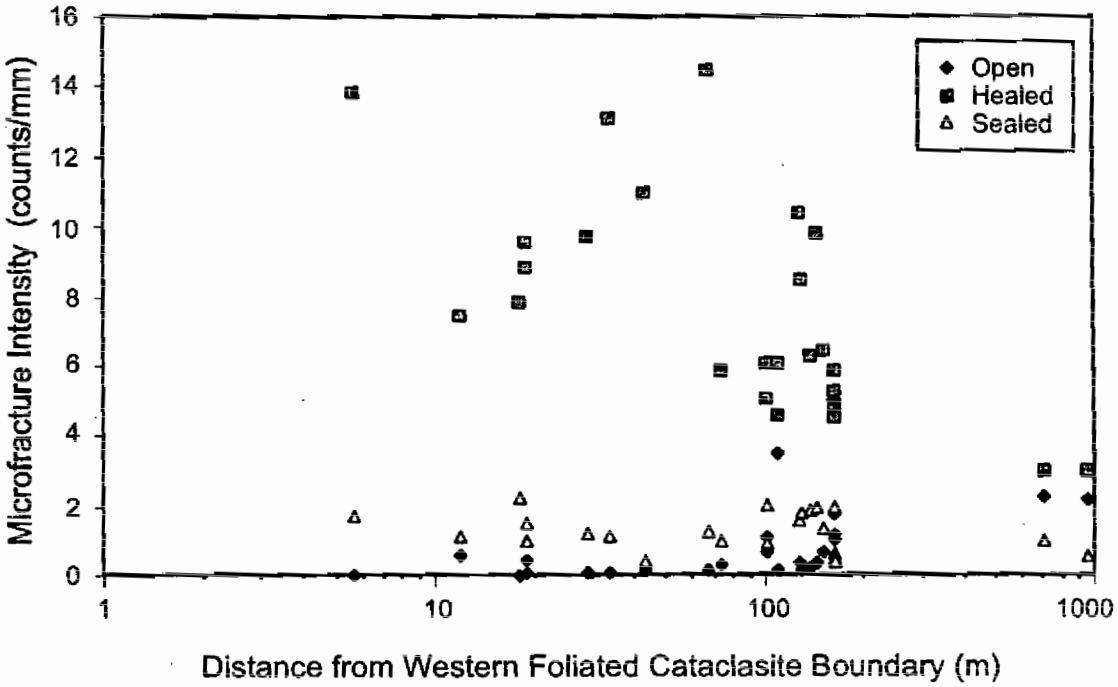

Figure 12. Intensity of open, sealed, and healed microfractures. Intensity is plotted as a function of distance west of the western foliated cataclasite boundary. Samples from all four traverses are combined; see Figure 4 for sample locations. Microfracture intensity data are presented in Table 6.

Figure 13. Cataclasite zone characterization. Changes in petrology and deformational microstructures in quartz as a function of distance west of the western foliated cataclasite/fractured rock boundary along the North Central Traverse. Mineral percentages determined by point count of 200 grains per thin section. Microfracture counts represent the average liner microfracture intensity within 30-50 quartz grains per section.

a) Calcite content. Calcite content increases toward the cataclastic zone and is absent in the Wagy Flat protolith.

b) Total feldspar and white mica/chlorite content. Total feldspar (plagioclase and potassium feldspar) decrease toward the cataclastic zone. Combined white mica/chlorite content increase toward the cataclastic zone.

c) Sum of all but open microfractures. The sum of healed, sealed, and recrystallized microfracture intensities increases toward the cataclastic zone. The total intensity is much greater than that of the protolith, but the individual samples have variably elevated microfracture intensities near the cataclastic zone.

d) Open microfractures. Open microfracture intensities decrease significantly near the cataclastic zone.

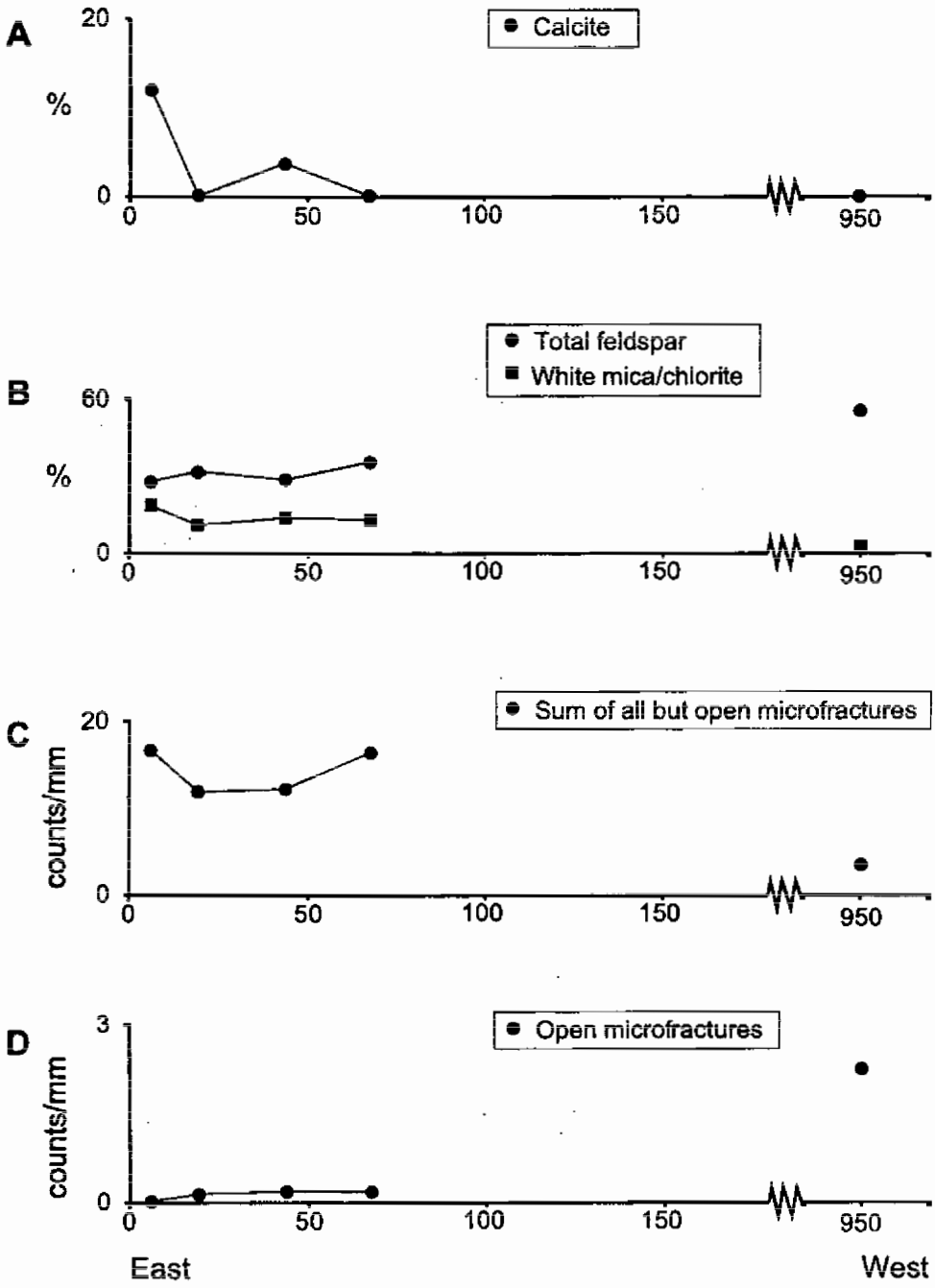
A
20
%
0
Calcite
0
50
100
150
950
B
60
%
0
Total feldspar
White mica/chlorite
0
50
100
150
950
C
20
counts/mm
0
Sum of all but open microfractures
0
50
100
150
950
D
3
counts/mm
0
Open microfractures
0
50
100
150
950
East
West
Distance (m) from Western Foliated Cataclasite Boundary

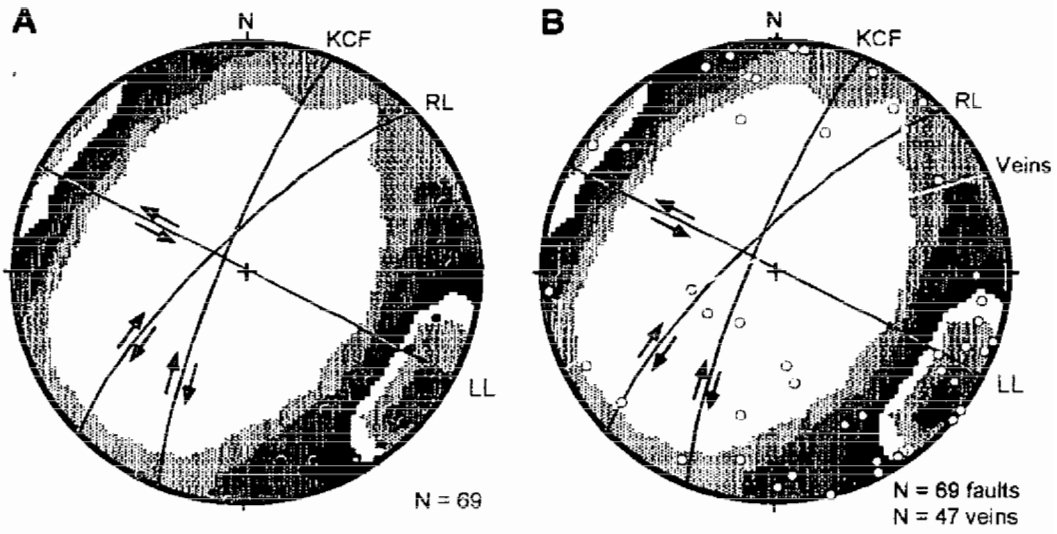

Figure 14. Fracture fabric of the east-side cataclastic zone. Contour plot of poles to all measured subsidiary faults in the intensely fractured zone on the east side of Engineer Point are overlain by great circles representing average orientation of the Kern Canyon Fault (KCF), average orientation of all faults with known right-lateral sense-of-shear (RL), and average orientation of all faults with known left-lateral sense-of-shear (LL). Plot (a) also shows the poles to known right-lateral faults (red dots), and poles to known left-lateral faults (green dots). Plot (b) shows poles to veins (yellow dots) and the average orientation of veins. Plots are lower hemisphere equal-area projections with north at the top. Kamb contours are shown at 2 sigma intervals. Data provided by J. Chester and F. Chester.